Interstellar-Terrestrial Relations: Variable Cosmic Environments, the Dynamic Heliosphere, and Their Imprints on Terrestrial Archives and Climate

K. Scherer (kls@tp4.rub.de), H. Fichtner (hf@tp4.rub.de) and T. Borrmann (tb@tp4.rub.de)
Institut für theoretische Physik, Weltraum- und Astrophysik, Ruhr-Universität Bochum, D-44780 Bochum, Germany

J. Beer (juerg.beer@eawag.ch)
Eidgenössische Anstalt für Wasserversorgung, Abwasserreinigung und Gewässerschutz, 133 Dübendorf, CH-8600, Switzerland

L. Desorgher (laurent.desorgher@phim.unibe.ch) and E. Flückiger (erwin.flueckiger@phim.unibe.ch)
Physikalisches Institut, Abteilung für Weltraumforschung und Planetologie, Sidlerstr. 5, CH-3012 Bern, Switzerland

H.-J. Fahr (hfahr@astro.uni-bonn.de)
Institut für Astrophysik und extraterrestrische Forschung der Universität Bonn, Auf dem Hügel 71, 53121 Bonn, Germany

S.E.S. Ferreira (fsksesf@puknet.puk.ac.za), U.W. Langner (fskuwl@puknet.puk.ac.za) and M.S. Potgieter (fskmsp@puknet.puk.ac.za)
Unit for Space Physics, School of Physics, North-West University, 2520 Potchefstroom, South Africa

B. Heber (heber@physik.uni-kiel.de)
Institut für Experimentelle und Angewandte Physik, Leibnizstraße 19, 24098 Kiel, Germany

J. Masarik (masarik@fmph.uniba.sk)
Commenius University, Department of Nuclear Physics & Bio Physics, 84248 Bratislava 4, Slovakia

N. Shaviv (shaviv@phys.huji.ac.il)
Hebrew University Jerusalem, 91904 Israel

J. Veizer (veizer@science.uottawa.ca)
Ottawa-Carleton Geoscience Center, University of Ottawa, 140 Louis Pasteur, Ottawa, Canada K1N 6N5

Abstract. In recent years the variability of the cosmic ray flux has become one of the main issues interpreting cosmogenic elements and additionally their connection with climate. In this review, an interdisciplinary team of scientist brings together our knowledge of the evolution and modulation of the cosmic ray flux from its origin in the Milky Way, during its propagation through the heliosphere, in its interaction with the Earth's magnetosphere, resulting, finally, in the production of cosmogenic isotopes in the Earth' atmosphere. The interpretation of the cosmogenic isotopes and the cosmic ray – cloud connection are also shortly discussed. Finally, we discuss some open questions.

Keywords: Cosmic Rays – Heliosphere – Comsogenic Isotopes – Climate

Table of Contents

I Introduction to the Problem **7**
- 1 Interstellar-Terrestrial Relations: Definition and Evidence 9
- 2 Cosmic Ray Forcing 10
- 3 Known Astronomical Effects 11
- 4 Structure of the Review 13

II General Theoretical Concepts **15**
- 5 The Fundaments for the Quantitative Modelling 17
  - 5.1 Cosmic Ray Transport 17
  - 5.2 The Dynamical Heliosphere 18

III Galactic Cosmic Rays **21**
- 6 Long-term Variation 23
  - 6.1 Star Formation Rate 23
  - 6.2 Spiral Arm Passages 25
  - 6.3 Cosmic Ray Record in Iron Meteorites 29
- 7 Cosmic Ray Spectra inside and outside of Galactic Arms 32
  - 7.1 Accelerations at Shocks 32
  - 7.2 Self-similar Blast Waves 34
  - 7.3 Galactic Cosmic Ray Spectra 35
  - 7.4 The Average GCR Spectrum inside Galactic Arms 38
  - 7.5 Escape into the Interarm Region 40

IV Heliospheric Modulation **45**
- 8 Propagation of Cosmic Rays inside the Heliosphere 47
  - 8.1 Solar Activity: 11-year and 22-year Cycles in Cosmic Rays 47
  - 8.2 Causes of the 11- and 22-year Modulation Cycles 50
- 9 Effects of the Heliospheric Structure and the Heliopause on the Intensities of Cosmic Rays at Earth 55
  - 9.1 Modulation Models 57

9.2 Changes in the Shape of the Heliosphere 57
9.3 Changes in the Size of the Heliosheath 58
9.4 Changes in the Termination Shock Compression Ratio 58
9.5 Modulation in the Heliosheath 61
9.6 Changes in the Local Interstellar Spectrum 61

V Effects of the Dynamical Heliosphere 67
10 3D (Magneto-)Hydrodynamic Modelling 69
10.1 3D Models without Cosmic Rays 69
10.2 3D Models with Cosmic Rays 69
11 Cosmic Ray Transport in a Dynamic Heliosphere 78
11.1 Cosmic Ray Transport 78
11.2 Transport Coefficients and the Compound Approach 79
11.3 Results of the Hybrid Model 82

VI Magnetospheric and Atmospheric Effects 87
12 Shielding by the Earth's Magnetosphere and Atmosphere 89
12.1 Cosmic Ray Propagation in the Earth's Magnetic Field 89
12.2 Cosmic Ray Interaction in the Atmosphere 94
13 Cosmic Ray Flux and Cosmogenic Isotopes 101
13.1 Calculation of Cosmogenic Nuclide Production Rates 104
13.2 Geometrical and Chemical Model of the Earth 104
13.3 Cosmic Ray Particle Fluxes and Cosmogenic Nuclide Production 105
13.4 The Geomagnetic Field and Cosmogenic Nuclide Production 106
13.5 Cross Sections for Cosmogenic Nuclide Production 109

VII Cosmic Ray Imprints in Terrestrial Archives and Their Implications to Climate 111
14 Imprints in Earth's archives 113
15 Implications to Climate 116
15.1 Celestial Climate Drivers and Amplifiers 118
15.2 Terrestrial Archives 121
15.3 Paleoclimate on Billion Year Time Scales 122
15.4 Paleoclimate on Million Year Time Scales 124

15.5 Paleoclimate on Multimillenial Time Scales 125
15.6 Postglacial Climate on Millenial to Centennial Time Scales 130
15.7 Post Little Ice Age Climate on Decadal Time Scales 133

VIII Resume 137
16 Where do we stand? 139

List of Abbreviations

accelerator mass-spectrometry (AMS)
anomalous cosmic ray (ACR)

before present (BP)

coronal mass ejections (CMEs)
cosmic ray (CR)
cosmic ray flux (CRF)

Energetic storm particles (ESP)

galactic cosmic ray (GCR)
general circulation model (GCM)
global merged interaction region (GMIR)
greenhouse gases (GHG)
Ground Level Enhancement (GLE)

heliospheric magnetic field (HMF)

interaction region (CIR)
International Geomagnetic Reference Field (IGRF)
International Geophysical Year (IGY)

Large Magellanic Cloud (LMC)
Little Ice Age (LIA)
local interstellar spectrum (LIS)

magneto-hydrodynamic (MHD)
Medieval Climate Optimum (MCO)
Milky Way (MW)

neutron monitor (NM)

pickup ion (PUI)
propagating diffusion barrier (PDB)

solar energetic particle (SEP)
Star Formation Rate (SFR)
supernova (SN)

termination shock (TS)
Total Solar Irradiance (TSI)

Part I

Introduction to the Problem

1. Interstellar-Terrestrial Relations: Definition and Evidence

There is evidence that the galactic environment of the Solar System leaves traces on Earth. Well-known are supernova explosions, which are responsible for an increased ^{3}He abundance in marine sediments (O'Brien et al., 1991), or catastrophic cometary impacts, which are considered as causes for biological mass extinctions (Rampino et al., 1997; Rampino, 1998). These and other events, to which also gamma ray bursts (Thorsett, 1995) or close stellar encounters (Scherer, 2000) can be counted, can be considered as 'quasi-singular' and belong to so-called *stellar-terrestrial relations*. From those one should distinguish 'quasi-periodic' events, which are connected to encounters of different interstellar gas phases or molecular clouds (Frisch, 2000), to the crossing of the galactic plane (Schwartz and James, 1984), and to the passage through galactic spiral arms (Leitch and Vasisht, 1998). As will be explained in the following, these quasi-periodic changes influence the Earth and its environment and are, therefore, called *interstellar-terrestrial relations*. The mediators of such environmental changes are the interstellar plasma and neutral gas as well as the cosmic rays, all of which affect the structure and dynamics of the heliosphere. The heliosphere, however, acts as a shield protecting the Earth from the direct contact with the harsh interstellar environment. From all particle populations that can penetrate this shield, only the flux variations of cosmic rays can be read off terrestrial archives, namely the depositories of cosmogenic isotopes, i.e. ice-cores, sediments, or meteorites.

The typical periods of interstellar-terrestrial relations seen in these archives are determined by external (interstellar) triggers on time-scales longer than about ten-thousand years, while those for shorter time-scales are governed by an internal (solar) trigger. The latter results from solar activity, which leads to variations of the cosmic ray flux with periods of the various solar cycles, like the Hale-, Schwabe- and Gleissberg-cycle amongst others.

The *interpretation* of the cosmogenic archives is of importance for our understanding of variations of the galactic cosmic ray spectra and of the solar dynamo and, therefore, of high interest to astrophysics. Moreover, the *correlation* of cosmogenic with climate archives gives valuable information regarding the question to what extent the Earth climate is driven by extraterrestrial forces. Candidates for such climate drivers are the variable Sun (solar forcing), the planetary perturbations (Milankovitch forcing), the variable cosmic ray flux (cosmic ray forcing), and the varying atomic hydrogen inflow into the atmosphere of Earth (hydrogen forcing).

The current debate concentrates on solar and cosmic ray forcing, because the Milankovitch forcing is well understood and the hydrogen forcing is highly speculative. While there exists a vast amount of literature, especially reviews and monographs, concerning the solar forcing, the work on cosmic ray forcing is still largely scattered and no comprehensive overview has been compiled so far. This review intends to make the first step to change that situation by bringing together our knowledge about cosmogenic archives, climate archives, cosmic ray transport and heliospheric dynamics.

2. Cosmic Ray Forcing

The idea that cosmic rays can influence the climate on Earth dates back to Ney (1959) who pointed out that if climate is sensitive to the amount of tropospheric ionization, it would also be sensitive to solar activity since the solar wind modulates the cosmic ray flux (CRF), and with it, the amount of tropospheric ionization. These principal considerations have been revived by Svensmark and Friis-Christensen (1997) and Svensmark (1998), who found from a study of satellite and neutron monitor data a correlation between cosmic ray intensity and the global cloud coverage on the 11-year time-scale of the solar activity cycle. While Marsh and Svensmark (2000a), Marsh and Svensmark (2000b), Palle Bago and Butler (2000) have significantly refined this correlation analysis. Usoskin et al. (2004b) have found that the CRF/low altitude cloud cover is as predicted. Namely, the amount of cloud cover change over the solar cycle at different latitudes is proportional to the change in tropospheric ionization averaged over the particular latitudes. Others have started to identify the physical processes for cloud formation due to high-energy charged particles in the atmosphere (Tinsley and Deen, 1991; Tinsley and Heelis, 1993; Eichkorn et al., 2002; Yu, 2002; Harrison and Stephenson, 2006). There is, however, also severe doubt regarding the significance of the correlation, see, e.g. Gierens and Ponater (1999), Kernthaler et al. (1999), Carslaw et al. (2002), Sun and Bradley (2002), Kristjánsson et al. (2004), Sun and Bradley (2004).

The critics rather favour the most evident external climate driver, namely the solar irradiance. While on the 11-year time-scale (Schwabe cycle) both the cosmic ray forcing and the solar forcing act in an indistinguishable manner, on the 22-year time-scale (Hale cycle), there should be a difference because, in contrast to the solar irradiation, the cosmic ray flux is sensitive to the heliospheric magnetic field polarity as a consequence of drift-related propagation (Fichtner et al., 2006).

Other clues result from the study of the climate and cosmogenic archives for intermediate and very long time-scales. Regarding the former, the so-called grand minima of solar activity have been investigated (van Geel et al., 1999a; Caballero-Lopez et al., 2004; Scherer and Fichtner, 2004) because temperature was generally lower during these periods (Grove, 1988). There is evidence from historical sunspot observations and cosmogenic archives that both forcing processes could have been responsible for this climate variation so that, unfortunately, no decision can be expected unless the 22-year Hale cycle is detected in the data, a claim that has been made already (Miyahara et al., 2005).

The situation is different on very long time-scales. Opposite to the shorter time-scales, on which the cosmic ray flux variations are dominated by solar activity, on longer time scales they are influenced by processes external to the heliosphere, like interstellar environment changes (Yabushita and Allen, 1998) or spiral arm crossings (Shaviv, 2003a). So, one should expect corresponding climate variations on time-scales of millions of years. Indeed, Shaviv and Veizer (2003) have found a correlation between the cosmic ray flux and Earth temperature for the last 500 million years that can be related to the spiral arm crossings of the heliosphere occuring with a quasi-period of about 135 million years. Because there is no reason to expect that solar activity and, in turn, solar irradiance is triggered by spiral arm crossings or interstellar environment changes, any cosmic ray climate correlation on such time-scales is a strong argument in favour of cosmic ray forcing.

3. Known Astronomical Effects

Quite early the influence of interstellar clouds on the climate on Earth has been discussed (Shapley, 1921; Hoyle and Lyttleton, 1939; McCrea, 1975; Eddy, 1976; Dennison and Mansfield, 1976; Begelman and Rees, 1976; McKay and Thomas, 1978) and revisited by Yeghikyan and Fahr, Yeghikyan and Fahr (2004b, 2004a). A possible influence of interstellar dust particles on the climate was discussed in Hoyle (1984). A review of the possible long-term fluctuations of the Earth environment and their possible astronomical causes was given by McCrea (1981). The influence of a neutral interstellar particle fluxes on the terrestrial environment was studied by Bzowski et al. (1996)

In the middle of the last century (Milankovitch, 1941) discussed the planetary influence on terrestrial climate, especially on the ice ages. The secular variations of the Earth's orbital elements caused by the other planets, lead to periodically changes in the inclination and eccentricity (with the most significant periods of: 19, 23, 41, 100 400 kyr), which in turn affects the absorption of solar irradiation (the latitudinal dependence), insolation, the length of the seasons, etc. causing climatic changes, e.g. Berger (1991),Ruddiman (2006). These and other periods can be found in Figure 1 taken from Mitchell (1976). Concentrating on

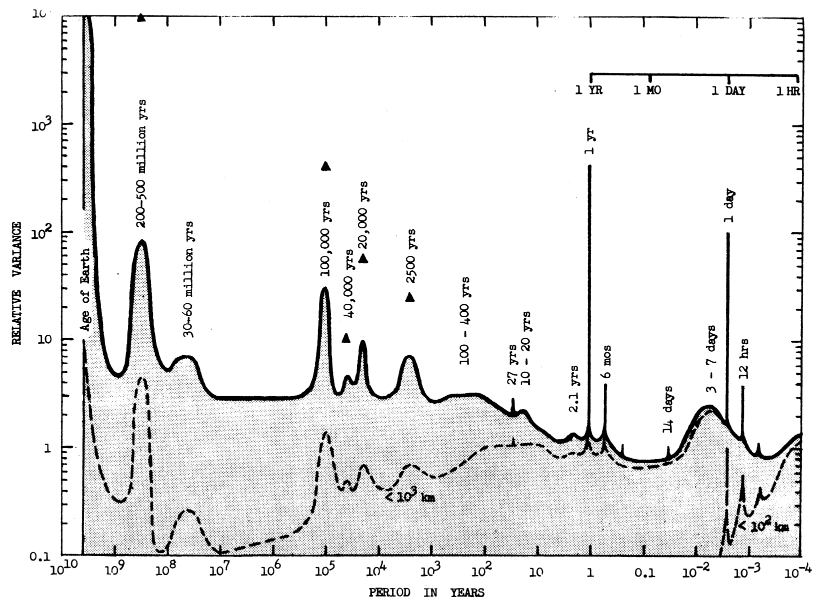

Figure 1. Compilation of the climatic changes on Earth on all times scales (after Mitchell 1976).

variations longer than one year in Figure 1 the different periods can be identified in the following ways: While the Milankovitch cycle is more or less confirmed, all periods for the external forcing of the climate listed above are still under debate. Recently, Lassen and Friis-Christensen (1995) pointed to the connection of the solar cycle length and the temperature variation in the northern hemisphere. These external effects have the major drawback, that up to now no detailed process is known which drives the related climate changes. The 2400–year period is probably connected with the relative motion of the Sun around the center of mass (barycentre) of the solar system (Charvatova, 1990). The 30–Myr peak coincides with the galactic plane crossing of the heliosphere, and the (220–500)−Myr peak corresponds to the revolution period of the Sun around the galaxy (see section 6). In table I, some alternative explanations are listed, too.

Other astronomical effects of sporadic nature are, for example, supernovae explosions (Ruderman, 1974), gamma-ray bursts (Thorsett, 1995), and stellar encounters (Scherer, 2000) and will not be discussed further.

Table I. Possible astronomical or geological explanations of the different periods observed in Figure 1.

Years	Explanation	
	Astronomical	Geological
10–20	solar cycle variations	
100-400	long term solar variations	
2400	motion of Sun around solar system barycentre	deep-sea thermohaline circulations
19000, 23000	precession parameter (Milankovitch cycle)	
41000	obliquity (Milankovitch cycle)	
100000	eccentricity (Milankovitch cycle)	
$(30–60)\times10^6$	galactic plane crossing	tectonism
$(200–500)\times10^6$	orbital revolution of the Sun around galactic center	tectonism

4. Structure of the Review

The general physical ideas for cosmic ray acceleration and modulation together with magneto-hydrodynamic (MHD) concepts are briefly presented in part II.

In part III the problem of determining the local interstellar cosmic ray spectra is considered. This is done in two sections: First, in section 6 the distribution of matter and stars in the galaxy along the orbit of the Sun and their influences on the cosmic ray flux is discussed (N. Shaviv). Second, in section 7 the galactic cosmic ray spectra inside and outside of galactic spiral arms are computed (H.-J. Fahr, H. Fichtner, K. Scherer).

The heliospheric modulation of present-day interstellar spectra due to the solar activity cycle is subject of part IV. While in section 8 the time dependence of the modulation processes are described for the 11- and 22-year solar cycles (M.S. Potgieter), section 9 concentrates on the spatial aspect of the modulation, in particular its dependence on the outer heliospheric structure (U.W. Langner, M.S. Potgieter).

For the considerations in part III and IV a stationary heliosphere was assumed. This approximation is dropped in part V. A general description of hydrodynamic modeling of heliospheric plasma structures given in section 10 (H. Fichtner, T. Borrmann) is followed by section 11 with a presentation of results of hybrid modeling, including the kinetic transport equation of cosmic rays (S.E.S. Ferreira, K. Scherer).

The interaction of cosmic rays with the environment of the Earth is studied in part VI. After discussing the magnetospheric and atmospheric propagation of cosmic rays as well as the corresponding ionization and energy deposition in the atmosphere in section 12 (B. Heber, L. Desorgher, E. Flückiger), the production of cosmogenic nuclei is described in section 13 (J. Masarik, J. Beer).

The imprints of cosmic rays on Earth and their implications for climate processes are subject of part VII. The emphasis in section 14 is put on the storage of cosmogenic isotopes in various archives (K. Scherer, J. Beer), while in section 15 the evidence of cosmic ray driven climate effects on different time scales is presented (J. Veizer).

In the final part VIII an attempt is made to identify and formulate the crucial questions in this new interdisciplinary field.

Part II

General Theoretical Concepts

5. The Fundaments for the Quantitative Modelling

The fundamental equations for quantitative studies are presented in the following two sections. The transport equation of cosmic rays discussed in the section 5.1 is used to describe the acceleration and propagation of cosmic rays through the galaxy as well as through the heliosphere. For the latter plasma structure the magneto-hydrodynamic (MHD) equations are presented in section 5.2 with their general assumptions.

5.1. Cosmic Ray Transport

The transport of cosmic rays is calculated by solving the transport equation (Parker, 1965)

$$\frac{\partial f}{\partial t} = \nabla \cdot \left(\overleftrightarrow{\kappa} \, \nabla f \right) - (\vec{v} + \vec{v}_{dr}) \cdot \nabla f + \frac{p}{3} (\nabla \cdot \vec{v}) \frac{\partial f}{\partial p} + S(\vec{r}, \vec{p}, t) \quad (1)$$

The description is based on the isotropic phase space distribution function $f(\vec{r}, p, t)$ depending on location $\vec{r}$, magnitude of momentum p and time t. Often instead of the momentum p the rigidity $R = pc/q$ is used, with c and q denoting the speed of light and the particle charge, respectively. The equation contains, in addition to the effects of convection velocity $\vec{v}$ and drift $\vec{v}_{dr}$ in the magnetic field $\vec{B}$ a fully anisotropic diffusion tensor:

$$\overleftrightarrow{\kappa} = \begin{pmatrix} \kappa_{\perp r} & 0 & 0 \\ 0 & \kappa_{\perp \theta} & 0 \\ 0 & 0 & \kappa_{\|} \end{pmatrix} \quad (2)$$

This tensor, denoted here in spherical polar coordinates (r, θ, φ), is formulated with respect to the local magnetic field, see Fig. 2. Various suggestions for the explicit form of its elements have been made,

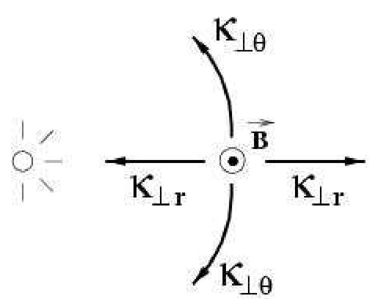

Figure 2. Illustration of the elements of the diffusion tensor. The coefficient $\kappa_{\|}$ describes the diffusion along the local magnetic field $\vec{B}$.

see, e.g., Burger and Hattingh (1998), Fichtner et al. (2000), Ferreira et al. (2001), Matthaeus et al. (2003), Bieber et al. (2004), or Shalchi and Schlickeiser (2004). The transport equation is generally solved numerically using mixed boundary conditions.

For quantitative studies of interstellar-terrestrial relations it is necessary to have a model of a three-dimensional heliosphere, which is immersed in a dynamic local interstellar medium. There are at least two reasons why such model should be three-dimensional. First, a comprehensive and self-consistent treatment of the cosmic ray transport must take into account the three-dimensional structure of the turbulent heliospheric plasma and, second, the heliosphere can be in a disturbed state for which no axisymmetric description can be justified. The present state-of-the-art of the modelling of a dynamic heliosphere with a self-consistent treatment of the transport of cosmic rays is reviewed in Fichtner (2005). As is pointed out in that paper, the major challenge is the development of a three-dimensional hybrid model. This task requires, on the one hand, the generalisation of the modelling discussed in the following section and, on the other hand, the formulation of three-dimensional models of the heliospheric plasma dynamics.

5.2. The Dynamical Heliosphere

The model of the dynamical heliosphere is in most cases based on the following (normalized) magneto-hydrodynamical equations

$$\frac{\partial}{\partial t}\begin{pmatrix}\rho\\ \rho\vec{v}\\ e\\ \vec{B}\end{pmatrix}+\nabla\cdot\begin{pmatrix}\rho\vec{v}\\ \rho\vec{v}\vec{v}+(p_{th}+\frac{1}{2}B^2)\hat{I}-\vec{B}\vec{B}\\ (e+p_{th}+\frac{1}{2}B^2)\vec{v}-\vec{B}(\vec{v}\cdot\vec{B})\\ \vec{v}\vec{B}-\vec{B}\vec{v}\end{pmatrix}=\begin{pmatrix}Q_\rho\\ \vec{Q}_{\rho\vec{v}}\\ Q_e\\ 0\end{pmatrix} \tag{3}$$

for each thermal component taken into account. Here, ρ is the mass density, $\vec{v}$ the velocity, e the total energy density and p_{th} the thermal pressure of a given component. $\vec{B}$ is the magnetic field and $\hat{I}$ the unity tensor. The terms $Q_\rho, \vec{Q}_{\rho\vec{v}}$ and Q_e describe the exchange of mass, momentum and energy between the thermal components and with the cosmic rays if present. For the closure of Eq. (3) an equation of state for each component is needed, for which usually the ideal gas equation is taken.

Alternatively, the treatment of hydrogen atoms can be based on their kinetic transport equation:

$$\frac{\partial f_H}{\partial t}+\vec{w}\cdot\nabla f_H+\frac{\vec{F}}{m_p}\cdot\nabla_w f_H=P-L \tag{4}$$

Here f_H is the distribution function of hydrogen atoms with velocity $\vec{w}$. The force $\vec{F}$ is the effect of gravity and radiation pressure, while P and L describe the sources and sinks, respectively. This equation takes into account, that the atoms may not collide sufficiently frequent, to allow a single-fluid approach (Baranov and Malama, 1993; Lipatov et al., 1998; Müller et al., 2000; Izmodenov, 2001). Heerikhuisen et al. (2006) have demonstrated, however, that a multifluid approach for hydrogen leads to a reasonable accurate description of the global heliosphere, comparable to the kinetic models.

To keep computing time for the solution of Eqs. (3) affordable, in most cases the number of species in 3-D models is restricted to protons and neutral hydrogen atoms (Zank, 1999; Fahr, 2004; Izmodenov, 2004; Borrmann and Fichtner, 2005). In sophisticated MHD models, which nowadays have been developed (Ratkiewicz et al., 1998; Opher et al., 2004; Pogorelov, 2004; Pogorelov et al., 2004; Washimi et al., 2005), computing time is even more critical and therefore only protons are treated, except in Pogorelov and Zank (2005) who include also hydrogen atoms.

In order to include more species the space dimension has to be reduced. In the 2-D hydrodynamic codes so far up to five species could simultaneously and self-consistently be included, namely in addition to protons and hydrogen also pickup ions (PUIs) as seed for the anomalous cosmic ray (ACR) component and the galactic cosmic rays (GCRs) (Fahr et al., 2000).

Recent developments allow to combine the kinetic modeling of the cosmic ray transport equation (1) with the five species approach, resulting in a hybrid model (Scherer and Ferreira, 2005a; Scherer and Ferreira, 2005b; Ferreira and Scherer, 2005).

The dynamics of the heliosphere includes time varying boundary conditions for both the solar activity cycle and the changing interstellar medium. The inner boundary condition determines the structure of the global heliosphere as well as the cosmic ray flux at the Earth on time scales of tens to thousands of years. For the longer periods, i.e. millions of years, the changes of the outer boundary conditions is more important. Details of modelling and its support by data are discussed in the following sections.

Part III

Galactic Cosmic Rays

6. Long-term Variation

The galactic cosmic ray flux reaching the outskirts of the Milky Way (MW) is often regarded as a constant. However, on long enough time scales, the galactic environment varies, and with it so does the density of cosmic rays in the vicinity of the solar system. In this section, we will concentrate on these variations, which are larger than the short term modulations by the solar wind. In particular, we expect variations from spiral arm passages over the 10^8 yr time scale, while Star Formation Rate (SFR) variations in the Milky Way are expected to be a dominant cause of Cosmic Ray Flux (CRF) variability on even longer time scales. We discuss here the expected variability over these scales, together with the empirical evidence used to reconstruct the actual variations. On shorter time scales, local inhomogeneities in the galactic environment or the occurrence of a nearby supernova can give rise to large variations. These variations will not be discussed since no definitive predictions yet exist nor do reliable reconstructions of the CRF on these shorter scales, which are still long relative to the cosmogenic records on Earth.

6.1. Star Formation Rate

The local and overall SFR in the MW is not constant. Variations in the SFR will in turn control the rate of supernovae. Moreover, supernova remnants accelerate cosmic rays (at least with energies $\lesssim 10^{15}$ eV), and inject fresh high-Z material into the galaxy. Thus, cosmic rays and galactic nuclear enrichment, is proportional to the SFR.

Although there is a lag of several million years between the birth and death of massive stars, this lag is small when compared to the relevant time scales at question. Over the "galactic short term", i.e., on time scales of 10^8 yr or less, the record of nearby star formation is "Lagrangian", i.e., the star formation in the vicinity of the moving solar system. This should record passages through galactic spiral arms. On longer time scales, of order 10^9 yr or longer, mixing is efficient enough to homogenize the azimuthal distribution in the Galaxy (Wielen, 1977). In other words, the long-term star formation rate, as portrayed by nearby stars, should record the long term changes in the Milky Way SFR activity. These variations may arise, for example, from a merger with a satellite or a nearby passage of one.

Scalo (1987), using the mass distribution of nearby stars, concluded that the SFR had peaks at 0.3 Gyr and 2 Gyr before present (BP). Barry (1988), and a more elaborate and recent analysis by Rocha-Pinto et al. (2000), measured the star formation activity of the Milky Way using chromospheric ages of late type dwarfs. They found a dip between 1 and 2 Gyr and a maximum at 2-2.5 Gyr b.p. (see also Fig. 3).

The data in Fig. 3 are not corrected for selection effects (namely, the upward trend with time is a selection effect, favorably selecting younger clusters more of which did not yet dissolve). Since the clusters in the catalog used are spread to cover two nearby spiral arms, the signal arising from the passage of spiral arms is smeared, such that the graph depicts a more global SFR activity (i.e., in our galactic 'quadrant'). On longer time scales (1.5 Gyr and more), the galactic azimuthal stirring is efficient enough for the data to reflect the SFR in the whole disk. There is a clear minimum in the SFR between 1 and 2 Gyr BP, and there are two prominent peaks around 0.3 and 2.2 Gyr BP. Interestingly, the Large Magellanic Cloud (LMC) perigalacticon should have occurred sometime between 0.2 and 0.5 Gyr BP in the last passage, and between 1.6 and 2.6 Gyr BP in the previous passage. This might explain the peaks in activity seen. This is corroborated with evidence of a very high SFR in the LMC about 2 Gyr BP and a dip at 0.7-2 Gyr BP (Gardiner et al., 1994; Lin et al., 1995). Also depicted are the periods during which glaciations were seen on Earth: The late Archean (3 Gyr) and mid-Proterozoic (2.2-2.4 Gyr BP) which correlate with the previous LMC perigalacticon passage (Gardiner et al., 1994; Lin et al., 1995) and the consequent SFR peak in the MW and LMC. The lack of glaciations in the interval 1-2 Gyr BP correlates with a clear minimum in activity in the MW (and LMC). Also, the particularly long Carboniferous-Permian glaciation, correlates with the SFR peak at 300 Myr BP and the last LMC perigalacticon. The late Neo-Proterozoic ice ages correlate with a less clear SFR peak around 500-900 Myr BP. Since both the astronomical and the geological data over these long time scales have much to be desired, the correlation should be considered as an assuring consistency. By themselves, they are not enough to serve as the basis of firm conclusions.

Another approach for the reconstruction of the SFR, is to use the cluster age distribution. A rudimentary analysis reveals peaks of activity around 0.3 and 0.7 Gyr BP, and possibly a dip between 1 and 2 Gyr (as seen in Fig. 3). A more recent analysis considered better cluster data and only nearby clusters, closer than 1.5 kpc (de La Fuente Marcos and de La Fuente Marcos, 2004). Besides the above peaks which were confirmed with better statistical significance, two more peaks were found at 0.15 and 0.45 Gyr. At this temporal and spatial resolution, we are seeing the spiral arm passages. On longer time scales, cluster data reveals a notable dip between 1 and 2 Gyr (Shaviv, 2003a; de La Fuente Marcos and de La Fuente Marcos, 2004).

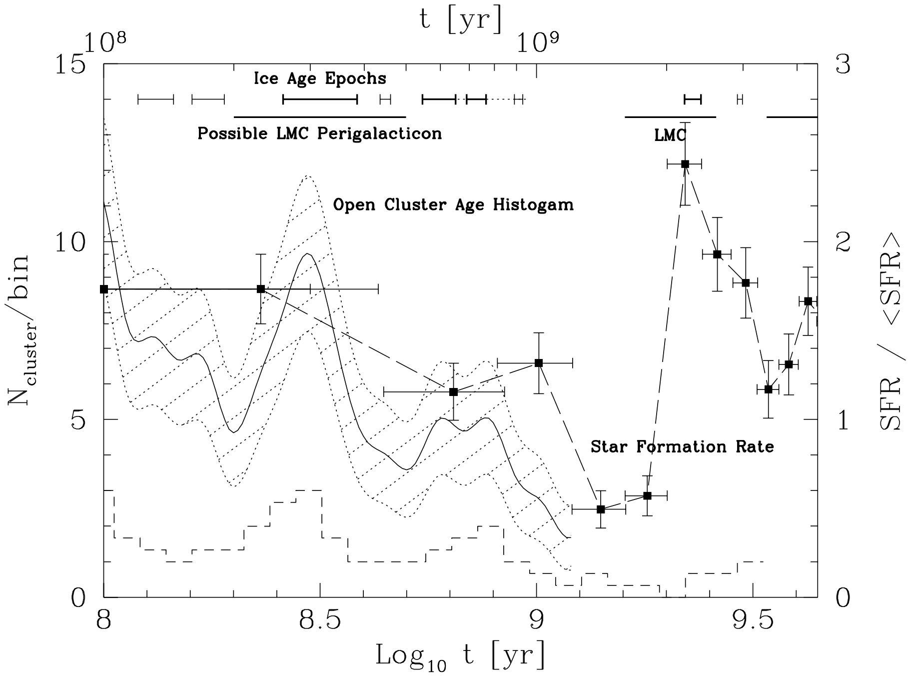

Figure 3. The history of the SFR. The squares with error bars are the SFR calculated using chromospheric ages of nearby stars (Rocha-Pinto et al., 2000), which is one of several SFR reconstructions available. These data are corrected for different selection biases and are binned into 0.4 Gyr bins. The line and hatched region describe a 1-2-1 average of the histogram of the ages of nearby open clusters (using the Loktin et al. (1994), catalog), and the expected 1-σ error bars.

6.2. Spiral Arm Passages

On time scales shorter than those affecting global star formation in the Milky Way, the largest perturber of the local environment is our passages through the galactic spiral arms.

The period with which spiral arms are traversed depends on the relative angular speed around the center of the galaxy, between the solar system with $\Omega_\odot$ and the spiral arms with Ω_p:

$$\Delta T = \frac{2\pi}{m\,|\Omega_\odot - \Omega_p|}, \tag{5}$$

where m is the number of spiral arms.

Our edge-on vantage point is unfortunate in this respect, since it complicates the determination of both the geometry and the dynamics of the spiral arms. This is of course required for the prediction of the spiral arm passages. In fact, the understanding of neither has reached a consensus.

Claims in the literature for a 2-armed and a 4-armed structure are abundant. There is even a claim for a combined 2+4 armed structure (Amaral and Lepine, 1997). Nevertheless, if one examines the $v-l$ maps of molecular gas, then it is hard to avoid the conclusion that *outside* the solar circle, there are 4 arms[1] (Blitz et al., 1983; Dame et al., 2001). Within the solar circle, however, things are far from clear. This is because $v-l$ maps become ambiguous for radii smaller than $R_\odot$, such that each arm is folded and appears twice ($R_\odot$ is the present distance of the Sun from the galactic center). Shaviv (2003a) has shown that if the outer 4 arms obey the simple density wave dispersion relation, such that they cannot exist beyond the 4:1 Lindblad resonances then two sets of arms should necessarily exist. In particular, the fact that these arms are apparent out to $r_{out} \approx 2R_\odot$ necessarily implies that their inner extent, the inner Lindblad radius, should roughly be at $R_\odot$. Thus, the set of arms internal to our radius should belong to a set other than the outer 4 arms.

The dynamics, i.e., the pattern speed of the arms, is even less understood than the geometry. A survey of the literature (Shaviv, 2003a) reveals that about half of the observational determinations of the relative pattern speed $\Omega_\odot - \Omega_p$ cluster around 9 to 13 km s^{-1}kpc^{-1}, while the other half are spread between -4 and 5 km s^{-1}kpc^{-1}. In fact, one analysis revealed that both $\Omega_\odot - \Omega_p = 5$ and 11.5 km s^{-1}kpc^{-1} fit the data equally well (Palous et al., 1977).

Interestingly, if spiral arms are a density wave (Lin and Shu, 1964), as is commonly believed (e.g., Binney and Tremaine, 1987), then the observations of the 4-armed spiral structure in HI outside the Galactic solar orbit (Blitz et al., 1983) severely constrain the pattern speed to satisfy $\Omega_\odot - \Omega_p \gtrsim 9.1 \pm 2.4$ km s^{-1}kpc^{-1}, since otherwise the four armed density wave would extend beyond the outer 4:1 Lindblad resonance (Shaviv, 2003a).

This conclusion provides theoretical justification for the smaller pattern speed. However, it does not explain why numerous different estimates for Ω_p exist. A resolution of this "mess" arises if we consider the possibility that at least two spiral sets exist, each one having a different pattern speed. Indeed, in a stellar cluster birth place analysis, which allows for this possibility, it was found that the Sagittarius-Carina arm appears to be a superposition of two arms (Naoz and Shaviv, 2004). One has a relative pattern speed of $\Omega_\odot - \Omega_{P,Carina,1} = 10.6^{+0.7}_{-0.5 sys} \pm$

[1] Actually, 3 are seen, but if a roughly symmetric set is assumed, then a forth arm should simply be located behind the galactic center.

1.6_{stat} km s^{-1}kpc^{-1} and appears also in the Perseus arm external to the solar orbit. The second set is nearly co-rotating with the solar system, with $\Omega_\odot - \Omega_{P,Carina,2} = -2.7^{+0.4}_{-0.5sys} \pm 1.3_{stat}$ km s^{-1}kpc^{-1}. The Perseus arm may too be harboring a second set. The Orion "armlet" where the solar system now resides (and which is located in between the Perseus and Sagittarius-Carina arms), appears too to be nearly co-rotating with us, with $\Omega_\odot - \Omega_{p,Orion} = -1.8^{+0.2}_{-0.3sys} \pm 0.7_{stat}$ km s^{-1}kpc^{-1}.

For comparison, a combined average of the 7 previous measurements of the 9 to 13 km s^{-1}kpc^{-1} range, which appears to be an established fact for both the Perseus and Sagittarius-Carina arms, gives $\Omega_\odot - \Omega_p = 11.1 \pm 1$ km s^{-1}kpc^{-1}. At reasonable certainly, however, a second set nearly co-rotating with the solar system exists as well.

The relative velocity between the solar system and the first set of spiral arms implies that every $\sim$ 150 Myr , the environment near the solar system will be that of a spiral arm. Namely, we will witness more frequent nearby supernovae, more cosmic rays, more molecular gas as well as other activity related to massive stars. We will show below that there is a clear independent record of the passages through the arms of the first set. On the other hand, passages through arms of the second set happen infrequently enough for them to have been reliably recorded.

To estimate the variable CRF expected while the solar system orbits the galaxy, one should construct a simple diffusion model which considers that the sources reside in the Galactic spiral arms. A straight forward possibility is to amend the basic CR diffusion models (e.g., Berezinskiĭ et al. (1990)) to include a source distribution located in the Galactic spiral arms. Namely, one can replace a homogeneous disk with an arm geometry as given for example by Taylor and Cordes (1993), and solve the time dependent diffusion problem as was done by Shaviv (2003a). Heuristically, such a model is sketched in Fig. 4.

The main model parameters include a CR diffusion coefficient, a halo half width (beyond which the CRs diffuse much more rapidly) and of course the angular velocity $\Omega_\odot - \Omega_p$ of the solar system *relative* to the spiral arm pattern speed. The latter number is obtained from the above observations, while typical diffusion parameters include a CR diffusion coefficient of $D = 10^{28}$cm^2/s, which is a typical value obtained in diffusion models for the CRs (Berezinskiĭ et al., 1990; Lisenfeld et al., 1996; Webber and Soutoul, 1998), or a halo half-width of 2 kpc, which again is a typical value obtained in diffusion models (Berezinskiĭ et al., 1990). Note that given a diffusion coefficient, there is a relatively narrow range of effective halo widths which yields a Be age consistent with observations (Lukasiak et al., 1994).

For the nominal values chosen in the diffusion model and the pattern speed found above, the expected CRF changes from about 25% of the

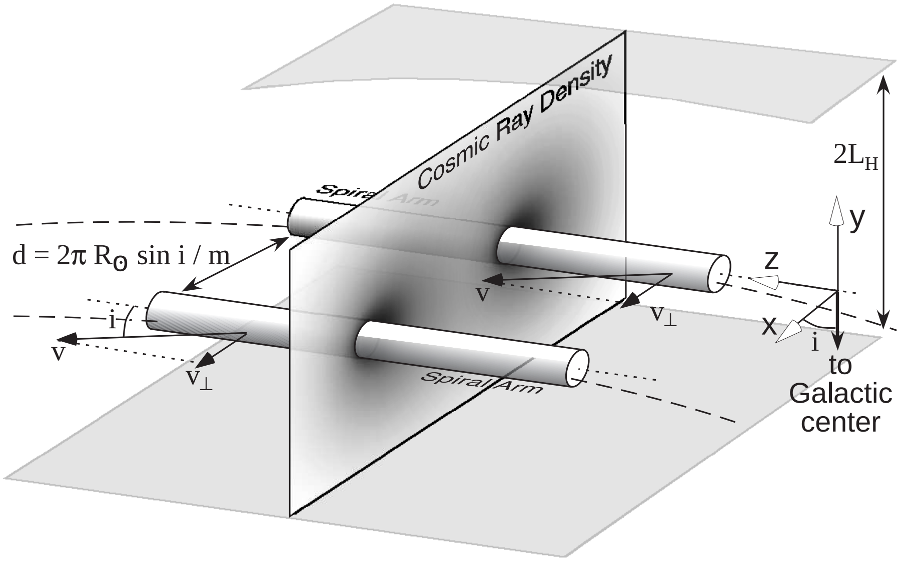

Figure 4. The components of the diffusion model constructed to estimate the Cosmic Ray flux variation. We assume for simplicity that the CR sources reside in Gaussian cross-sectioned spiral arms and that these are cylinders to first approximation. This is permissible since the pitch angle i of the spirals is small. The diffusion takes place in a slab of half width l_H, beyond which the diffusion coefficient is effectively infinite.

current day CRF to about 135%. Moreover, the average CRF obtained in units of today's CRF is 76%. This is consistent with measurements showing that the average CRF over the period 150-700 Myr BP, was about 28% lower than the current day CRF (Lavielle et al., 1999).

Interestingly, the temporal behavior is both skewed and lagging after the spiral arm passages (Fig. 5). The lag arises because the spiral arms are defined through the free electron distribution. However, the CRs are emitted from which on average occur roughly 15 Myr after the average ionizing photons are emitted. The skewness arises because it takes time for the CRs to diffuse after they are emitted. As a result, before the region of a given star reaches an arm, the CR density is low since no CRs were recently injected in that region and the sole flux is of CRs that succeed to diffuse to the region from large distances. After the region crosses the spiral arm, the CR density is larger since locally there was a recent injection of new CRs which only slowly disperse. This typically introduces a 10 Myr lag in the flux, totaling about 25 Myr with the delay. This lag is actually observed in the synchrotron emission from M51, which shows a peaked emission trailing the spiral arms (Longair, 1994).

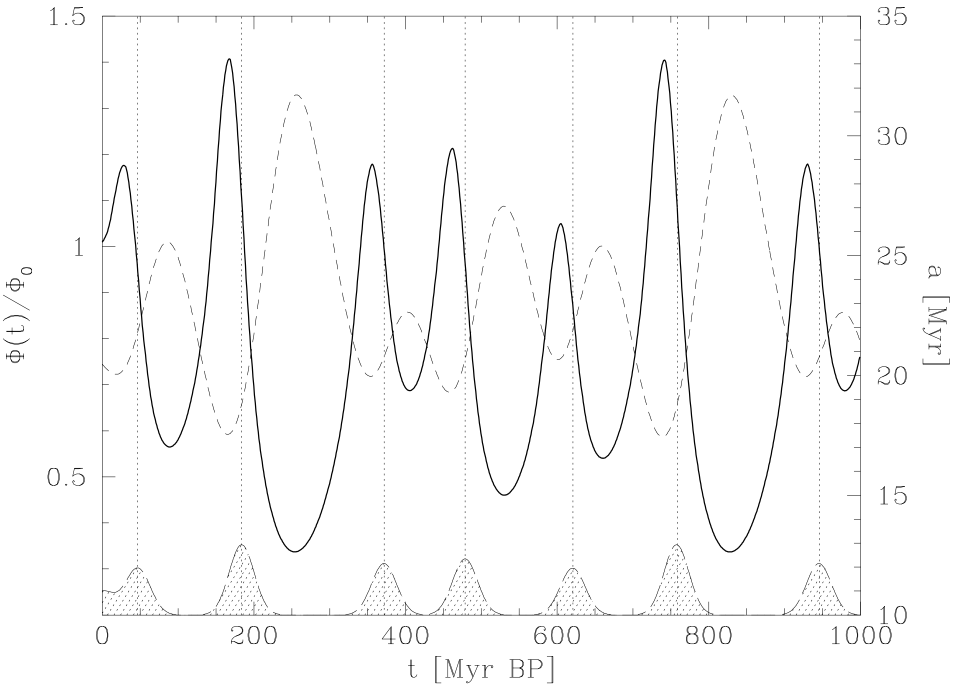

Figure 5. The cosmic-ray flux variability and age as a function of time for $D = 10^{28}\,\mathrm{cm}^2/\mathrm{s}$ and $l_H = 2\,\mathrm{kpc}$. The solid line is the cosmic-ray flux, the dashed line is the age of the cosmic rays as measured using the Be isotope ratio. The shaded regions at the bottom depict the location, relative amplitude (i.e., it is not normalized) and width of the spiral arms as defined through the free electron density in the Taylor and Cordes model. The peaks in the flux are lagging behind the spiral arm crosses due to the SN-HII lag. Moreover, the flux distribution is skewed towards later times.

6.3. Cosmic Ray Record in Iron Meteorites

Various small objects in the solar system, such as asteroids or cometary nuclei, break apart over time. Once the newly formed surfaces of the debris are exposed to cosmic rays, they begin to accumulate spallation products. Some of the products are stable and simply accumulate with time, while other products are radioactive and reach an equilibrium between the formation rate and their radioactive decay. Some of this debris reaches Earth as meteorites. Since chondrites (i.e., stony meteorites) generally "crumble" over $\lesssim 10^8$ yr, we have to resort to the rarer iron meteorites, which crumble over $\lesssim 10^9$ yr, if we wish to study the CRF exposure over longer time scales.

The cosmic ray exposure age is obtained using the ratio between the amount of the accumulating and the unstable nuclei. Basically, the exposure age is a measure of the integrated CRF, as obtained by the accumulating isotope, in units of the CRF "measured" using the unstable nucleus. Thus, the "normalization" flux depends on the average flux over the last decay time of the unstable isotope and not on the average flux over the whole exposure time. If the CRF is assumed constant, then the flux obtained using the radioactive isotope can be assumed to be the average flux over the life of the exposed surface. Only in such a case, can the integrated CRF be translated into a real age.

Already quite some time ago, various groups obtained that the exposure ages of iron meteorites based on "short" lived isotopes (e.g., ^{10}Be) are inconsistent with ages obtained using the long lived unstable isotope ^{40}K, with a half life of ~ 1 Gyr. In essence, the first set of methods normalize the exposure age to the flux over a few million years or less, while in the last method, the exposure age is normalized to the average flux over the life time of the meteorites. The inconsistency could be resolved only if one concludes that over the past few Myr, the CRF has been higher by about 28% than the long term average (Hampel and Schaeffer, 1979; Schaeffer et al., 1981; Aylmer et al., 1988; Lavielle et al., 1999).

More information on the CRF can be obtained if one makes further assumptions. Particularly, if one assumes that the parent bodies of iron meteorites tend to break apart at a constant rate (or at least at a rate which only has slow variations), then one can statistically derive the CRF history. This was done by Shaviv (2003a), using the entire set of ^{40}K dated iron meteorites. To reduce the probability that the breaking apart is real, i.e., that a single collision event resulted with a parent body braking apart into many meteorites, each two meteorites with a small exposure age difference (with $\Delta a \leq 5\times10^7$ yr), and with the same iron group classification, were replaced by a single effective meteor with the average exposure age.

If the CRF is variable, then the exposure age of meteorites will be distorted. Long periods during which the CRF was low, such that the exposure clock "ticked" slowly, will appear to contract into a short period in the exposure age time scale. This implies that the exposure ages of meteorites is expected to cluster around (exposure age) epochs during which the CRF was low, while there will be very few meteors in periods during which the CRF was high.

Over the past 1 Gyr recorded in iron meteorites, the largest variations are expected to arise from our passages through the galactic spiral arms. Thus, we expect to see cluster of ages every ~ 150 Myr. The actual exposure ages of meteorites are plotted in Fig. 6, where periodic clustering in the ages can be seen. This clustering is in agreement with

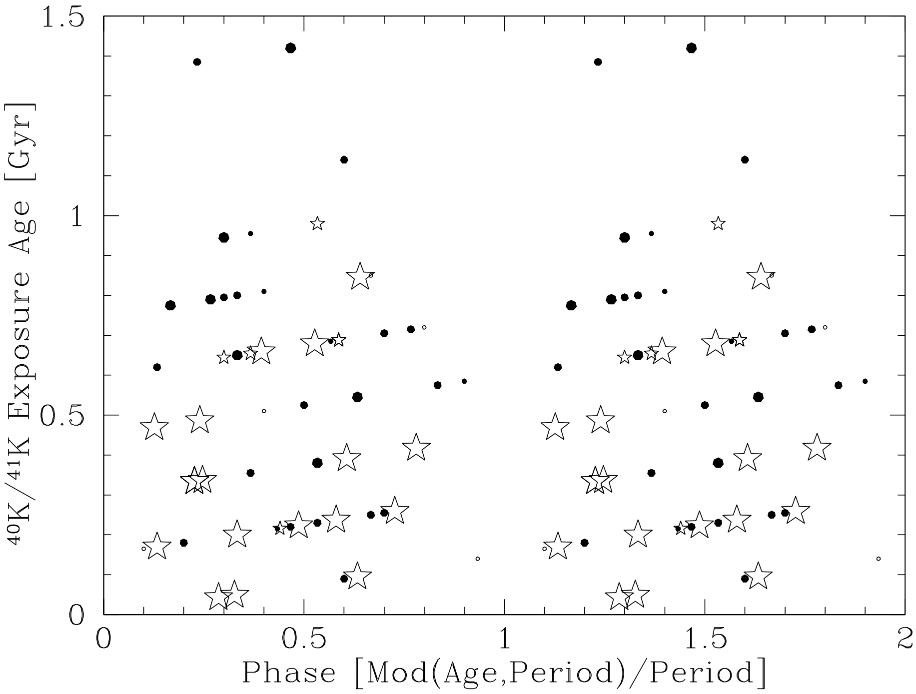

Figure 6. The exposure age of iron meteorites plotted as a function of their phase in a 147 Myr period. The dots are the ^{40}K exposure ages (larger dots have lower uncertainties), while the stars are ^{36}Cl based measurements. The K measurements do not suffer from the long term "distortion" arising from the difference between the short term (10 Myr) CRF average and the long term (1 Gyr) half life of K (Lavielle et al. 1999). However, they are intrinsically less accurate. To use the Cl data, we need to "correct" the exposure ages to take into account this difference. We do so using the result of Lavielle et al. (1999). Since the Cl data is more accurate, we use the Cl measurement when both K and Cl are available for a given meteorite. When less than 50 Myr separates several meteorites of the same iron group classification, we replace them with their average in order to discount for the possibility that one single parent body split into many meteorites. We plot two periods such that the overall periodicity will be even more pronounced. We see that meteorites avoid having exposure ages with given phases (corresponding to epochs with a high CRF). Using the Rayleigh Analysis, the probability of obtaining a signal with such a large statistical significance as a fluke from random Poisson events, with *any* period between 50 and 500 Myr, is less than 0.5%. The actual periodicity found is 147 ± 6 Myr, consistent with both the astronomical and geological data.

the expected variations in the cosmic ray flux. Namely, iron meteorites recorded our passages through the galactic spiral arms.

Interestingly, this record of past cosmic ray flux variations and the determination of the galactic spiral arm pattern speed is different in its nature from the astronomical determinations of the pattern speed.

This is because the astronomical determinations assume that the Sun remained in the same galactic orbit it currently occupies. The meteoritic measurement is "Lagrangian". It is the measurement relative to a moving particle, the heliosphere, which could have had small variations in its orbital parameters. In fact, because of the larger solar metalicity than the solar environment, the solar system is more likely to have migrated outwards than inwards. This radial diffusion gives an error and a bias when comparing the effective, i.e., "Lagrangian" measured $\tilde{\Omega}_p$, to the "Eulerian" measurements of the pattern speed:

$$\tilde{\Omega}_p - \Omega_p = 0.5 \pm 1.5\,\mathrm{km\ s^{-1}kpc^{-1}} \qquad (6)$$

Taking this into consideration, the observed meteoritic periodicity, with $P = 147 \pm 6$ Myr , implies that $\Omega_\odot - \Omega_p = 10.2 \pm 1.5_{sys} \pm 0.5_{stat}$, where the systematic error arises from possible diffusion of the solar orbital parameters. This result is consistent with the astronomically measured pattern speed of the first set of spiral arms.

7. Cosmic Ray Spectra inside and outside of Galactic Arms

In this section we want to follow the line of argumentations of the previous one, but shall approach the problem based on more fundamental physical considerations. The passage of the heliosphere through dense interstellar clouds has many interesting direct effects (see e.g. Yeghikyan and Fahr, 2003, 2004a, 2004b) and also influences via decreased modulation the near-Earth flux intensities of GCRs and of anomalous cosmic rays (ACRs) (see Scherer, 2000, Scherer et al., 2001b, Scherer et al., 2001a). Here we study the problem of GCR spectra which are to be expected inside and outside of galactic arms.

7.1. Accelerations at Shocks

Shocks, for a long time already, have been recognized as effective astrophysical sites for particle acceleration. This is because particles, which strongly interact with scattering centers embedded in astrophysical magnetohydrodynamic plasma flows can easily and effectively profit from strong velocity gradients occuring in these flows. Most effective in this respect are velocity gradients which are established at astrophysical MHD shocks. One may characterize the transition from upstream to downstream velocities at such a shock by a typical transition scale δ and by the extent H of the whole region over which the acceleration procedure is considered. Then the particle transport equation (1) given in section 5 needs to be solved for the case $\delta \ll r_g \ll \lambda \ll H$ with r_g and

λ being the gyroradius and the mean scattering length parallel to the background magnetic field, respectively. For a quasi one-dimensional shock, and for stationary conditions, at positions not too far from the shock it transforms into the following one-dimensional equation:

$$u\frac{\partial f}{\partial x} - \frac{\partial}{\partial x}\left[D_{\|}\cos\theta\frac{\partial f}{\partial x}\right] = \frac{1}{3}(u_{+} - u_{-})\delta(x)\frac{\partial f}{\partial \ln p} \tag{7}$$

where $\pm$ denote the plasma parameters upstream (+) and downstream (−) of the shock structure, respectively, u is the corresponding plasma bulk speed, and $D_{\|}$ the coefficient of spatial diffusion along the magnetic field.

Criteria, that in any case should be fulfilled by a formal solution of the above equation, are:

A: steadiness of differential particle density at the shock, i.e.:

$$f_{+}(p, x = 0) = f_{-}(p, x = 0)$$

B: Continuity of differential streaming at the shock, i.e.:

$$\left[uf - \kappa\frac{df}{dx}\right]_{+,0} = \left[uf - \kappa\frac{df}{dx}\right]_{-,0}$$

C: Continuity of differential energy flow at the shock, i.e.:

$$\left[-u\frac{\partial f}{\partial \ln p^3} - \kappa\frac{df}{dx}\right]_{+,0} = \left[-u\frac{\partial f}{\partial \ln p^3} - \kappa\frac{df}{dx}\right]_{-,0}$$

Far from the shock one may assume unmodulated spectra with asymptotic solutions given by $f_{\pm}(p, x \to \pm\infty) = f_{\pm\infty}(p)$. Downstream of the shock ($x \geq 0$) it is expected that f is independent on x, i.e.: $f = f_{+\infty}(p)$.

Upstream of the shock ($x \leq 0$), however, f must be expected to be modulated, i.e. given by:

$$f = f_{-\infty}(p) + (f_{+\infty}(p) - f_{-\infty}(p))\exp\left[u_{-}\int_0^x \frac{dx}{\kappa}\right] \tag{8}$$

The full solution for $f_{+\infty}(p)$ matching all the above requirements then is given by the following formal solution:

$$f_{+\infty}(p) = qp^{-q}\int_0^p f_{-\infty}(p')p'^{(q-1)}dp' \tag{9}$$

where the power index q is given by the expression: $q = 3s/(s-1)$ with the shock compression ratio s given by: $s = u_{-}/u_{+}$.

Given the spectral distribution far upstream of the shock in the form $f_{-\infty}(p) \sim p^{-\Gamma}$ with $\Gamma \leq q$ then Eq. (9) yields:

$$f_{+\infty}(p) \sim qp^{-q} \int_0^p p'^{-\Gamma} p'^{q-1} dp' = qp^{-q} \left(\frac{p^{q-\Gamma}}{q-\Gamma} \right) \Bigg|_0^p = \frac{q}{q-\Gamma} p^{-\Gamma} \quad (10)$$

Assuming, on the other hand, that $f_{-\infty}(p) \sim p^{-\Gamma}$, with $\Gamma = \Gamma_0 \leq q$ for $p \leq p_0$ only, and with $\Gamma \geq q$ for $p \geq p_0$, then Eq. (9) in contrast gives:

$$f_{+\infty}(p) \sim qp^{-q} \left[\int_o^{p_0} p'^{q-\Gamma_0-1} dp' + \int_{p_0}^{p} p'^{q-\Gamma-1} dp' \right] \quad (11)$$

with the solutions for

$$f_{+\infty}(p) \sim \begin{cases} \dfrac{q}{q-\Gamma_0} p^{-\Gamma_0} & ; \quad p \leq p_0 \\ qp^{-q} \left[\dfrac{1}{q-\Gamma_0} p_0^{q-\Gamma_0} + \dfrac{1}{q-\Gamma} \left| p^{q-\Gamma} - p_0^{q-\Gamma} \right| \right] & ; \quad p \geq p_0 \end{cases} \quad (12)$$

which finally evaluates to:

$$f_{+\infty}(p) \sim \frac{q}{\Gamma - q} \left(\frac{p}{p_0} \right)^{-q} \left[\frac{\Gamma - q}{q - \Gamma_0 p_0^{-\Gamma_0} + p_0^{-\Gamma} + p_0}^{-\Gamma} \left(\frac{p}{p_0} \right)^{-\Gamma} \right]$$

and simply is of the twin-power law form:

$$f_{+\infty}(p) = A \left(\frac{p}{p_0} \right)^{-q} + B \left(\frac{p}{p_0} \right)^{-\Gamma} \quad (13)$$

One should keep in mind that here $\Gamma \geq q$ was assumed, which makes it evident that the first term clearly is the leading term for $p \gg p_0$ meaning that here one obtains a simple mono-power law:

$$f_{+\infty}(p \geq p_0) \sim \frac{q}{\Gamma - q} \left(\frac{p}{p_0} \right)^{-q} \left[\frac{\Gamma - q}{q - \Gamma_0} p_0^{-\Gamma_0} + p_0^{-\Gamma} \right] \sim \left(\frac{p}{p_0} \right)^{-q} \quad (14)$$

In the following this solution for the shock-related GCR distribution is to be applied to giant astrophysical shock waves like supernova blast waves sporadically running out from collapsing stars.

7.2. Self-similar Blast Waves

Supernova shock waves are considered in terms of spherical blast waves under the assumption of self-similarity (see Sedov, 1946). For the purpose of justifying this concept the outside pressure must be expected to be equal to $P_0 \simeq 0$. The consideration starts with the adiabatic

Sedov phase which implies the initial explosion-induced SN energy release E_B is converted into kinetic energy of the dynamics of the mass-accumulating SN shell. The problem in this adiabatic phase is fully determined by two quantities, namely E_B and the mass density ρ_0 of the unperturbed, pristine interstellar medium.

In a spherically symmetric problem all hydrodynamic functions only are functions of the distance r from the SN explosion center and of the time t elapsed since the explosion event, and all solutions should allow a self-similar scaling by $r(t) = \alpha(t)r(t_0)$. Since the quantity $\Psi = E_B/\rho_0$ has the dimension $[cm^5 \sec^{-2}]$, one can thus introduce the following self-similar normalization:

$$\xi = r/x(t) = r \left(\frac{\rho_0}{E_B t^2}\right)^{1/5} \tag{15}$$

The special point R_s of the shock front location with the normalized value ξ_s as function of time hence behaves like:

$$R_s(t) = \xi_s \left(\frac{E_B}{\rho_0}\right)^{1/5} t^{2/5} \tag{16}$$

As consequence from the above relation one easily derives the expansion velocity of the SN shock front by:

$$u_- = \frac{dR_s}{dt} = \frac{2}{5}\frac{R_s}{t} = \xi_s \frac{2}{5}\left(\frac{E_B}{\rho_0}\right)^{1/5} t^{-3/5} \tag{17}$$

The upstream Mach number of the SN shock is permanently decreasing with time after the explosion event according to:

$$M(t) = M_0 \left(\frac{t}{t_0}\right)^{\eta-1} = \frac{\eta R_0}{t_0 C_0}\left(\frac{t}{t_0}\right)^{\eta-1} \tag{18}$$

where $\eta = 2/5$ in a homogeneous low-pressure medium and M_0 and C_0 are the initial SN shock Mach number and the sound velocity of the unperturbed interstellar medium. Roughly it can be estimated that the adiabatic Sedov expansion starts, when the initial SN explosion energy is converted into kinetic energy of the shell matter, i.e. when $(4\pi/3)\rho_0 R_{s0}^3 C^2 M_0^2 = E_{SN}$ holds. This yields the time t_0 after the explosive event $t = 0$ when the adiabatic phase of the shock expansion starts as related to the initial shock distance by:

$$R_{s0} = 13.5 \left(\frac{mE_{SN}}{\rho_0}\right)^{1/5} t_0^{2/5}\,[pc] \tag{19}$$

7.3. Galactic Cosmic Ray Spectra

Based on a stochastic occurrence of SN events within the spiral arm regions it may be necessary, before an inner-arm particle spectrum can be estimated, to inspect various important time periods characterizing the course of relevant physical processes, like the SN-occurrence period, the SN shock passage time to the borders of the arm, the mean capture time of energetic particles within the arm region or the diffusion time, and the average particle acceleration time near the expanding SN shock surface.

Starting from theoretical solutions of the cosmic ray transport equation as presented by Axford (1981), O'C Drury (1983) or Malkov and O'C Drury (2001), where, as described above, a one-dimensional shock geometry is assumed, one finds the following upstream solution $f_-(x,p)$ for the spectrum of shock-accelerated energetic particles:

$$f_-(x,p) = \frac{C}{A}\left(\frac{p}{p_0}\right)^{-q}\exp\left(\frac{u_-}{\kappa(p)}x\right) \tag{20}$$

Here C is a constant and the coordinate x denoting the linear distance from the planar shock surface is counted negative in the direction upstream of the shock. The speed by which the shock passes over the galactic material amounts to u_- and may be of the order of 1000 to 2500 km/s. Downstream of the shock it is assumed that the spatial derivative of f_+ vanishes, i.e. $\partial f_+/\partial x \simeq 0$, meaning that $f_+ \simeq const.$

The absolute value of the distribution function f_- has not yet been specified. Thus the value C needs to be fixed such as to fulfill flux continuity relations at the shock expressing the fact that the total outflow Φ of the GCR fluxes to the left and to the right side of the SN shock (i.e. the sum of the upstream and downstream streamings, respectively, e.g. see Jokipii (1971), Gleeson and Axford (1968) has to be identical with the flux of particles above the injection threshold $p = p_0$ which are convected from the upstream side into the shock and can serve as the seed of SN-accelerated GCRs. This requirement expresses in the form (see Fahr, 1990):

$$\begin{aligned}&\int\left[\frac{1}{3}f_-u_- - \frac{1}{3}u_-p\frac{\partial f_-}{\partial p} - \kappa_-\frac{\partial f_-}{\partial x}\right]p^2dp\\ +&\int\left[\frac{1}{3}f_+u_+ - \frac{1}{3}u_+p\frac{\partial f_+}{\partial p} - \kappa_+\frac{\partial f_+}{\partial x}\right]p^2dp \;=\; \varepsilon(p_0)u_+n_+\end{aligned} \tag{21}$$

where $\varepsilon(p_0)n_+$ is the number of particles with momenta $p\mu \leq -p_0$ upstream of the shock which can serve as seed of the GCRs. Evaluating the above equation with the expression for $f_\pm$ given in Eq. (20)

then, when reminding that at $x = 0$ the upstream and downstream distribution functions are identical, i.e. $f_- = f_+$ leads to:

$$\int u_- f_- \left[\frac{1}{3}(1+\frac{1}{s})\frac{4s-1}{s-1} - 1\right] p^2 dp = \varepsilon(p_0) u_- n_0 \tag{22}$$

The above expression can finally be evaluated with the distribution function given by Eq. (20):

$$\frac{s^2+6s-1}{3(s^2-s)} \int f_0 p^2 dp = \frac{s^2+6s-1}{3(s^2-s)} C p_0^3 \int_1^\infty x^{-\frac{2+s}{s-1}} dx = \varepsilon(p_0) n_0 \tag{23}$$

which delivers for the quantity C:

$$C = \frac{3s\varepsilon(p_0)n_0}{(3s^2+2s-3)p_0^3} \tag{24}$$

As a surprise the above result does not anymore show the explicit dependence of C on the upstream plasma velocity u_-. This dependence, however, implicitly is hidden in the value p_0 for the critical momentum of the particle injection into the shock acceleration. In order to inject particles into the diffusive acceleration process, it is necessary that these particles have the dynamic virtue due to which they are not simply convected over the electric potential wall of the SN shock but become reflected at this wall at least for the first time (see e.g. Chalov and Fahr, 1995, Chalov and Fahr, 2000). For this to happen the following relation simply needs to be fulfilled:

$$\frac{1}{2}m(u_- - \frac{p_0}{m})^2 \leq \frac{1}{2}m(u_-^2 - u_+^2) \;\; \Rightarrow \;\; p_0 \geq m u_-(1 - \sqrt{1-\frac{1}{s^2}}) \tag{25}$$

The percentage of particles with momenta $p\mu \leq -p_0$ in the shifted Maxwellian distribution function, describing particles comoving with the upstream plasma flow, is then given by;

$$\epsilon\,(p_0) = \frac{1}{\pi^{1/2}} \int_{x_0}^\infty \exp(-x^2)dx = 1 - \frac{1}{\sqrt{\pi}}\mathrm{erf}(x_0) = 1 - \frac{1}{\sqrt{\pi}}\mathrm{erf}(\kappa(s)M_s) \tag{26}$$

where $x_0^2 = p_0^2/2KT_0m = mu_-^2 g^2(s)/2KT_0 = \kappa^2(s)M_s^2$. Here the following notations have been used: $g(s) = (1-(1-s^{-1})^{-1/2})$ with the Mach number of the upstream plasma defined by $M_s^2 = mu_-^2/\gamma KT_0$.

This finally delivers for C the expression:

$$C = 3sn_0 \frac{1-\pi^{-1/2}\mathrm{erf}(\kappa(s)M_s)}{(3s^2+2s-3)p_0^3} \tag{27}$$

This result expresses the fact that the absolute value of f_- given by C is determined by the upstream flow velocity u_-, the upstream

Mach number M_s, the compression ratio s as function of M_s and the upstream plasma density n_0 which is known to be greater by a factor of about 10 in the spiral arms compared to inter-arm regions.

To describe the evolution in time and space of spectra for GCRs originating at SN shock waves one furthermore needs to know something about the evolution of the SN shock at its propagation in circumstellar space. Relying on the Sedov solution for the SN blast wave evolution at its propagation into the ambient interstellar medium one can describe the propagation velocity $U_1 = U_1(t)$ as a function of time by the following relation (see Krymskii, Krymskii (1977b, 1977a)):

$$U_1(t) = \frac{2}{5}(\frac{2E_{SN}}{\rho_1})^{1/5}t^{-3/5} \tag{28}$$

where E_{SN} denotes the total energy released by the SN explosion, and ρ_1 is the ambient interstellar gas mass density ahead of the propagating shock.

Keeping in mind that the compression ratio s as given by the Rankine-Hugoniot relations writes:

$$s(t) = \frac{(\gamma+1)M_1^2(t)}{(\gamma-1)M_1^2(t)+2} \tag{29}$$

where $M_1(t)$ denotes the upstream Mach number depending on SN shock evolution time t and is given by:

$$M_1^2(t) = \frac{\rho_1 U_1^2(t)}{\gamma P_1} = \frac{4}{25}\frac{\rho_1^{3/5}}{P_1}(2E_{SN})^{2/5}t^{-6/5} \tag{30}$$

one can predict the temporal change ds/dt of the SN shock compression ratio. It then clearly turns out that the typical period τ_s by which the strength of the SN shock changes in time is large with respect to $\tau_a(p)$, i.e. that:

$$\tau_s = -\frac{s}{ds/dt} \geq \tau_a(p) = \frac{6s}{s-1}\frac{\kappa_1}{U_1^2} \tag{31}$$

7.4. The Average GCR Spectrum inside Galactic Arms

To calculate the average GCR spectrum for a casually placed space point within the galactic arm regions we shall assume that such a point is at a random distance with respect to casually occuring SN shock fronts, the latter being true as consequence of stochastic occurrences of SN explosions at random places in the arms. We shall denote the casual x-axis position of an arbitrary space point with respect to the center of a stochastic SN explosion by X. At time t, after the explosion took place, the SN shock front has an actual x-axis position of $R_x(t) = \int_0^t U_1(t')dt'$ and thus the average GCR spectrum should be obtainable by the following expression:

$$\overline{f(p)} = \frac{1}{X_{\max} t_{\max}} \int_{X_{\min}}^{X_{\max}} dX \int_{t_{\min}}^{t_{\max}} dt' C(t') \left[\left(\frac{p}{p_0} \right)^{-q(t')} + B' \left(\frac{p}{p_0} \right)^{-\Gamma} \right] \times \exp \left[- \frac{U_1(X - R_x(t'))}{\kappa(p)} H(R_x(t') - X) \right] \quad (32)$$

Here the function $H(\lambda)$ is the well known step function with $H(\lambda) = 0$ for positive values of λ.

The quantity $X_{\max} \simeq R_a$ is to determine the maximum distance which a stochastically placed detector point may have to the SN explosion center. This maximum distance, for physical reasons and in order to make the expression (32) statistically relevant, should be selected such that within the counted arm volume $V_{\max} = \pi R_a^2 X_{\max}$ during a time $t_{\max}$ one obtains the probability "1" for a next SN explosion to occur. With an SN- explosion rate ς per unit of time and volume within the arm region one then finds $X_{\max} = \left[\pi R_a^2 \varsigma t_{\max} \right]^{-1}$ The quantity $t_{\max}$ is taken as the time after SN explosion till which the evolving SN shock front has upstream Mach numbers larger than or equal to 1 and thus accelerates GCRs. One can conclude that diffusive acceleration of GCRs can continue till the propagation speed $U_1(t)$ of the SN shock front falls below the local Alfvén speed v_{A1} impeding the pile-up of MHD turbulences which act as scattering centers for GCRs bouncing to and fro through the shock. From Eq. (30) one thus derives:

$$t_{\max} \simeq \left(\frac{2E_{SN}}{\rho_1} \right)^{1/3} \left(\frac{5}{2} v_{A1} \right)^{-5/3} \quad (33)$$

which for values given by Hartquist and Morfill (1983) (i.e. $\mathrm{E}_{SN} = 10^{51} erg$; $\rho_1/m = 10 cm^{-3}$; $v_{A1=} 10^6 cm/s$) evaluates to $t_{\max} \simeq 6 Myr$. The distance $X_{\min}$ denotes the SN shock distance from the SN explosion center at time $t_{\min}$ after explosion given by:

$$t_{\min} \simeq \left(\frac{2E_{SN}}{\rho_1} \right)^{1/3} \left(\frac{5}{2} U_{1,\max} \right)^{-5/3} \quad (34)$$

where $U_{1,\max}$ is the maximum SN shock speed just after shock formation. For estimate purposes we may assume here that the following connection can be assumed $\frac{4\pi}{3} X_{\min}^3 \rho_1 U_{1,\max}^2 = E_{SN}$ and that a maximum shock speed of $U_{1,\max} = 3500 km/s$ can be adopted at the beginning of the Sedov phase.

7.5. Escape into the Interarm Region

Assuming that the expression for $f(p)$ given by the Eq. (32) is valid for all space points located within a cylindrical tube along the central axis of the spiral arm, i.e. $f(p)$ represents an axially and temporally averaged GCR spectrum for all near axis points within a galactic arm, and adopting an arm-parallel magnetic field, then in addition to the very efficient spatial diffusion parallel to the magnetic field a much less efficient diffusion perpendicular to the field operates everywhere which eventually lets GCR particles escape into the interarm region. We describe this diffusion with respect to the cylindric coordinate r as a source-free, time-independent diffusion ($\nabla \cdot (\overleftrightarrow{\kappa}\ f) = 0$) which gives in cylindrical coordinates

$$\left(r\kappa_{\perp} \frac{\partial f}{\partial r} \right) = \text{const} = (r\kappa_{\perp} \frac{\partial f}{\partial r})_0 = -\pi r_0^2 \frac{f_0}{\tau_e} \tag{35}$$

where r_0 is the radius of an inner tube within which the distribution function f_0 prevails, and where τ_e is the period of GCR escape into the interarm region. Then the solution for $f = f(r)$ is obtained from the expression:

$$f(r,p) = f(r_0,p) + \int_{r_0}^{r} \frac{\text{const}}{r'\kappa_{\perp}} dr' = f(r_0,p) \left(-\frac{\pi r_0^2}{\tau_e \kappa_{\perp}} \ln(\frac{r}{r_0}) \right) \tag{36}$$

At the border $r = R_a$ of the arm to the interarm region the identity at both sides of both GCR flux and the spectral intensity is required yielding the following two relations:

$$R_a \kappa_{i\perp} \left| \frac{\partial f_i}{\partial r} \right| = R_a \kappa_{a\perp} \left| \frac{\partial f_a}{\partial r} \right| \quad \text{and} \quad |f_i|_{R_a} = |f_a|_{R_a} \tag{37}$$

where $\kappa_{a\perp}$ and $\kappa_{i\perp}$ denote spatial diffusion coefficients in the arm and the interarm region, respectively. With these requirements one obtains the distribution function $f_i(r,p)$ in the interarm region as given in the form:

$$f_i(r,p) = f(r_0,p) \left[1 - \frac{\pi r_0^2}{\tau_e} \left(\frac{1}{\kappa_{a\perp}} \ln\left(\frac{R_a}{r_0}\right) + \frac{1}{\kappa_{i\perp}} \ln\left(\frac{r}{R_a}\right) \right) \right] \tag{38}$$

To achieve consistency with the assumptions made in the derivations above one should be able to justify a time-independence of the GCR distribution function, i.e. the fact that $\partial f / \partial t = 0$ is assumed. From a simplified phase-space transport equation one can then derive the requirement that time-independence of f is achieved, if the average galactic arm SN occurrence period τ_{SN} and the escape period τ_e are related by:

$$\tau_e = \frac{\tau_{SN}}{(1 - \frac{1}{p^3} q \chi n_1 \tau_{SN})} = \frac{\tau_{SN}}{[1 + 4(\frac{p_{i0}}{p})^3 \frac{\tau_{SN}}{\tau_{i0}}]} \tag{39}$$

where $q = 3s/(s-1)$ is the power index of the GCR spectrum and where the momentum loss of GCR particles due to gas ionisations has been assumed as $\dot{p}_i \simeq -\chi n_1 p^{-2}$, for details see Lerche and Schlickeiser, Lerche and Schlickeiser, Lerche and Schlickeiser (1982a, 1982c, 1982b). The second identity follows with $q \simeq 4$ and $n_1 \simeq 10 cm^{-3}$ and $\tau_{i0} = \tau_i(p_{i0}) = 10^8 s$ and $p_{i0} = p(100 MeV)$. The standard period τ_{SN} might be quantified by: $\tau_{SN} \simeq 10^{10} s$.

Now we try to obtain a reasonably well supported value for the dimension r_0 within the above derived calculation. Going back to Eq. (35) one first finds:

$$\left(r\kappa_\perp \frac{\partial f}{\partial r} \right)_{R_a} \simeq R_a \kappa_\perp \frac{f_0 - f_{R_a}}{R_a} = \pi r_0^2 \frac{f_0}{\tau_e} \tag{40}$$

from which with the help of Eq. (36) one furthermore derives

$$\pi r_0^2 = \kappa_\perp \tau_e \frac{f_0 - f_{R_a}}{f_0} = \kappa_\perp \tau_e \left[1 - 1 + \frac{\pi r_0^2}{\tau_e \kappa_\perp} \ln(\frac{R_a}{r_0}) \right] \tag{41}$$

simply requiring $r_0 = R_a/\exp(1)$.

With help of Eq. (39) one now can use Eq. (38) to display the spectral flux intensity of GCRs as function of the off axis-distance r from the axis of the galactic arms.

Based on formula (38) one can estimate the variation of the galactic cosmic ray spectra along the trajectory of the Sun, in particular inside and outside galactic spiral arms. In a first step, we compute an arm spectrum from the expression

$$j_a(r_0, p) = j(r_\odot, p) \left[1 - \frac{\pi r_0^2}{\tau_e} \left(\frac{1}{\kappa_{a\perp}} \ln\left(\frac{R_a}{r_0}\right) + \frac{1}{\kappa_{i\perp}} \ln\left(\frac{r_\odot}{R_a}\right) \right) \right]^{-1} \tag{42}$$

assuming that the present-day local interstellar spectrum derived from observations can be represented as (Reinecke et al., 1993)

$$j(r_\odot, p) = p^2 f(r_\odot, p) = \frac{12,41\,\mathrm{v}/c}{(E_k + 0.5\,E_0)^{2.6}}\ \mathrm{part./m^2/s/srad/MeV} \tag{43}$$

where v is the speed of a proton with kinetic energy E_k in GeV and E_0 is the proton rest energy in GeV.

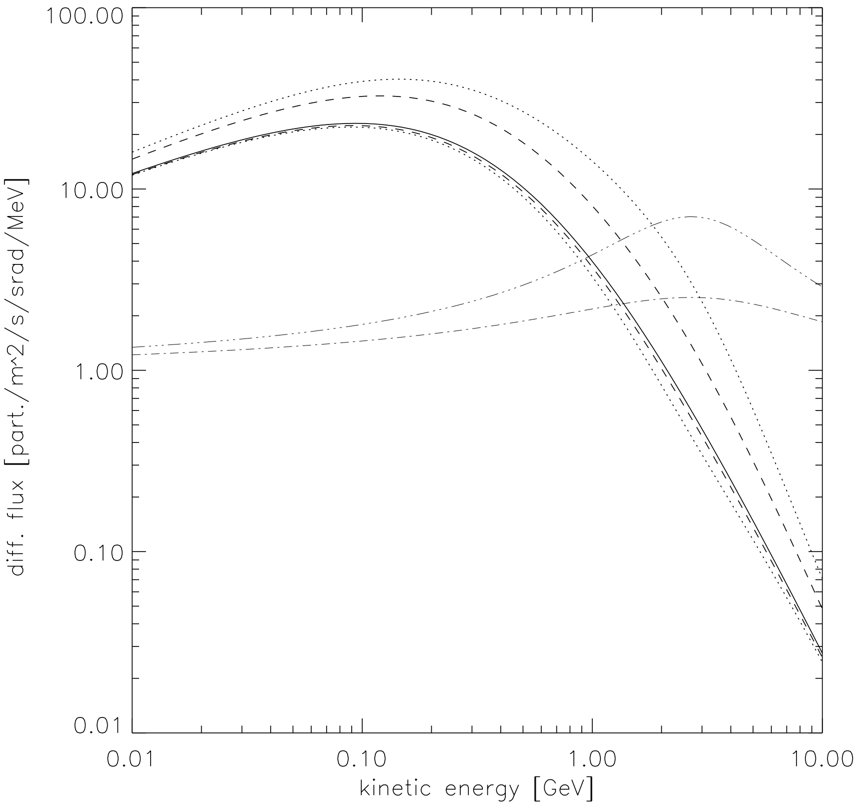

Figure 7. Galactic cosmic ray spectra inside and outside galactic spiral arms: the solid line gives the present-day spectrum according to Reinecke et al. (1993), the upper dashed line is the arm spectrum computed from formula 45 assuming that the Sun is located 1 kpc outside the next main spiral arm, the lower dashed line shows the spectrum in the middle between two arms, and the dash-dotted line is the ratio of the arm to the interarm spectrum for a spiral arm radius of R_a=0.35 kpc, r_0=0.1 kpc, $\kappa_{i\perp} = 3 \cdot 10^{28}\,\mathrm{cm}^2/\mathrm{s}$, and $\kappa_{a\perp} = 0.1\kappa_{i,\perp}$, and $\tau_e = 7.1 \cdot 10^6$ a. The other lines give the corresponding spectra for a 20% wider spiral arm.

For the present location of the Sun relative the next main spiral arm with radius R_a=0.35 kpc we use $r_\odot$=1 kpc. Interpreting the interarm diffusion coefficient as that one considered in galactic propagation models we select a typical value of $\kappa_{i\perp} = 3 \cdot 10^{28}\,\mathrm{cm}^2/\mathrm{s}$. For the diffusion coefficient inside an arm we adopt $\kappa_{a\perp} = 0.1\kappa_{i\perp}$ corresponding to about three times higher turbulence level inside an arm than outside.

As we are computing spectral rather than just total flux variations, we have to take into account the dependence of the diffusion on rigidity P. We use

$$\kappa_{i\perp} = 1.5 \left(\frac{P}{P_0}\right)^{\xi} \quad ; \quad \xi = \frac{aP + bP_0}{P + P_0} \tag{44}$$

which avoids the spectral break of the expression given by Büsching et al. (2005) and approximate the latter with the values $a = 0.51$ and $b = -0.39$.

Because the time scale τ_e resulting from Eq. (41) is even shorter than τ_{SN}, its use in Eq. (38) would not be consistent with the diffusion time scale $R_a^2/\kappa_{a\perp} = 7.1 \cdot 10^6$ yr, which we therefore use instead of τ_e.

The resulting arm spectrum is shown as the upper dashed line in Fig. 7. From the latter we subsequently computed the spectrum approximately in the middle between to spiral arm from

$$j_i(r_m, p) = j(r_a, p)\left[1 - \frac{\pi r_0^2}{\tau_e}\left(\frac{1}{\kappa_{a\perp}}\ln\left(\frac{R_a}{r_0}\right) + \frac{1}{\kappa_{i\perp}}\ln\left(\frac{r_m}{R_a}\right)\right)\right] \tag{45}$$

with r_m=3 kpc resulting in the lower dashed curve in the figure. The dotted lines are at the same locations inside and outside an spiral arm but for a 20% greater R_a. That there is not much variation of the spectra in the interarm region is consistent with the rather high diffusion coefficient which cannot result in strong modulation over a few kpc.

Obviously, we obtain the expected variation of factors two to seven depending on parameters, compare with the chapter 6. In our approach, however, this variation is computed as a function of kinetic energy, see the dash-dotted lines in the Fig. 7. Interestingly, the maximum variation occurs at around 3 GeV , which means that also the modulated spectra at Earth should exhibit a variation. This modulation of the interstellar spectra within the heliosphere is the subject of the following part, while the interactions of CRs in the atmosphere are described in part VI.

Part IV

Heliospheric Modulation

8. Propagation of Cosmic Rays inside the Heliosphere

8.1. Solar Activity: 11-year and 22-year Cycles in Cosmic Rays

In the heliosphere three main populations of cosmic rays, defined as charged particles with energies larger than 1 MeV, are found. They are: (1) Galactic cosmic rays, mainly protons and some fully ionized atoms, with a spectral peak for protons at about 2 GeV at Earth. (2) The anomalous component, which is accelerated at the solar wind termination shock after entering the heliosphere as neutral atoms that got singly ionized. For a review of these aspects, see Fichtner (2001). (3) The third population is particles of mainly solar origin, which may get additionally accelerated by interplanetary shocks. A prominent strong electron source of up to 50 MeV is the Jovian magnetosphere, with the Saturnian magnetosphere much less pronounced.

We are protected again CRs by three well-known space "frontiers", the first one arguably the less appreciated of the three: (1) The solar wind and the accompanying relatively turbulent heliospheric magnetic field extending to distances of more than 500 AU in the equatorial plane and to more than 250 AU in the polar plane. The heliospheric volume may oscillate significantly with time depending on solar activity, and where the solar system is located in the galaxy, see part V. (2) The Earth's magnetic field, which is not at all uniform, e.g. large changes in the Earth's magnetic field are presently occurring over southern Africa. This means that significant changes in the cut-off rigidity at a given position occur. These changes seem sufficiently large over the past 400 years that the change in CRF impacting the Earth may approximate the relative change in flux over a solar cycle (Shea and Smart, 2004). The magnetosphere also withstands all the space weather changes that the Sun produces, and can reverse its magnetic polarity on the long-term. (3) The atmosphere with all its complex physics and chemistry. The cosmic ray intensity decreases exponentially with increasing atmospheric pressure. The Sun contributes significantly to atmospheric changes through, e.g. variations in solar irradiance, and variations in the Earth's orbit (Milankovitch cycles).

The dominant and the most important variability time scale related to solar activity is the 11-year cycle. This quasi-periodicity is convincingly reflected in the records of sunspots since the early 1600's and in the GCR intensity observed at ground and sea level since the 1950's when neutron monitors (NMs) were widely deployed, especially as part of the International Geophysical Year (IGY). These monitors have been remarkably reliable, with good statistics, over five full 11-year

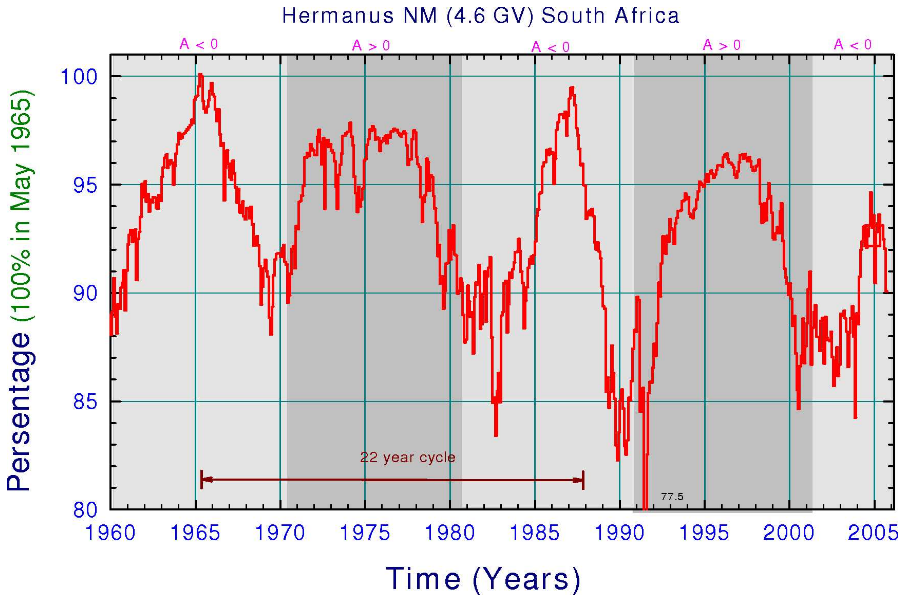

Figure 8. Cosmic ray flux measured by the Hermanus NM (at sea-level with a cut-off rigidity of 4.6 GV) in South Africa. Note the 11-year and 22-year cycles.

cycles. An example of this 11-year cosmic ray cycle is shown in Fig. 8, which is the flux measured by the Hermanus NM in South Africa. The intensity is corrected for atmospheric pressure to get rid of seasonal and daily variations. This means that atmospheric pressure must also be measured very accurately at every NM station.

In Fig. 8 another important cycle, the 22-year cycle, is shown. This cycle is directly related to the reversal of the solar magnetic field during each period of extreme solar activity and is revealed in CR modulation as the alternating flat and sharp profiles of consecutive solar minimum modulation epochs when the CR intensity becomes a maximum (minimum modulation). The causes and the physics of the 11-year and 22-year cycles will be discussed below, but first a short discussion in the context of this paper will be given about other variabilities related to CRs in the heliosphere.

Short periodicities are evident in NM and other cosmic ray data, e.g. the 25–27-day variation owing to the rotational Sun, and the daily variation owing to the Earth's rotation. These variations seldom have magnitudes of more than 1% with respect to the previous quite times. The well-studied corotating effect is caused mainly by interaction regions (CIRs) created when a faster solar wind overtakes a previously released slow solar wind. They usually merge as they propagate outwards to form various types of interaction regions, the largest ones are known as global merged interaction regions - GMIRs (Burlaga et al., 1993). Such a GMIR caused the very large cosmic ray decrease in 1991, shown in Fig. 8. They are related to what happened to the solar magnetic field at some earlier stage and are linked to coronal mass ejections (CMEs), which are always prominent with increased solar activity but dissipate completely during solar minimum. They propagate far outward in the heliosphere with the solar wind speed, even beyond the solar wind termination shock around 90–95 AU. Although CIRs may be spread over a large region in azimuthal angle, they cannot cause long-term periodicities on the scale (amplitude) of the 11 year cycle. An isolated GMIR may cause a decrease similar in magnitude than the 11-year cycle but it usually lasts only several months to about a year. A series or train of GMIRs, on the other hand, may contribute significantly to modulation during periods of increased solar activity, in the form of large discrete steps, increasing the overall amplitude of the 11-year cycle (le Roux and Potgieter, 1995). The Sun also occasionally accelerates ions to high energies but with a highly temporal and anisotropic nature, which are known as solar energetic particle (SEP) events.

The 11-year and 22-year cycles are modulated by longer term variability on time scales from decades to centuries, perhaps even longer. There are indications of periods of 50–65 years and 90–130 years, also for a periodicity of about 220 and 600 years. It is not yet clear whether these variabilities should be considered "perturbations", stochastic in nature or truly time-structured to be figured as superpositions of several periodic processes. Cases of strong "perturbations" of the consecutive 11-year cycles are the "grand minima" in solar activity, with the prime example the Maunder Minimum (1645–1715) when sunspots almost completely disappeared. Assuming the solar magnetic field to have vanished or without any reversals during the Maunder minimum would be an oversimplification as some studies already seem to illustrate (Caballero-Lopez et al., 2004; Scherer and Fichtner, 2004). The heliospheric modulation of CRs could have continued during this period but much less pronounced (with a small amplitude). It is reasonable to infer that less CMEs, for example, occurred so that the total flux of CRs at Earth then should have been higher than afterwards. However, to consider the high levels of sunspot activity for the last few 11-year cycles as unprecedented is still inconclusive. From Fig. 8 follows that the maximum levels of CRs seem to gradually decrease.

The CRF is also not expected to be constant along the trajectory of the solar system in the galaxy. Interstellar conditions, even locally, should therefore differ significantly over long time-scales, for example, when the Sun moves in and out of a spiral arm (Shaviv, 2003a, see also part III). The CRF at Earth is therefore expected to be variable over time scales of 10^5 to 10^9 years (e.g. Scherer, 2000, Scherer et al., 2004, and the references therein).

It is accepted that the concentration of ^{10}Be nuclei in polar ice exhibits temporal variations in response to changes in the flux of the primary CRs (Beer et al., 1990, Masarik and Beer, 1999, and references therein). McCracken et al. (2002, 2004) showed that the ^{10}Be response function has peaked near 1.8 GeV/nucleon since 1950. They also claim that the NM era represents the most extreme cosmic ray modulation events over the past millennium and that this period is not the typical condition of the heliosphere. There is the hypothesis that short-term (one month or less) increases in the nitrate component of polar ice are the consequence of SEPs (Shea et al., 1999). The observed concentration of ^{10}Be is also determined by both production and transport processes in the atmospheric, and a terrestrial origin for many of the noticeable enhancements in ^{10}Be is possible, a major uncertainty that inhibits the use of cosmogenic isotopes for the quantitative determination of the time variations of galactic CRs on the same scales for which ^{10}Be is available.

Exploring cosmic ray modulation over time scales of hundreds of years and during times when the heliosphere was significantly different from the present epoch is a very interesting development. Much work is still needed to make the apparent association (correlations) more convincing, being very complex is well recognized, than what e.g. McCracken et al. (2004) and Usoskin and Mursula (2003) discussed. However, the association between the ^{10}Be maxima and low values of the sunspot number is persuasive for the Maunder and Dalton minima.

8.2. Causes of the 11- and 22-year Modulation Cycles

Although there is a large number of solar activity indices, the sunspot number is the most widely used index. From a CR modulation point of view, sunspots are not very useful, because the large modulation observed at Earth is primarily caused by what occurs, in three-dimensions, between the outer boundary (heliopause) and the Earth (or any other observation point). In this sense the widely used “force-field” modulation model (e.g. Caballero-Lopez and Moraal, 2004) is very restricted, ignoring all the important latitudinal modulation effects e.g., perpendicular diffusion, gradient and curvature drifts.

Our present understanding of cosmic ray modulation is based on the cosmic ray transport equation (1). For this equation, with a full description of the main modulation mechanisms and the main physics behind them, the reader is referred to Potgieter (1995, 1998) and Ferreira and Potgieter (2004), and the references therein, for more details see section 5. The individual mechanisms are well-known but how they combine to produce cosmic ray modulation, especially with increasing solar activity, is still actively studied. Basically it works as follows. GCRs scatter from the irregularities in the heliospheric magnetic field as they attempt to diffuse from the heliospheric boundary toward the Earth. With these irregularities frozen into the solar wind, the particles are convected outward at the solar wind speed. In the process, they experience adiabatically energy losses, which for nuclei can be quite significant. Gradient and curvature drift is the fourth major mechanism, and gets prominent during solar minimum conditions when the magnetic field becomes globally well structured. In the $A > 0$ drift cycle (see Fig. 8) the northern field points away from the Sun, consequently positively charged particles drift mainly from high heliolatitudes toward the equatorial plane and outward primarily along the current sheet, giving the typical flat intensity-time profiles. The current (neutral) sheet separates the field in two hemispheres and becomes progressively inclined and wavy, due to solar rotation, with increasing solar activity (Smith, 2001). The extent of inclination or "tilt angle" changes from about 10° at solar minimum to 75° at solar maximum (theoretically 90° is possible but the current sheet on the Sun becomes unrecognizable long before then; Hoeksema, 1992). In the $A < 0$ cycle the drift directions are reversed, so that when positive particles drifting inward along the wavy current sheet, the intensity at Earth becomes strongly dependent on the tilt angle and consequently exhibits a sharp intensity-time profile for about half of the 11-year cycle. For negatively charged particles the drift directions reverse so that a clear charge-sign dependent effect occurs, a phenomenon that has been confirmed by observations from the Ulysses mission for more than a solar cycle (Heber et al., 2003). The CRF thus varies in anti-correlation with the 11-year solar activity cycle indicating that they are indeed modulated as they traverse the heliosphere. The extent of this modulation depends on the position and time of the observation, and strongly on the energy of the cosmic rays. The 22-year cycle, originating from the reversal of the solar magnetic field roughly every 11 years, is superimposed on the 11-year cycle with an amplitude less than 50% of the 11-year cycle. As shown in Fig. 8, the NM intensity-time profiles exhibit the expected peak-like shapes around the solar minima of 1965 and 1987 ($A < 0$), while around 1954, 1976 and 1998 ($A > 0$) they were conspicuously flatter. Shortly after the extraordinary flat profile around 1976 was observed, two research groups, in Arizona (Jokipii et al., 1977) and in South Africa, quickly recognized that gradient and curvature drifts, together with current sheet drifts, could explain these features (Potgieter and Moraal, 1985, and references therein). After the revealing of drifts as a major modulation mechanism, the "tilt angle" of the current sheet, being a very good proxy of its waviness which on its turn is directly related to solar activity, has became the most useful solar activity "index" for cosmic ray studies.

While the cosmic ray intensity at NM energies are higher in $A < 0$ cycles at solar minimum than in the $A > 0$ cycles - see Fig. 8 - the situation is reversed for lower energies e.g., for 200 MeV protons, confirmed by spacecraft observations. This requires the differential spectra of consecutive solar minima to cross at energies between 1 and 5 GeV (Reinecke and Potgieter, 1994). The maxima in these spectra also shift somewhat up or down in energy depending on the drift cycle because the energy losses are somewhat less during $A > 0$ cycles than during $A < 0$ cycles. Convincing experimental evidence of drift effects followed since the 1970's, e.g. when it was discovered that NM differential spectra based on latitude surveys showed the 22-year cycle, and when the intensity-time profiles of cosmic ray electrons depicted the predicted "opposite" profiles. It further turned out that the $A > 0$ minimum in the 1990's was not as flat as in the 1970's, by allowing the solar minima modulation periods to be less drift dominated, as predicted (Potgieter, 1995). This fortuitous flat shape during of the 1970's is therefore not entirely owing to drifts but also to the unique unperturbed way in which solar activity subsided after the 1969-70 solar maximum. The period from 1972–1975 became known as a "mini-cycle", interestingly close to the 5-year cycle that McCracken et al. (2002) reported. It is also known that the sharp profiles are consistently asymmetrical with respect to the times of minimum modulation, with a faster increase in cosmic ray flux before than after the minima (about 4 years to 7 years, respectively). The 11-year solar cycle thus has an asymmetric shape, also evident from "tilt angle" calculations, and should therefore be evident in the cosmogenic archives.

In the mid-1990's, le Roux and Potgieter (1995) illustrated that the waviness of the current sheet cannot be considered the only time-dependent modulation parameter because large step decreases occurred in the observed CR intensities (McDonald et al., 1981). These steps are prominent during increased solar activity when the changes in the current sheet are no longer primarily responsible for the modulation. In order to successfully model CR intensities during moderate to higher solar activity requires some form of propagating diffusion barriers (PDBs). The extreme forms of these diffusion barriers are the GMIRs, mentioned above. They also illustrated that a complete 11-year modulation cycle could be reproduced by including a combination of drifts and GMIRs in a time-dependent model. The addition of GMIRs convincingly explains the step-like appearance in the observed cosmic ray intensities. The periods during which the GMIRs affect long-term modulation depend on the radius of the heliosphere, their rate of occurrence, the speed with which they propagate, their amplitude, their spatial extent, especially in latitude, and finally also on the background turbulence (diffusion coefficients) they encounter. Drifts, on the other hand, dominate the solar minimum modulation periods so that during an 11-year cycle there always is a transition from a period dominated by drifts to a period dominated by diffusive propagating structures. During some 11-year cycles these periods of transition happen very gradually, during others it can be very quickly, depending on how the solar magnetic field transforms from a dominating dipole structure to a complex higher order field. For reviews on long-term modulation, see e.g. Heber and Potgieter (2000) and Potgieter et al. (2001).

If there is a direct relation between ^{10}Be concentrations and CRs impacting Earth, large decreases like the one in 1991 which reduced the flux of relatively high energy significantly, should show up in the time-profiles of ^{10}Be.

A third improvement in our understanding of 11-year and 22-year cycles came when Potgieter and Ferreira (2001) generalized the PDBs concept by varying also all the relevant diffusion coefficients with an 11-year cycle, in a fully time-dependent model directly reflecting the time-dependent changes in the measured magnetic field magnitude at Earth. These changes were propagated outwards at the solar wind speed to form effective PDBs throughout the heliosphere, changing with the solar cycle. This approach simulated an 11-year modulation cycle successfully for cosmic ray at energies > 10 GeV, but it resulted in far less modulation than what was observed at lower energies. They therefore introduced the compound approach, which combines the effects of the global changes in the heliospheric magnetic field magnitude, related to all diffusion coefficients, with global and current sheet drifts in a complex manner, not merely approximately proportional to $1/B$, with B the magnetic field magnitude, to produce realistic time-dependent relations between the major modulation parameters (Ferreira and Potgieter, 2004). This approach has so far provided the most successful modeling of the 11-year and 22-year cycles. An example is given in Fig. 9, where the 11-year simulation done with the compound numerical model is shown compared to the Hermanus NM count rates expressed as percentage values for the period of 1980–1992.

This inversion CR-B method is used to derive values of the solar magnetic field back in time, after the modulation model is calibrated to CR observations, typically for minimum modulation like in May 1965, and further by assuming a direct relation between CRs and the

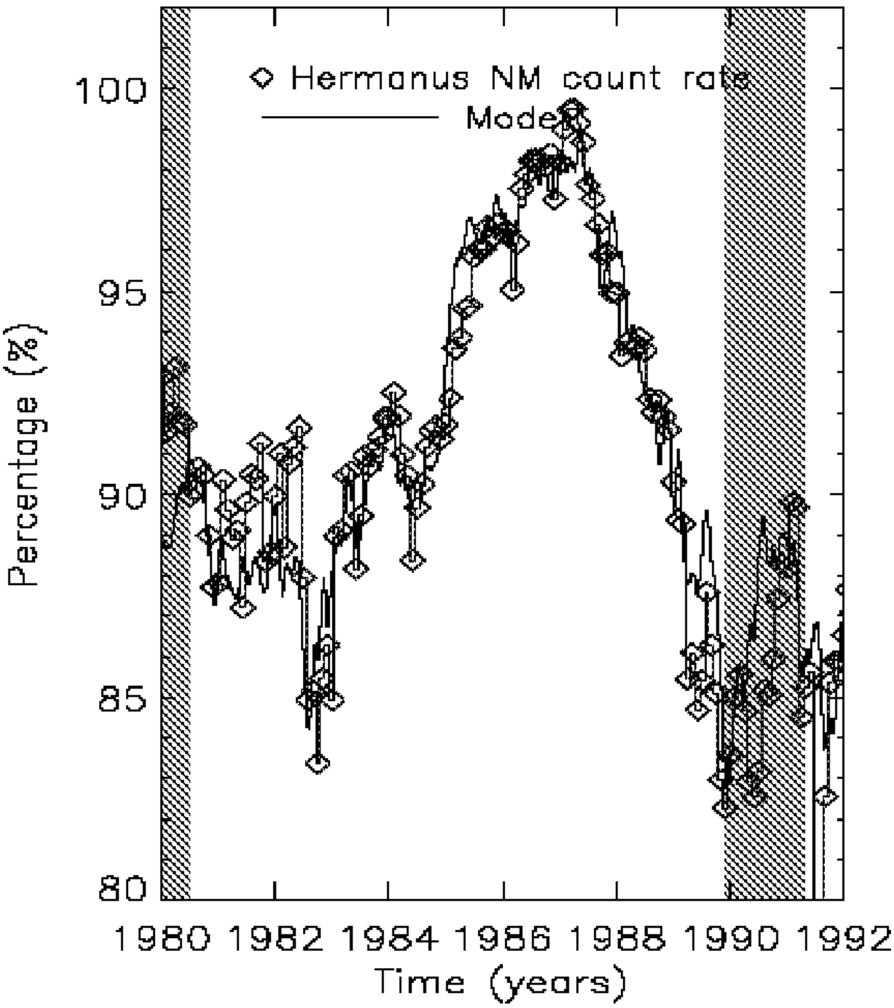

Figure 9. Model computations, based on the compound approach (Ferreira and Potgieter, 2004), shown with the Hermanus NM count rates expressed as percentage values for 1980–1992. Shaded areas indicate when the solar magnetic field polarity was not well defined.

long-term cosmogenic isotope time-profiles. This produces interesting results but further investigation is required because these computations are highly model dependent. It is apparent that for the reconstruction of sunspot numbers from the rate of cosmogenic isotopes, one needs to take into account drift effects described above. Using sunspot numbers as a proxy for the long-term changes in the interplanetary magnetic field over long periods of time and hence the cosmic ray intensity is not reasonable.

The structural features and geometry of the heliosphere, including the solar wind termination shock, the heliosheath and heliopause, especially their locations, also influence the cosmic ray fluxes at Earth. This is the topic of the next section. Together with these features, one has to take into account the possible variability of the local interstellar spectrum for the various cosmic ray species as the heliosphere moves around the galactic center as discussed in part III. The impact of these global heliospheric features on very long-term cosmic ray modulation will be intensively studied in future, with the interest already being enhanced by the recent encounter (Stone et al., 2005) of the solar wind termination shock of the Voyager 1 spacecraft.

9. Effects of the Heliospheric Structure and the Heliopause on the Intensities of Cosmic Rays at Earth

As the heliosphere moves through interstellar space, various changes in its environment could influence and change its structure. In this section the purpose is to show how changes in the geometrical structure of the heliosphere can affect the modulation of cosmic rays at Earth from a test particle model point of view. The next two subsections will discuss the hydrodynamic point of view. The main focus will be on the modulation effects of the outer heliospheric structures: (1) The solar wind termination shock (TS) where charged particles are getting re-accelerated to higher energies. (2) The outer boundary (heliopause) where the local interstellar spectra (LIS) of different particle species are encountered; and (3) the heliosheath, the region between the TS and the heliopause. The TS is described as a collisionless shock, i.e. a discontinuous transition from supersonic to subsonic flow speeds of the solar wind, in order for the solar wind ram pressure to match the interstellar thermal pressure, accompanied by discontinuous increases in number density, temperature and pressure inside the heliosheath. The heliopause is a contact discontinuity; a surface in the plasma through which no mass flow occurs, and which separates the solar and interstellar plasmas. For a review of these features, see Zank (1999) and also part V.

With the recent crossing of the TS by the Voyager 1 spacecraft at $\approx$94 AU a compression ratio, between the upstream and downstream solar wind plasmas, was measured between $\approx$2.6 (Stone et al., 2005) and $\approx$3 (Burlaga et al., 2005). This implies that the TS is rather weak, as assumed in our modeling. The TS may move significantly outwards and inwards over a solar cycle (Whang et al., 2004). Many factors influence the position of the heliopause, making it less certain, but it

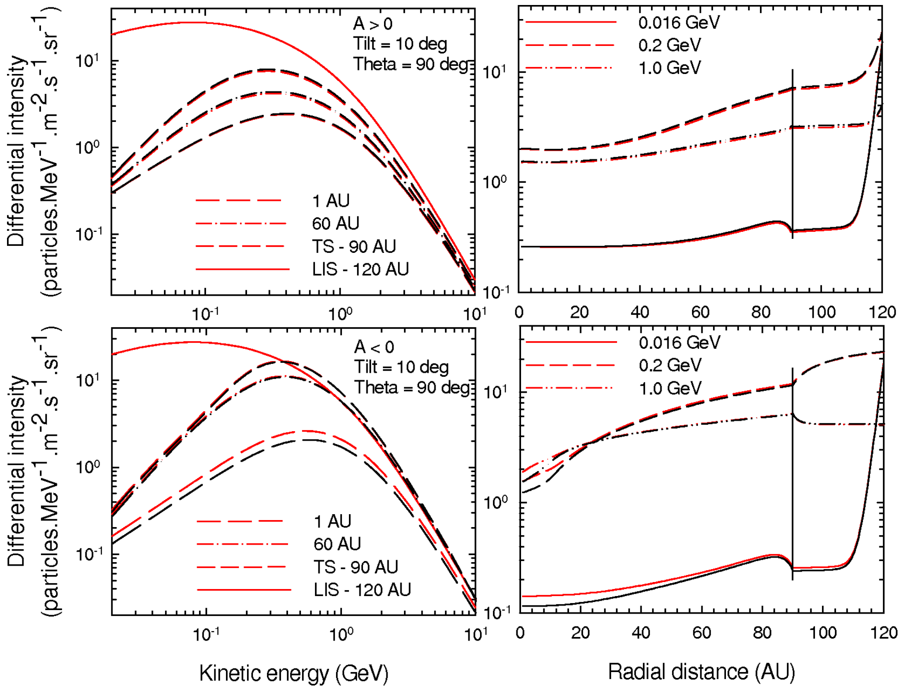

Figure 10. Solutions for a symmetric (red curves) and an asymmetric heliosphere (black curves) shown for the nose region ($\alpha = 20°$), for solar minimum conditions ($\alpha = 90°$), and for the $A > 0$ polarity cycle (top panels) and the $A < 0$ polarity cycle (bottom panels), respectively. Left panels: Energy spectra at radial distances of 1 AU, 60 AU, at the TS position and at the LIS position. Right panels: Differential intensities as a function of radial distance at energies of 16 MeV, 200 MeV, and 1 GeV, respectively. Here $r_s = 90$ AU and $r_{HP} = 120$ AU for both heliospheric shapes, but only in the nose direction, for the asymmetrical shape $r_s = 100$ AU and $r_{HP} = 180$ AU in the tail direction. The LIS is specified at r_{HP}. (From Langner and Potgieter 2005b).

is probably at least 30–50 AU beyond the TS in the nose direction, the region in which the heliosphere is moving, but significantly larger in the tail direction of the heliosphere, because the dimensions of the heliosphere should be affected by its relative motion through the local interstellar medium (Scherer and Fahr, 2003; Zank and Müller, 2003). The configuration and position of the TS and the heliopause will also change if the heliosphere would move in and out of a denser region in the interstellar medium, like a crossing of the galactic spiral arm.

The effects on the intensities of CRs at Earth of some assumptions and unknowns in heliospheric modeling are shown in this part; these effects may just as well be interpreted as caused by changes in the local interstellar space.

9.1. Modulation Models

Modulation models are based on the numerical solution of the time-dependent CR transport equation (Parker, 1965), see also section 5. The details of the model used to obtain the results shown below, were discussed by Langner et al. (2003) and Langner and Potgieter (2005c). Eq. (1) was solved time-dependently as a combined diffusive shock acceleration and drift modulation model, neglecting any azimuthal dependence. The heliospheric magnetic field (HMF) was assumed to have a basic Archimedian geometry in the equatorial plane, but was modified in the polar regions similar to the approach of Jokipii and Kota (1989). The solar wind was assumed to be radially outward, but with a latitudinal dependence. The current sheet tilt angle α was assumed to represent solar minimum modulation conditions when $\alpha = 10°$, and solar maximum when $\alpha = 75°$, for both the magnetic polarity cycles, respectively called $A > 0$ (e.g. ≈1990–2001) and $A < 0$ (e.g. 1980–1990). The position of the outer modulation boundary (heliopause) was assumed at $r_{HP} = 120$ AU, except where explicitly indicated, where the proton LIS of Strong et al. (2000) was specified, or the interstellar spectra of Moskalenko et al. (2002, 2003) for boron (B) and carbon (C). The position of the TS was assumed at $r_s = 90$ AU, with a compression ratio $s = 3.2$ and a shock precursor scale length of $L = 1.2$ AU (Langner et al., 2003), except where explicitly indicated.

9.2. Changes in the Shape of the Heliosphere

An example of the effects on galactic CR protons at Earth due to a change in the shape of the heliosphere is illustrated in Fig. 10 for both HMF polarity cycles for $\alpha = 10°$. The shape of the heliosphere is changed from symmetrical, with $r_{HP} = 120$ AU and $r_s = 90$ AU, to asymmetrical with $r_{HP} = 120$ AU and $r_s = 90$ AU in the nose direction and $r_{HP} = 180$ AU and $r_s = 100$ AU in the tail direction. In the left panels the energy spectra are shown at radial distances of 1 AU, 60 AU, and at r_s and r_{HP}. In the right hand panels the differential intensities are shown at energies of 16 MeV, 200 MeV, and 1 GeV, respectively. The 16 MeV profiles are shown for illustrative purposes only.

The comparison of these spectra illustrates that no significant difference occurs for the $A > 0$ cycle for solar minimum between a symmetrical and asymmetrical heliosphere, despite a difference of a factor of 1.5 in the position of the heliopause in the equatorial tail direction; even when the heliopause is moved from 120 AU to 200 AU and the TS from 90 AU to 105 AU. For the $A < 0$ polarity cycle differences remain insignificant in the nose direction, but they increase towards the Sun with decreasing radial distances, for all latitudes. Changes in the shape of the heliosphere therefore have an influence on the CR intensities at Earth, although relatively small (Langner and Potgieter, 2005c).

9.3. Changes in the Size of the Heliosheath

In Fig. 11 the computed spectra for galactic protons are shown for both magnetic polarity cycles and for solar minimum conditions with $\alpha = 10°$. The spectra and differential intensities are shown at the same distances and energies as in Fig. 11. The LIS is specified first at $r_{HP} = 120$ AU and then with $r_{HP} = 160$ AU. All the modulation parameters including the diffusion coefficients were kept the same for both situations. Qualitatively the results for the different heliopause positions look similar, but quantitatively they differ, especially as a function of radial distance. The spectra for $r_{HP} = 120$ AU in all four panels are higher than for the 160 AU position. The differences between the differential intensities are most prominent for energies $\leq$1 GeV and increase with decreasing energy indicative of the wider heliosheath. In the equatorial plane the TS effects are most prominent in the $A < 0$ cycle judged by the amount and at what energies the spectra at 90 AU and even at 60 AU exceed the LIS value. This "excess" effect is reduced when the heliopause is moved further out. As a function of radial distance these effects are quite evident for the chosen energies, e.g. the 0.20 GeV intensities are lower at all radial distances.

The "barrier" effect, the sharp drop in intensities over relatively small radial distances in the outer heliosphere, becomes more prominent (covers a larger distance) when the heliopause is moved outward, especially during the $A > 0$ cycles when it happens over an extended energy range. The width of this modulation "barrier" is dependent on the modulation conditions (diffusion coefficients) close to the outer boundary. For energies $\leq$200 MeV most of the modulation happens in the heliosheath for both cycles, but especially because of the barrier covering relatively small distances near the heliopause during the $A > 0$ cycle. For CR intensities at Earth the position of the TS proved to be not as significant as the position of the heliopause (Langner and Potgieter, 2004; Langner and Potgieter, 2005a; Langner and Potgieter, 2005b).

9.4. Changes in the Termination Shock Compression Ratio

The modulation obtained with the TS model with respect to the carbon LIS, as a typical example of the modulation of CR nuclei, is shown in the left panels of Fig. 12 Potgieter and Langner (2004) for boron spectra, with a detailed discussion. The spectra and differential intensities are now also shown for $\alpha = 75°$, for a model with a TS and then

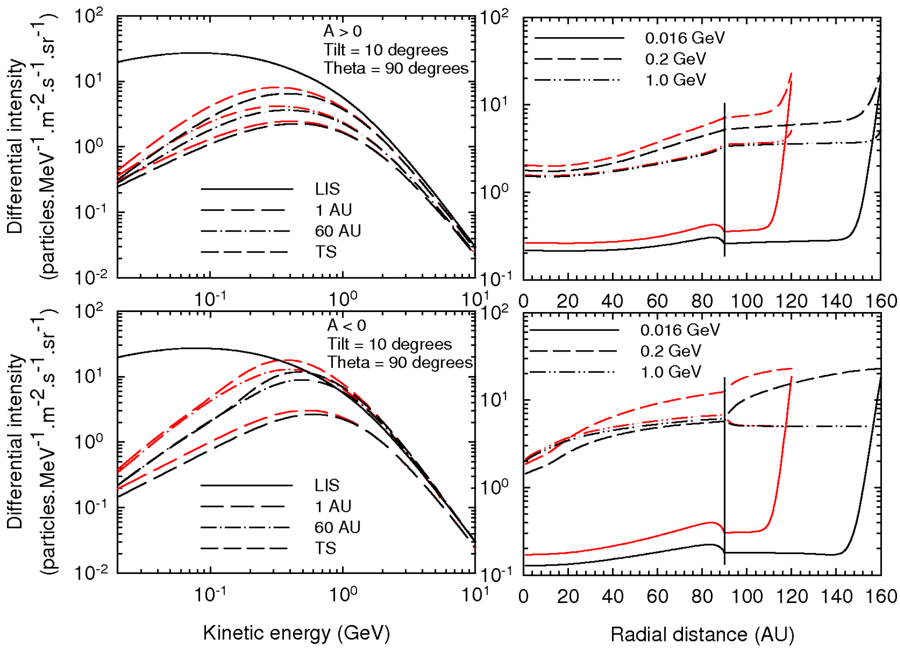

Figure 11. Left panels: Computed differential intensities for galactic protons with $\alpha = 10°$ as a function of kinetic energy for both polarity cycles, at 1 AU, 60 AU, and the TS location (bottom to top) in the equatorial plane ($\theta = 90°$). Right panels: The corresponding differential intensities as function of radial distance for 0.016, 0.2 and 1.0 GeV, respectively at the same latitude as in the left panels. The TS is at 90 AU, as indicated, with the LIS specified at 120 AU (red lines) and 160 AU (black lines), respectively. (From Langner and Potgieter 2005a).

without a TS, respectively. The modulation of C is clearly affected by incorporating a TS. Note the manner in which the modulation changes from solar minimum to moderate solar maximum activity and how the effects increase with solar activity.

The effect of the TS on the modulation of C is for the larger part of the heliosphere significant; it drastically decreases the intensities at lower energies (e.g. at 100 MeV/nuc) but increases it at higher energies (e.g. at 1 GeV/nuc), as the lower energy particles are being accelerated to higher energies. The adiabatic spectral slopes are also altered in the process. The intensities at low energies are, therefore, lower at Earth with the TS than without it in the $A > 0$ polarity cycle, but not for the $A < 0$ cycle, because in this cycle the low energy particle population are supplemented by the modulation of the larger population of high energy particles at the TS, emphasizing the role of particle drifts. These differences can be seen at Earth, and it is clear that a change in the compression ratio will have consequences on the intensities at Earth.

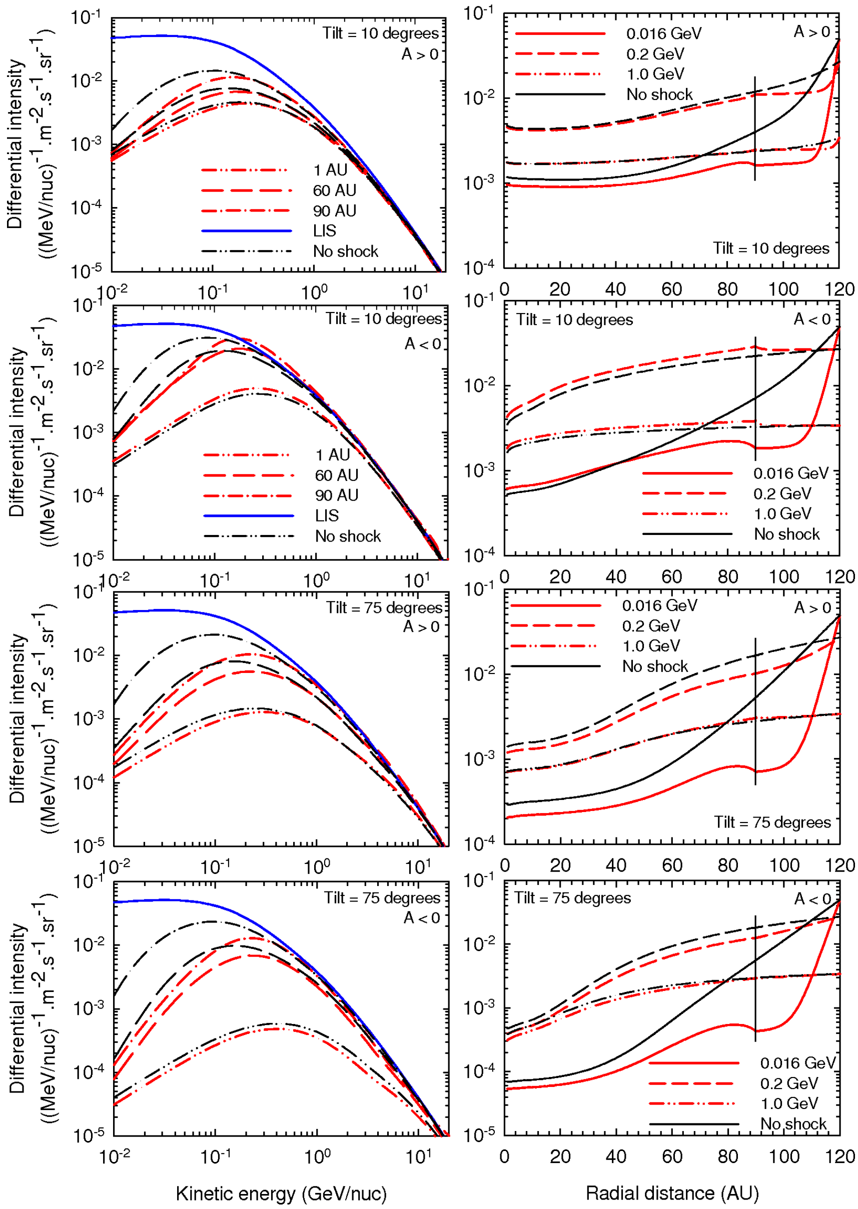

Figure 12. Left panels: Computed spectra for galactic carbon for both polarity cycles, at 1 AU, 60 AU and 90 AU (bottom to top) in the equatorial plane. Right panels: Corresponding differential intensities as a function of radial distance for 0.016, 0.2 and 1.0 GeV, respectively. The TS is at 90 AU, as indicated, with the LIS (blue lines) at 120 AU, with $\alpha = 10°$ and $75°$, respectively. Solutions without a TS are indicated by black lines for the same radial distances and energies. Note the scale differences. (From Potgieter and Langner, 2004).

The differences between the two approaches are most significant with $E \leq 100\,\mathrm{MeV/nuc}$ and $r \geq 60\,\mathrm{AU}$. Similar results were found for CR protons and helium (He) (Langner et al., 2003; Langner and Potgieter, 2004).

9.5. Modulation in the Heliosheath

Also shown in the right panels of Fig. 12 is that the modulation in the heliosheath is an important part of the total modulation for C. Barrier type modulation is caused by the heliosheath as was previously mentioned for galactic protons. It differs significantly for different energies, from almost no effect at high energies to the largest effect at low energies, and with changes in HMF polarity cycle. The TS plays in this regard a prominent role and can be regarded as a main contributor to the barrier modulation effect at low energies. For a discussion of these effects for protons, see Langner et al. (2003).

In Fig. 13 the computed modulation to take place in the heliosheath, between r_b and r_s, is compared to what happens between r_b and 1 AU (LIS to Earth) and between r_s and 1 AU (TS to Earth). This comparison is emphasized by showing in this figure the intensity ratios j_{LIS}/j_1, j_{LIS}/j_{90} and j_{90}/j_1 for B and C in the equatorial plane for both polarity cycles with $\alpha = 10°$. Note that for a few cases the ratios become less than unity. Obviously, all these ratios must converge at a high enough energy where no modulation takes place. According to this figure a significant level of modulation occurs in the heliosheath when $A > 0$ with $E \leq 200\,\mathrm{MeV/nuc}$ for solar minimum ($\alpha = 10°$). This is also true for $A < 0$ but at a somewhat lower energy. The level of modulation in the heliosheath decreases significantly for $E > 200\,\mathrm{MeV/nuc}$ in contrast with that of j_{90}/j_1 for the $A < 0$ cycle but to a lesser extent for the $A > 0$ cycle. From this it is clear that the heliosheath can play an important role for CR intensities at Earth, because at low energies most of the modulation of CRs happens in this region.

9.6. Changes in the Local Interstellar Spectrum

By comparing the energy spectra and radial dependence of the intensities for the chosen energies in Fig. 14 it can be seen that the modulation for B and C differs as a function of radial distance. This is primarily because of the much steeper spectral slope for the local interstellar spectrum (LIS) below 100 MeV/nuc for B compared to C. This implies that the C modulation should have a much larger radial gradient below ≈200-500 MeV/nuc in the outer heliosphere than for B. The spectral slopes at low energies change with increasing radial distance as the adiabatic energy loss effect gets less. Despite the rather flat LIS for C

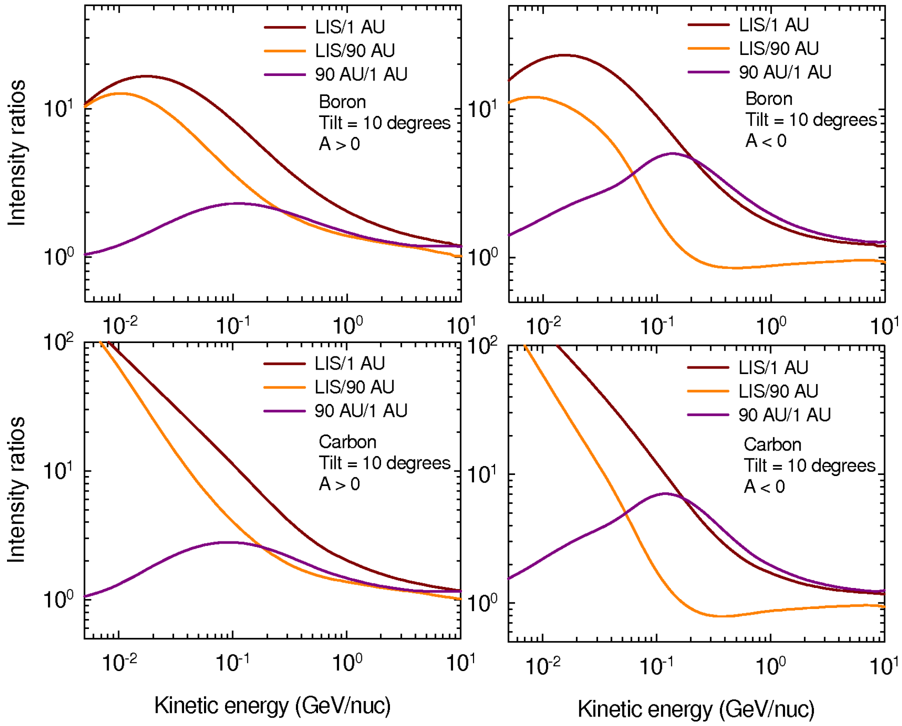

Figure 13. Intensity ratios j_{LIS}/j_1, j_{LIS}/j_{90} and j_{90}/j_1 (120 to 1 AU, 120 to 90 AU and 90 to 1 AU) for boron and carbon as a function of kinetic energy in the equatorial plane with $\alpha = 10°$; left panels: for $A > 0$, right panels for $A < 0$. Interstellar spectra are considered local interstellar spectra (LIS) at 120 AU and the TS is positioned at 90 AU. Note the scale differences. (From Potgieter and Langner, 2004).

below 100 MeV/nuc, the modulated spectra at 1 AU look very similar for B and C, a characteristic of large adiabatic “cooling”. The computed differential intensities for B and C are also shown at Earth for both polarity cycles compared to B and C observations. These comparisons are shown for two sets of LIS as mentioned in the figure caption. This second approach contains a new, local component to spectra of primary nuclei and is probably closer to what can be considered a LIS. The B to C ratios as functions of kinetic energy are also shown compared to the observations, with the interstellar B/C at 120 AU as a reference (Potgieter and Langner, 2004).

As noted before the spectral shapes at 1 AU are very similar for B and C owing to adiabatic energy loses between 120 AU and 1 AU. This causes a steady B/C below 200-300 MeV/nuc. This ratio will systematically decrease with increasing radial distances to eventually coincide with the LIS ratios. However, the spectral slopes at 1 AU are slightly different for the two polarity epochs owing to the different particle drift

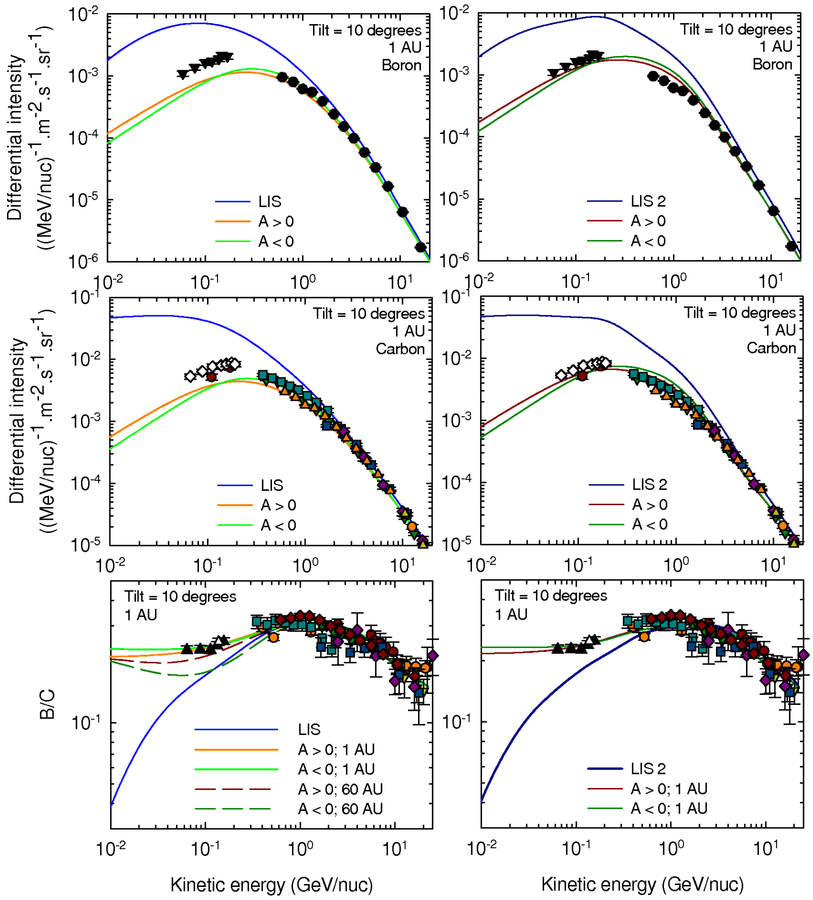

Figure 14. Top and middle panels: Computed differential intensities for boron (top) and carbon (middle) at Earth for both polarity cycles compared to observations. Computations are done with the IS for boron and carbon by Moskalenko et al. (2002) (left panels) and by Moskalenko et al. (2003) (right panels). Bottom panel: B/C as a function of kinetic energy for both polarity cycles with $\alpha = 10^{\circ}$ compared to corresponding observations. The computations are compared to the interstellar B/C at 120 AU as a reference (blue lines). The data compilation is taken from Moskalenko et al. (2003). (From Potgieter and Langner, 2004).

directions during the two magnetic polarity cycles. This causes the well-known crossing of the spectra for successive solar minima, seen here between 100–200 MeV/nuc (Reinecke and Potgieter, 1994). The LIS of (Moskalenko et al., 2002) is most reasonable above 500 MeV/nuc, although a more reasonable fit is obtained below 300 MeV/nuc by using the second LIS of (Moskalenko et al., 2003), which from 200 MeV/nuc to ≈4 GeV/nuc is higher than the previous one. Unfortunately these modified LIS produce modulated spectra that do not represent the

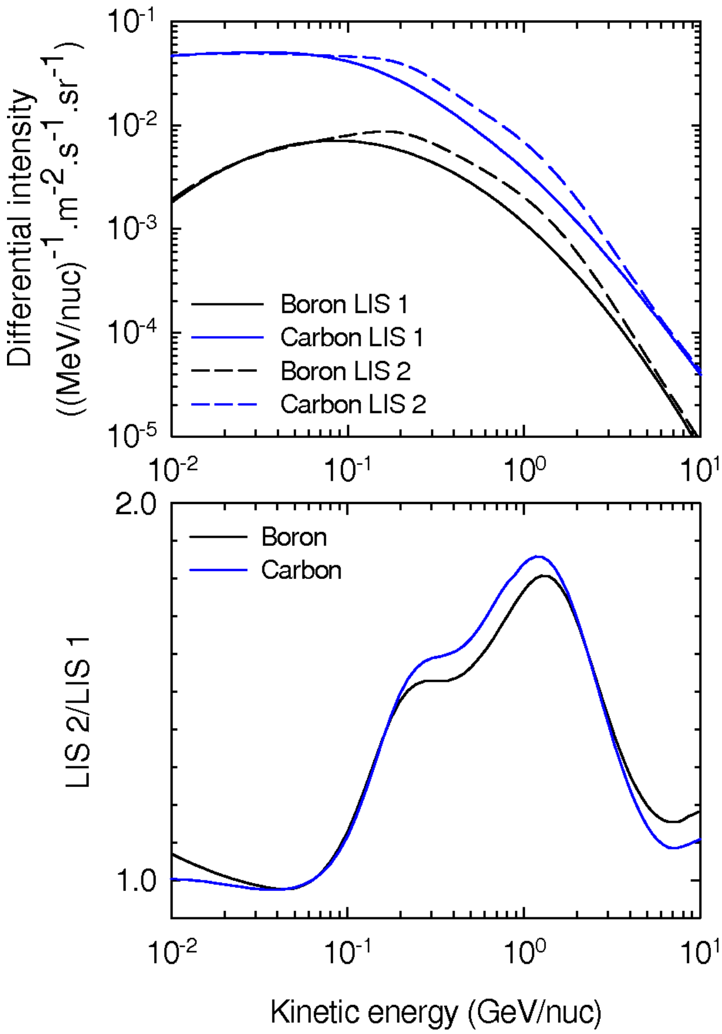

Figure 15. A comparison of the two sets of interstellar spectra for boron (black lines) and carbon (blue lines); lower values (LIS1; solid lines) by Moskalenko et al. (2002), higher values (LIS2- dashed lines) by Moskalenko et al. (2003). The latter contains a local interstellar contribution to spectra of primary nuclei as proposed by Moskalenko et al. (2003) and is probably closer to what can be considered a LIS for carbon. In the lower panel the corresponding ratios (LIS2/LIS1) are shown as a function of energy/nuc. (From Potgieter and Langner, 2004).

observations well between ≈200 MeV/nuc and ≈1 GeV/nuc for both B and C, with the fit to the low-energy B/C still in place. This aspect is emphasized in Fig. 15 by showing the two sets of LIS, with the changes introduced by Moskalenko et al. (2003), and the corresponding ratios as a function of energy.

These differences in the intensities at Earth, caused by different local interstellar spectra, are therefore a clear indication that even small changes in the spectral shape of the LIS can play an important role in the measured intensities of CRs at Earth, if it would occur at high enough energy not to be hidden by adiabatic energy losses.

Changes in the heliospheric structure and in the heliosheath can play a measurable part on the CR intensities at Earth. Qualitatively the modulation for B, C, protons, and He are similar, with certainly quantitative differences. Although these studies were done with a different compression ratio and position for the TS than what was recently observed, the results will qualitatively stay the same. Even though each of the discussed changes cause only small effects at Earth, which alone may seem insignificant, it is clear that a superposition of changes, strongly dependent on energy and on the HMF polarity cycle, may cause a significant effect on the intensities of CRs at Earth.

Part V

Effects of the Dynamical Heliosphere

10. 3D (Magneto-)Hydrodynamic Modelling

For quantitative studies of interstellar-terrestrial relations it is necessary to have a model of a three-dimensional heliosphere, which is immersed in a dynamic local interstellar medium. There are at least two reasons why such model should be three-dimensional. First, a comprehensive and self-consistent treatment of the cosmic ray transport must take into account the three-dimensional structure of the turbulent heliospheric plasma and, second, the heliosphere can be in a disturbed state for which no axisymmetric description can be justified. The present state-of-the-art of the modeling of a dynamic heliosphere with a self-consistent treatment of the transport of cosmic rays is reviewed in Fichtner (2005). As is pointed out in that paper, the major challenge is the development of a three-dimensional hybrid model. This task requires, on the one hand, the generalisation of the modeling discussed in the following section and, on the other hand, the formulation of three-dimensional models of the heliospheric plasma dynamics. The fundamental equations are discussed in section 5 for both the cosmic ray transport as well as the MHD-fluid equations. In the following we discuss different approaches based on these fundamental equations (1) to (3).

10.1. 3D Models without Cosmic Rays

Several three-dimensional models without cosmic rays have been presented. Following early work, which is reviewed in Zank (1999), Fichtner (2001), Fahr (2004), and Izmodenov (2004), nowadays sophisticated MHD models have been developed, see Washimi et al. (2005), Opher et al. (2004), Pogorelov (2004), Pogorelov et al. (2004) and Pogorelov and Zank (2005). Their results are not discussed further, because this review is focused on models containing cosmic rays.

10.2. 3D Models with Cosmic Rays

So far, a truly dynamical, three-dimensional model for the large-scale heliosphere that also includes self-consistently a sophisticated cosmic ray transport comprising fully anisotropic diffusion and drifts is still missing. For the existing three-dimensional models including the cosmic ray transport rather over-simplifying approximations had to be made. Common to all these models is their pure hydrodynamical character, i.e. the fact that the heliospheric magnetic field is included only kinematically. Further simplifications depend on the type of approach being used.

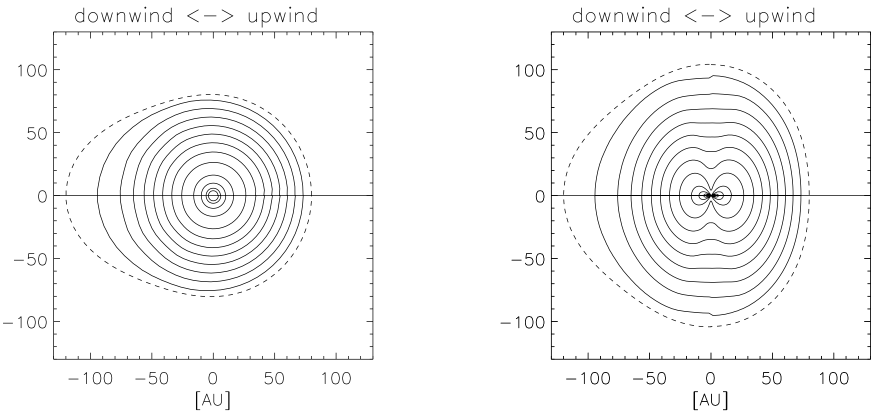

Figure 16. The (normalized) spatial distribution of anomalous protons with 31 MeV for the no-drift case (corresponding to solar activity maximum) in a non-spherical heliosphere. Both cuts are containing the upwind-downwind axis (horizontal solid line): the left panel is a cut perpendicular to the symmetry axis of the heliospheric magnetic field and the right panel is a cut containing it. The outermost dashed line indicates the heliospheric shock in these planes. The contours have, from the shock inwards, the values 1, 0.9, 0.8, 0.7, 0.6, 0.5, 0.4, 0.3, 0.2, 0.1, 0.05, 0.01 (taken from Sreenivasan and Fichtner (2001)).

10.2.1. *Models Based on a Kinetic Description of Cosmic Rays*

Those models that include the kinetic cosmic ray transport equation, are not self-consistent by prescribing the heliospheric plasma structure. This has been done, in extension of earlier work, by Sreenivasan and Fichtner (2001), who treated the kinetic, drift-free transport of anomalous cosmic rays within a three-dimensionally structured stationary heliosphere with a Parker field and excluded the region beyond the asymmetric termination shock. Despite these simplifications the resulting spatial cosmic ray distribution (see Fig. 16) gives a first impression of what one should expect quantitatively for the outer heliosphere.

The figure shows the spatial distribution of anomalous protons with a kinetic energy of 31 MeV for a non-spherical heliospheric shock (outermost dashed line) in the 'equatorial' plane (left), which is perpendicular to the symmetry axis of the heliospheric magnetic field and contains the upwind-downwind axis (horizontal solid line), and in a meridional plane (right) containing both the symmetry axis of the heliospheric magnetic field and the upwind-downwind axis. The shock is elongated in the polar and the downwind direction by factors of 1.3 and 1.5, respectively, as is found with the above-mentioned (M)HD studies. The resulting spectra are compared with those for a spherical heliosphere in Fig. 17.

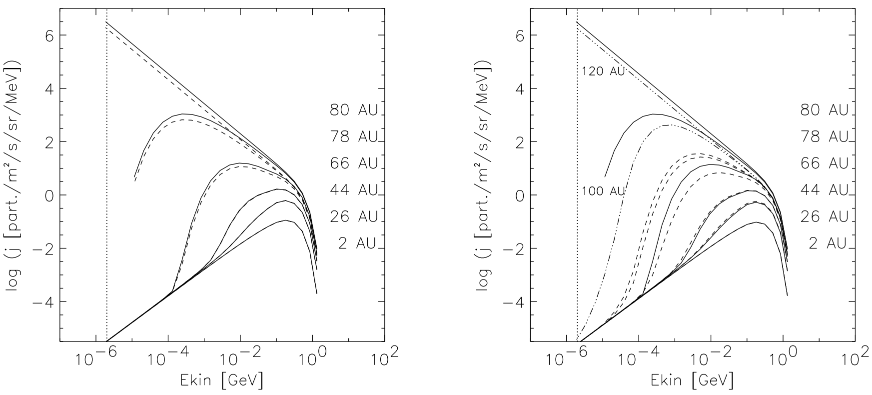

Figure 17. The spectral distribution of anomalous protons in the upwind (solid lines) and downwind (dashed lines) directions for the no-drift case applicable to maximum solar activity. Even for the spherical heliosphere (left panel) the source spectra in the upwind and the downwind direction (uppermost solid and dashed lines) are different due to an assumed variation in the flux of the ACR source population, i.e. the pick-up ions. The right panel is for a non-spherical heliosphere. In both panels the solid and dashed lines indicate (from bottom to top) the spectra at $2, 26, 44, 66, 78$ and 80 AU. Note that in the right panel there are two additional (separately labeled) spectra for 100 and 120 AU (dash-dotted lines) due to the downwind elongation of the non-spherical heliosphere. The vertical dotted line indicates $E_{kin} = 2$keV (taken from Sreenivasan and Fichtner, 2001).

From the figures it is obvious that the three-dimensional structure of the heliosphere is manifest in the spatial and spectral distributions of anomalous cosmic rays only in the outer heliosphere beyond about 50 AU. Thus, within the framework of the assumptions made for this work, one would not expect any effect of the large-scale heliospheric structure on the spectra at the orbit of the Earth.

This first attempt to incorporate the anisotropic diffusion tensor in a ‘realistically’ 3D-structured heliosphere has, of course, severe shortcomings. Some were addressed with 2D models, which are discussed in the following section. Concentrating here on the three-dimensional aspects, a next step was made by Burger and Hitge (2004) computing galactic proton spectra for a non-Parkerian heliospheric magnetic field as suggested by Fisk (1996). Their steady-state model is formulated in a frame corotating with the Sun. Figure 18 gives a comparison of the spectra at the Earth as well as the latitudinal gradients resulting for the Parker field and a hybrid field having Fisk- and Parker-field properties.

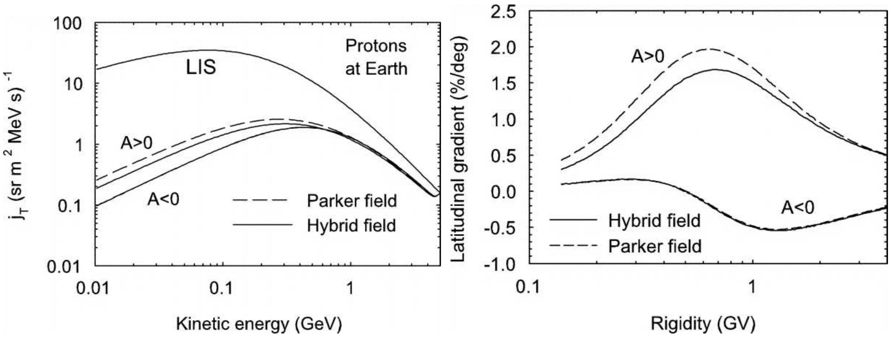

Figure 18. Proton energy spectra at the Earth (left panel) and proton latitudinal gradients as a function of rigidity (right panel) for a Parker field (dashed lines) and the hybrid field (solid lines). The upper two lines are for an $A > 0$ solar polarity epoch, and the lower two (almost identical) lines are for an $A < 0$ epoch. The gradients are calculated between 20^o and 90^o colatitude at a radial distance of 2 AU (taken from Burger and Hitge (2004)).

The finding with highest relevance for the present context is that the hybrid field reduces intensities compared to a Parker field when $qA > 0$, with the signed particle charge q and sign(A) indicating the two subcycles of the Sun's magnetic cycle. This reduction is stronger at high latitudes than at lower latitudes, and also stronger at low energies than at higher energies. Interestingly, for $qA < 0$ the global effects of the hybrid field are almost negligible.

In this model, however, the outer boundary of the computational domain was chosen as 50 AU and, thus, the entire outer heliosphere was neglected.

10.2.2. *Models Based on a Hydrodynamic Description of Cosmic Rays*

In order to get closer to a model of cosmic ray transport in a fully dynamic and complete heliosphere Borrmann (2005) developed a three-dimensional hydrodynamic model of heliospheric dynamics (Borrmann and Fichtner, 2005) that self-consistently includes a hydrodynamically treated galactic cosmic ray component, i.e. rather than the full kinetic transport equation 1, it is employing the moment equation

$$\frac{\partial p_{cr}}{\partial r} = \nabla \cdot \left(\langle \overleftrightarrow{\kappa} \rangle \nabla p_{cr} \right) - \vec{v}_{sw} \cdot \nabla p_{cr} - \gamma (\nabla \cdot \vec{v}_{sw})\, p_{cr} \qquad (46)$$

for the cosmic ray pressure

$$p_{cr}(\vec{r}, p, t) = \frac{4\pi}{3} \int p^3 w f(\vec{r}, p, t) dp \qquad (47)$$

with the particle speed w. Here, $\langle \overleftrightarrow{\kappa} \rangle$ is the momentum-average of the diffusion tensor given in Eq. (2). A typical result for the plasma

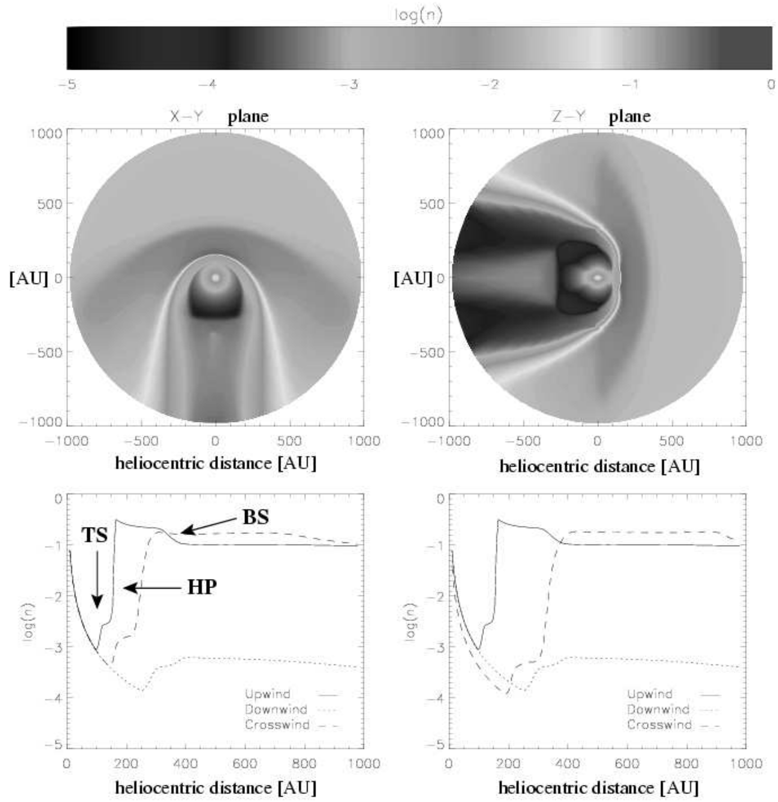

Figure 19. Contour plots of the proton number density in the equatorial ($X-Y$) and a meridional ($Y-Z$) planes along and with the associated number density profiles in the upwind (solid lines), the downwind (dotted lines), the crosswind (dashed lines in the lower left panel), and the polar directions (dashed lines in the lower right panel).

structure of the heliosphere at solar minimum activity is shown in Fig. 19.

The galactic proton distribution at a rigidity of about 0.6 GV for such a configuration is shown in Fig. 20, which is – not surprisingly – qualitatively similar to that shown in Fig. 16. It is quantitatively far more realistic, of course, as the whole heliosphere in particular the heliosheath and the local interstellar medium in the vicinity of the heliopause are fully included.

Again it is found with this study that the cosmic ray intensity at Earth remains unaffected by the large-scale asymmetry of the heliosphere.

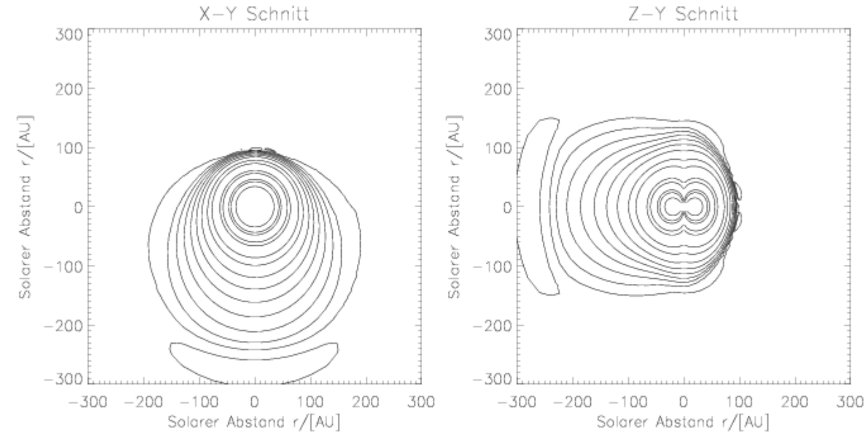

Figure 20. The (normalized) galactic proton distribution for a mean rigidity of 0.6 GV in the equatorial plane (left panel) and the meridional plane containing the heliospheric upwind-downwind axis (right panel). The contour values decrease by 0.1 between 1 (outermost line around the Sun) and 0.1 followed by 0.05, 0.01, 0.005, 0.001, 0.0005 and 0.0001.

This model allows one, however, for the first time, to compute the back reaction of three-dimensional galactic proton distributions on the large-scale structure of the heliosphere. This is illustrated in Figs. 21 and Fig. 22. The first gives the density and velocity contours for three different diffusion tensor models as used by Fichtner et al. (1996), Fichtner et al. (2000), and Ferreira et al. (2001).

From these figures it is evident that the effect of galactic cosmic rays on heliospheric structure is limited to the outer downwind heliosphere, where it manifests in a reduction of the heliocentric distance to the termination shock. This translates into the confirmation that the effect of galactic cosmic rays on the heliosphere is probably negligible and that their test particle treatment is well-justified. Note that this is probably not true for anomalous cosmic rays, which are supposedly accelerated at the termination shock and expected to modify the latter (Florinski et al., 2004). This has, however, not yet been studied with a 3D model.

This model by Borrmann (2005) has also been used for studies of the test particle transport of cosmic rays particularly including the heliosheath region, see the previous section and Langner et al. (2005b) and Langner et al. (2005a), where it is shown that, while the heliospheric asymmetry is not directly showing up in the 1 AU spectra of galactic and anomalous cosmic rays, the absolute levels of the isotropic fluxes are depending on the 3D-structure of the heliosphere.

More involved is an analysis of the consequence of a severely disturbed local interstellar medium. While also this has not been studied

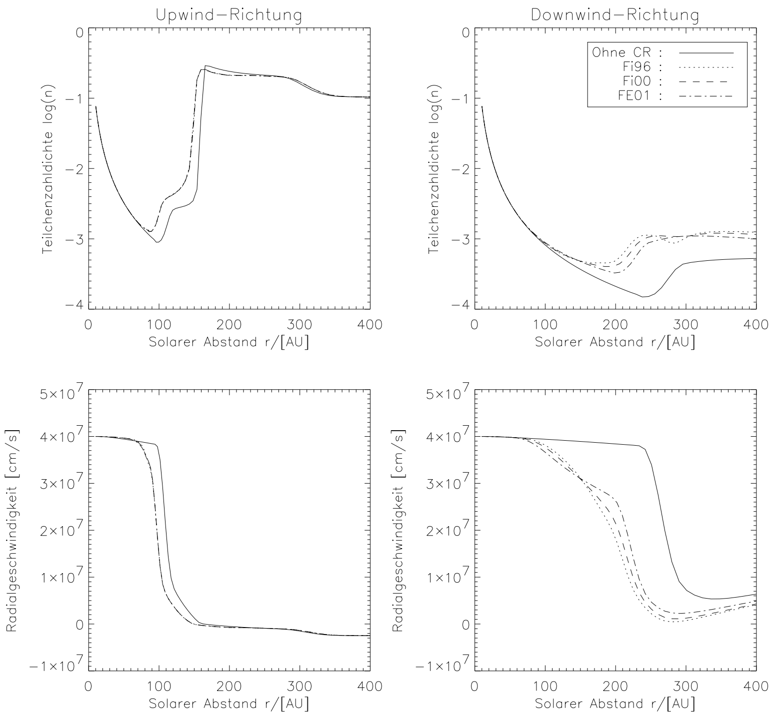

Figure 21. The number density (upper panels) and velocity (lower panels) of the solar wind plasma in the upwind (left) and the downwind direction (right) resulting from a a computation self-consistently including the back reaction of cosmic rays on heliospheric structure for three choices of the anisotropic diffusion tensor (dotted, dashed and dash-dotted lines) as compared to the case without cosmic rays (solid lines).

within the framework of a 3D model, certain principal aspects were investigated already by Zank and Frisch (1999) with axisymmetric computations. Borrmann and Fichtner (2005) presented the plasma structure of a severely disturbed heliosphere as a result of a changing inflow direction of a local interstellar medium whose density is increasing to a ten-fold higher value as it can happen when the heliosphere is entering a different interstellar cloud. For a transition period of roughly 400 years from one steady-state to another, the shape of the shrinking heliosphere is highly asymmetric, see Fig. 23, and one should expect a response of the spatial and spectral distribution of galactic cosmic rays.

Such cosmic ray response to heliospheric environment changes has been studied by Scherer et al., Scherer et al., Florinski and Zank (2001a,

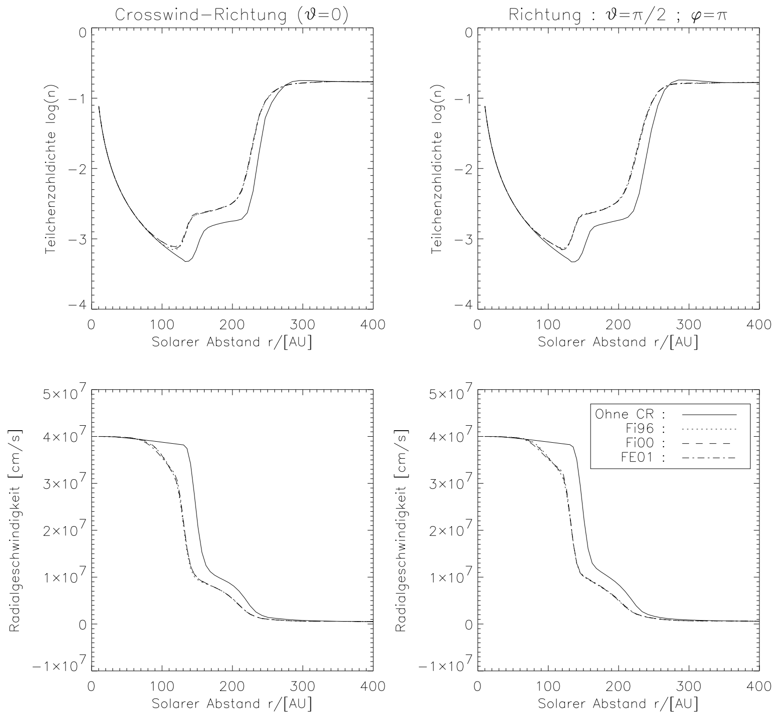

Figure 22. Same as Fig. 21 but for the polar (left panel) and the crosswind direction (right panel).

2002, 2005) with a 2D model. These authors show that a changing interstellar environment can cause the cosmic ray flux at the Earth to be higher or lower than at present as is shown in Fig. 24.

The resulting estimates of the corresponding ^{10}Be production rates (see part VI) amount to about 80% to 400% of the present rate (Florinski and Zank, 2005). The authors remark, however, that these values depend critically on the model of heliospheric turbulence determining the cosmic ray spectra at the Earth.

In summary one can state that the development of 3D models, which self-consistently include cosmic rays, is progressing but has not reached a satisfactory level. Given the rather high computational requirements of such modeling, progress will probably be slow. Therefore, 2D models will be very important tools with which many physical aspects can be studied in a rather good approximation. Also, they allow the incorporation of more physical processes and their refined treatment, like the

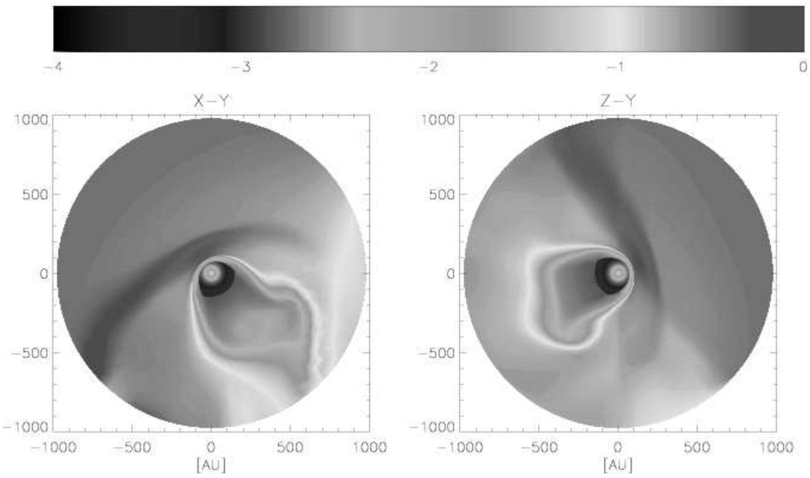

Figure 23. The structure of the heliosphere, here visualized with the proton number density $n[cm^{-3}]$, can be irregular in case of a time-varying local interstellar medium (taken from Borrmann and Fichtner (2005)).

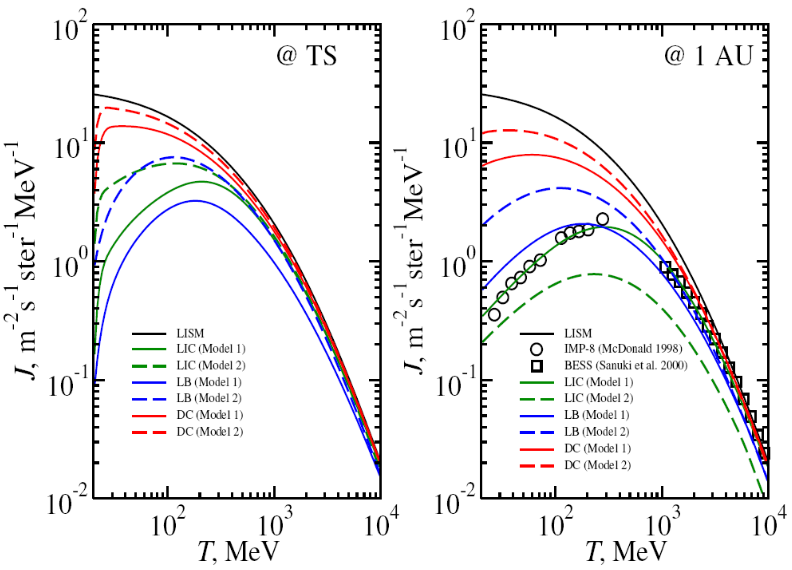

Figure 24. Spectra of galactic protons at 1.1 times the distance to the solar wind termination shock in the apex direction (left) and at 1 AU (right) for the three interstellar environments (taken from Florinski and Zank (2005)).

solution of the kinetic transport equation. These 2D hybrid models are reviewed in the following section.

11. Cosmic Ray Transport in a Dynamic Heliosphere

To model cosmic ray modulation over long timescales and for different energies requires knowledge of the most important modulation processes and in particular how these change over a solar cycle. (See Potgieter and Ferreira (2001) and Potgieter (1998) for a review, and also part IV.) Also of great importance is to know the geometry of the modulation volume (heliosphere) as well as the plasma flow inside, which includes a transition from super to subsonic speeds. This shock also acts as an accelerator of cosmic rays, which in their turn might alter the original plasma flow.

In view of the above argumentation a hybrid model is required, taking into account the hydrodynamic equations (3) and the kinetic transport equation (1). Because the magnetic field is not dynamically important, one can chose $B = 0$ in Eq. (3), but for the modulation of the CRs the magnetic field is not negligible, e.g. $B \neq 0$. To take care of this contradictory assumption, the Parker spiral field is calculate kinematically in the hydrodynamic part, in which it is not needed, but it is used in the kinetic part (Scherer and Ferreira, 2005a; Scherer and Ferreira, 2005b).

However, concerning the 11- and 22-year cosmic ray modulation propagating diffusion barriers (Burlaga et al., 1993) and drift effects (Jokipii et al., 1977) are important and are primarily responsible, especially at the higher energies, for time dependent modulation, see part IV. Apart from these, global changes in the HMF magnitude over a solar cycle also play an important role (Cane et al., 1999; Wibberenz et al., 2002). Both effects are combined into a compound approach (Ferreira and Potgieter, 2004) to calculate long-term cosmic ray modulation utilizing a self-consistent hybrid model. A short discussion of this approach and model is given below, together with some results which are presented thereafter.

11.1. Cosmic Ray Transport

The transport of ACRs and GCRs inside the heliosphere can be calculated by solving transport equation (1) for the differential intensity $j = R^2 f$, where f is the solution for distribution function and R is the rigidity. j is given in units of particles $\mathrm{m}^{-2}\,\mathrm{s}^{-1}\,\mathrm{sr}^{-1}\,\mathrm{MeV}^{-1}$.

To calculate j as self consistent as possible a hybrid model (Scherer and Ferreira, 2005a; Scherer and Ferreira, 2005b) was developed, in which three species are estimated hydrodynamically, the protons, neutral H-atoms and H-pick-up ions. Once the heliospheric geometry and plasma flow are calculated, they are transferred into the kinetic transport part (solving equation 1) to determine the spectra of the other two species, e.g. ACRs and GCRs, inside the heliosphere. This is all done dynamically including solar cycle related changes in $\vec{v}$ and $\overleftrightarrow{\kappa}$ which influences the heliospheric geometry particle transport therein. For the dynamics, it is assumed that the fast solar wind dissappears over the solar poles toward solar maximum as observed by Ulysses (McComas et al., 2001) and close to the ecliptic the solar wind is always constant at slow speeds. As shown by e.g. (Ferreira and Scherer, 2004) and (Scherer and Ferreira, 2005a) this influences the geometry of heliosphere.

Results of the hybrid model are presented in Fig. 25 showing the time evolution of the dynamic heliosphere including solar cycle related changes in the latitudinal profile of $\vec{v}$. Shown here is the proton ($\vec{v}$ and LISM) speed for selected periods over a 11-year cycle as three plots representing increasing solar activity from top to bottom. An interesting aspect is the so called "tornado alley" evident at high latitudes beyond the termination shock. In this narrow region the plasma speed significantly differs compared to that of the surroundings. However, as the fast solar wind (solar minimum) over the poles disappears and only an uniformly slow solar wind (solar maximum) is left, this structure is less evident and almost disappears for extreme solar maximum periods. The most important feature shown here, from a CR modulation point of view, is that as solar activity increases the termination shock moves inward, especially at the polar and tail regions. That has important consequences for CR particle acceleration and distribution in these regions.

The geometry of the heliosphere, as calculated by our hybrid model, is summarized in table II, where the radial distance of the shock and the heliopause are given for the nose, the pole, and tail, as well as the latitude 34°, corresponding to the Voyager 1 crossing of the termination shock. Note that the termination shock, and to a lesser extent the heliopause radius, depend on the plasma speed which changes over solar activity, emphasizing the need to compute these structures, and their effect on the CR distribution self-consistently. See Zank, Fichtner (1999, 2005) for a review. Note that solar cycle related changes in $\vec{v}$ also has a large effect on the cooling and acceleration of cosmic rays because of their dependence on $\nabla \cdot \vec{v}$.

11.2. Transport Coefficients and the Compound Approach

The two most important CR transport processes in Eq. 1, are diffusion and drifts found in $\overleftrightarrow{\kappa}$ where the following coefficients are of special interest

$$\kappa_{rr} = \kappa_{||} \cos^2 \psi + \kappa_{\perp r} \sin^2 \psi \tag{48}$$

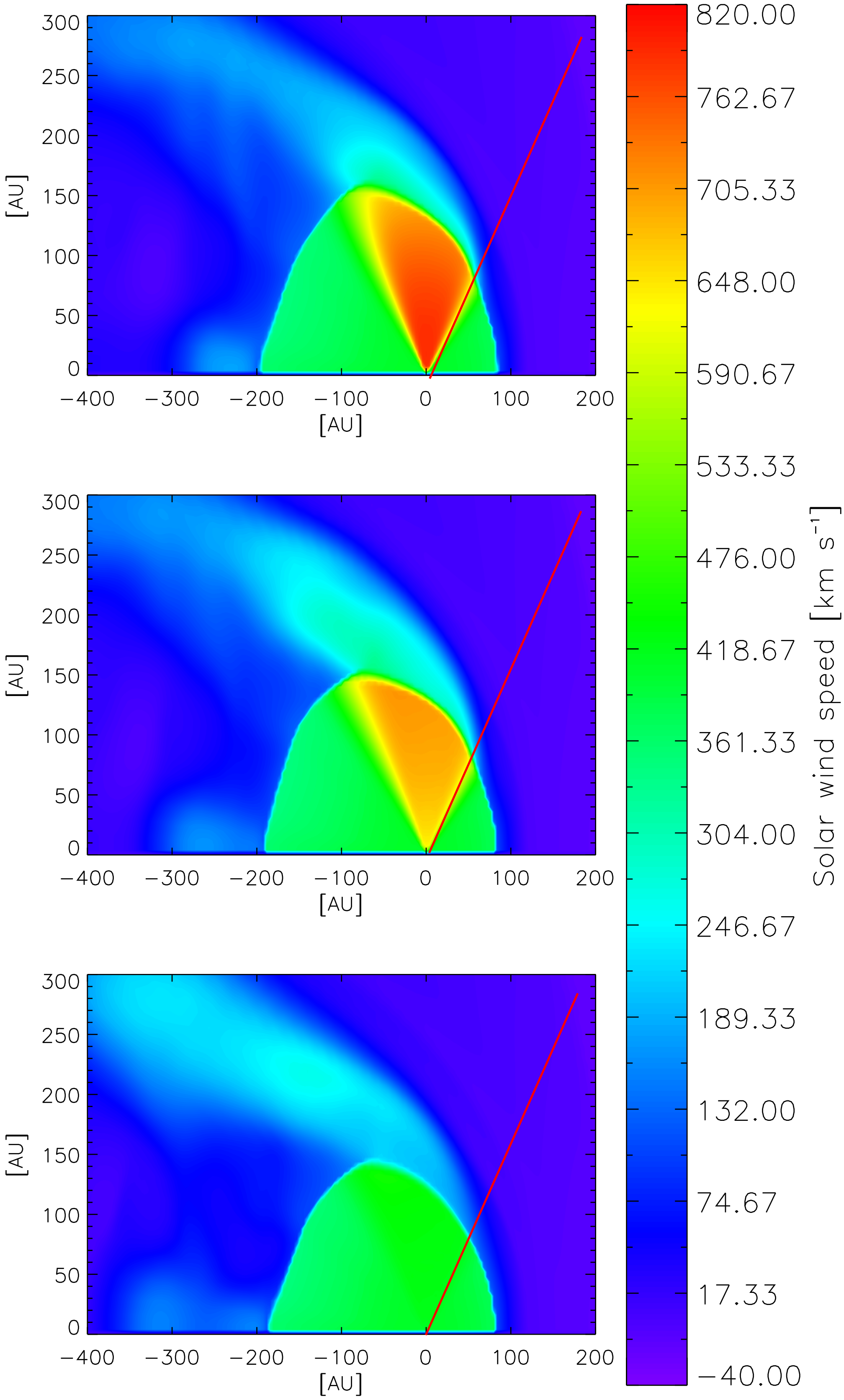

Figure 25. Time evolution of the dynamic heliosphere represented by the solar wind speed. The red line indicates the inclination at which Voyager 1 has crossed the termination shock

Table II. Heliospheric geometry during different levels of solar activity

Structure	Nose	Poles	Tail	Voyager 1
		Solar minimum		
Termination shock	85 AU	137AU	189AU	92AU
Heliopause	120AU	219AU	undefined	134AU
		Solar maximum		
Termination shock	85AU	130AU	173AU	93AU
Heliopause	121AU	228AU	undefined	135AU

$$\kappa_{\theta\theta} = \kappa_{\perp\theta} \tag{49}$$

$$\kappa_A = \frac{\beta P}{3B} \tag{50}$$

these are, from top to bottom, the radial and polar diffusion and drifts respectively, with heliospheric magnetic field B (Parker, 1958) and spiral angle ψ. Here $\kappa_{||}$ is diffusion parallel to the heliospheric magnetic field, $\kappa_{\perp r}$ perpendicular diffusion in the radial direction and $\kappa_{\perp\theta}$ perpendicular diffusion in the polar direction, compare with Fig. 2.

Concerning the time-dependence of the CR transport parameters, it was shown by Perko and Fisk (1983) and le Roux and Potgieter (1989), that the modulation over long periods requires some form of propagating diffusion barriers, see section 8. More recently Cane et al. (1999) and Wibberenz et al. (2002) argued that the CR step decreases observed at Earth could not be primarily caused by GMIRs because they occurred before any could form beyond 10 AU. Instead they suggested that time-dependent global changes in the HMF might be responsible for long-term modulation. These two ideas were combined by Ferreira (2002) and into the so-called compound approach, by simply multiplying all the diffusion (and drift) coefficients in $\overset{\leftrightarrow}{\kappa}$ by a time dependent function

$$f_2(t) = \left(\frac{B_0}{B(t)}\right)^n \tag{51}$$

with $n = \alpha/k$ with α the tilt angle and k a constant with the appropriate units. Equation (51) use as time-dependent input parameters the observed tilt angle and HMF magnitude. This function results in transport parameters which is roughly a factor of $\sim$10 smaller for solar minima compared to solar maxima, see also Cummings and Stone

(2001) and results in realistic time-dependent modulation (Ferreira and Potgieter, 2004; Ndiitwani et al., 2005).

11.3. Results of the Hybrid Model

Figure 26 shows the results from our hybrid model in the form of computed 30 MeV ACR and GCR combined intensities in the meridional plane of the heliosphere. The computations are presented as a series of "snapshots" corresponding to different solar activity conditions. The top left panel displays solar minimum, and then from left to right, bottom to top, each panel shows increasing solar activity with the last panel at the bottom showing the CR distribution at solar maximum. Demonstrated here is that, in general, irrespectively of solar activity the heliosphere and the CR distribution are highly asymmetrical due to the motion of the Sun through the LISM, as well as the poleward elongation of the termination shock and heliopause.

One can see in Fig. 26 that there is a minor decrease of particle intensities at the shock toward solar maximum. However, for the higher latitudes in the heliospheric flanks in the nose direction (typically the region where the fast solar wind dominates at solar minimum) there is a large decrease of CR particles. This is because less ACRs, which are accelerated in the equatorial regions, reach these high latitudes. For the heliospheric tail this is not as clear because of the interesting phenomenon that just after solar minimum, there is acceleration of particles at high latitudes. This occurs just below the so-called "tornado alley" which is an extension of a relatively high speed solar wind stream into the tail region (Scherer and Ferreira, 2005b). These authors showed that in this region at the termination shock, $\nabla \cdot \vec{v}$ is comparable to values in the equatorial regions of the nose, resulting in equally effective acceleration. However, this effect is depending on solar activity and disappears toward solar maximum conditions. Also of interest is the large modulation volume in the tail, and the symmetric distribution of CRs inside the termination shock, irrespective of solar activity (Langner and Potgieter, 2005a).

Showing time dependent modulation over all energies, in Fig. 27 computed spectra for the $A < 0$ polarity cycle (top panels) and for the $A > 0$ polarity cycle (bottom panels) are shown for galactic (left panels), anomalous (middle panels) and combined (right panels) proton intensities. From bottom to top the model solutions are plotted for 10, 60, 85 AU (which is the computed termination shock distance in the equatorial regions), and 120 AU (which is the computed heliopause distance at the stagnation line), respectively The solid lines correspond

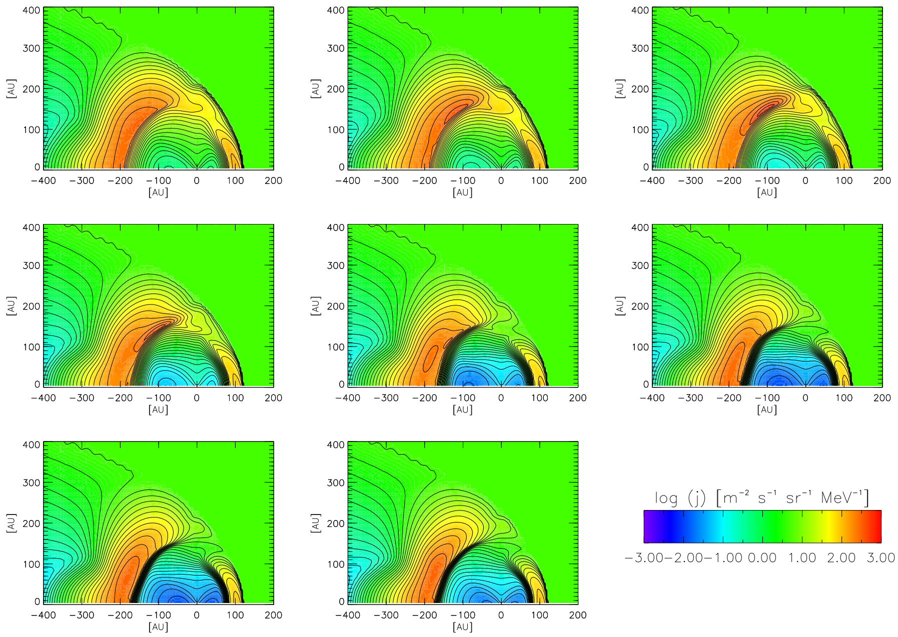

Figure 26. Computed 30 MeV ACR and GCR intensities in the meridional plane of the heliosphere. Results are shown as a series of snapshots corresponding to different solar activity conditions present in the heliosphere. The top left panel shows solar minimum, and then from left to right, bottom to top, each panel shows increasing solar activity with the middle panel at the bottom showing the cosmic ray distribution at solar maximum.

to solar minimum, and the dashed lines correspond to solar maximum conditions present in the heliosphere.

As solar activity increases, a reduction in the computed GCR intensities, as well as a reduction in the amount of particles accelerated at the termination shock occurs. The latter is especially evident for the $A < 0$ polarity cycle where, due to the reduction of drifts, CRs now enter the heliosphere from all latitudes and are not as effectively accelerated in the equatorial region where the compression ratio of the solar wind termination shock is the largest. Also for solar maximum conditions, low energy GCRs are much more modulated leading to lower intensities, compared to solar minimum, and, therefore, less particles are accelerated to higher energies. For the ACRs there are even less particles accelerated toward higher energies for both polarity cycles, as shown in the middle panels of Fig. 27. Concentrating on the spectrum at the shock, the model shows for the $A < 0$ polarity cycle, that, for the very low energies, there is not much difference between the computed intensities corresponding to different solar cycle conditions, due to the mono-energetic source which was specified at the termination shock.

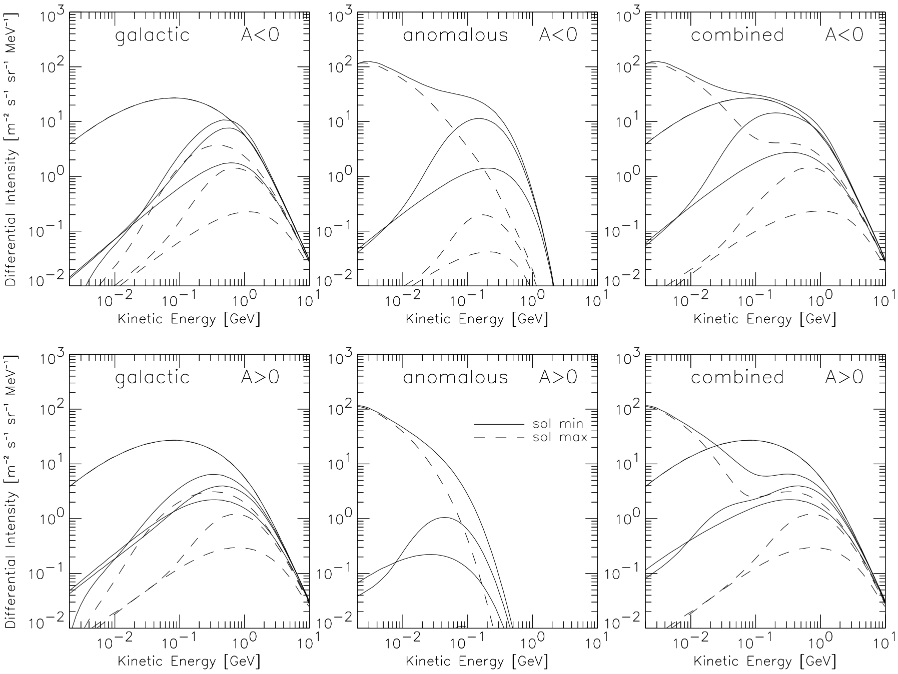

Figure 27. Computed spectra for the $A < 0$ heliospheric magnetic field polarity cycle (top panels) and $A > 0$ polarity cycle (bottom panels). Shown are computed galactic (left panels), anomalous (middle panels) and combined (right panels) proton spectra. Model solutions are shown from bottom to top at 10, 60, 85 AU (which is the computed termination shock distance at the stagnation line), and 120 AU (which is the computed heliopause distance in direction to the heliospheric nose). The solid lines correspond to computed intensities with solar minimum conditions, and the dashed lines correspond to solar maximum conditions present in the heliosphere

For increasing energy the two spectra at the shock start to diverge because of the different modulation conditions, resulting in e.g. a factor of ∼10 less particles at 100 MeV for solar maximum conditions. For the inner heliosphere, e.g. inside 10 AU, the effect of increasing modulation results in even a larger reduction of particle intensities reducing number of anomalous particles by a factor of ∼35 during solar maximum. For the $A > 0$ polarity cycle, the difference between the accelerated spectra at the shock, due to different heliospheric conditions, are not as pronounced. However, for regions inside the termination shock, especially in the inner heliosphere, the ACRs completely disappears (Lanzerotti and Maclennan, 2000; Reames and McDonald, 2003).

For the combined intensities it is shown that the solar modulation amplitude is depending on distance and rigidity (Webber and Lockwood, 2001; Webber and Lockwood, 2004). For example, at 200 MeV the ratio between the computed combined intensities for solar minima and solar maximum conditions at 10 AU is a factor $\sim$10, at 60 AU it is a factor $\sim$4, and it decreases towards the heliopause. Also shown is that for solar maximum conditions the computed combined spectra for both polarity cycles are almost the same for all distances. This is expected because of the reduction of drifts in the model via the compound approach which is essential in explaining charge-sign dependent modulation (Ferreira and Potgieter, 2004; Ndiitwani et al., 2005).

Part VI

Magnetospheric and Atmospheric Effects

12. Shielding by the Earth's Magnetosphere and Atmosphere

12.1. Cosmic Ray Propagation in the Earth's Magnetic Field

The Earth's magnetic field shields us partly against galactic cosmic rays and solar particles. The lower energy limit needed for a charged particle to cross the Earth's magnetosphere and access a specific position at the top of the atmosphere decreases with the geomagnetic latitude of the observer, resulting in a cosmic ray flux on Earth increasing pole-ward. The cosmic ray flux dependence on the geomagnetic latitude was already observed shortly after World War II. Fig. 28 represents the variation of the flux of fast neutrons in the atmosphere with geomagnetic latitude measured by Simpson (1951, 2000).

As a first approximation, the geomagnetic field can be represented by a dipole centered on the Earth with an axis tilted approximately 11° to the spin axis of the Earth. In reality the geomagnetic field is much more complex than a dipole. It is the result of the interaction of the solar wind with the Earth's internal magnetic field and ionosphere (McPherron, 1995). From this complex interaction several dynamical magnetospheric current systems develop, resulting in several modifications of the Earth's magnetic field, among which are the compression of the magnetic field lines in the day-side and their stretching in

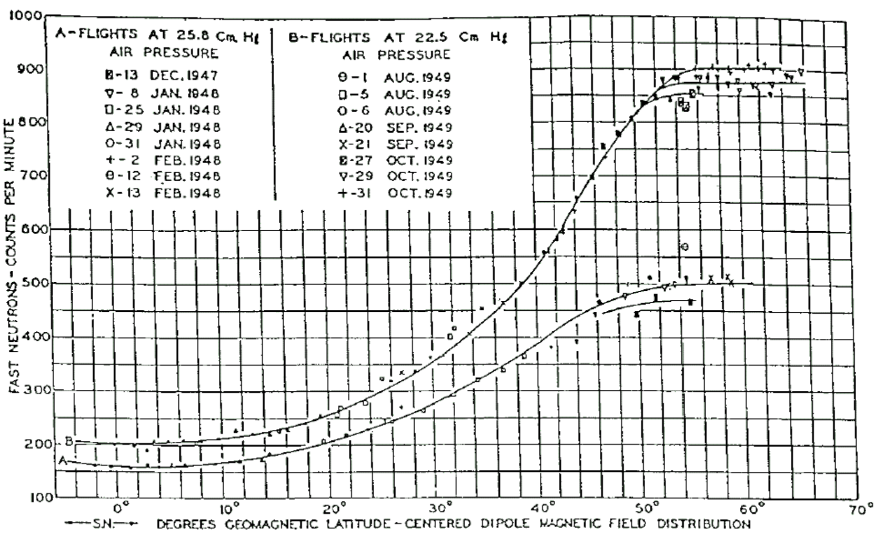

Figure 28. Geomagnetic latitude dependence of fast neutrons as observed by Simpson (1951), taken from Simpson (2000).

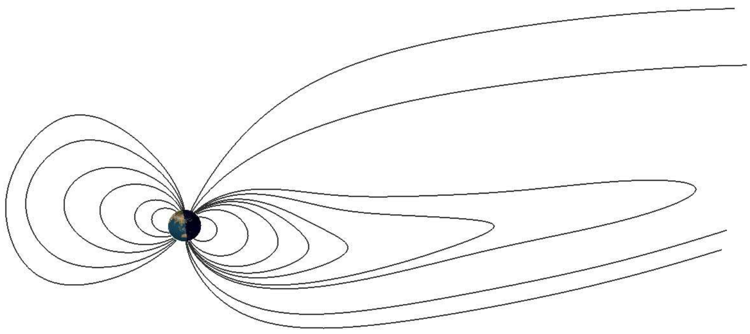

Figure 29. Configuration of the Earth's magnetosphere at 9 a.m. on January 1, 2005 as obtained by using the IGRF and Tsyganenko96 models for describing the internal and external geomagnetic field respectively (Langel, 1992; Tsyganenko, 1996). The different lines represent magnetic field lines which cross the Earth's surface on the noon-midnight meridian.

the night-side, leading to a magnetosphere configuration as illustrated in Fig. 29. The external geomagnetic field, also called the magnetospheric magnetic field, refers to the magnetic field induced by the magnetospheric currents. The International Geomagnetic Reference Field (IGRF) model represents the most frequently used model of the Earth's internal magnetic field for the period 1900 to the present (Langel, 1992). It is a spherical harmonic model, with coefficients derived from magnetic field measurements from geomagnetic stations, ship-towed magnetometers, and satellites. The spherical harmonic coefficients for a given period are obtained by interpolating and extrapolating the different IGRF parameters released every five years by the International Association of Geomagnetism and Aeronomy (IAGA). From continuous satellite measurements, different models of the external magnetic field depending on geomagnetic activity and solar wind parameters have also been developed (Olson and Pfitzer, 1982; Tsyganenko, 1989; Tsyganenko, 1995; Tsyganenko, 1996; Tsyganenko, 2002; Tsyganenko et al., 2003; Tsyganenko and Sitnov, 2005; Ostapenko and Maltsev, 2000; Alexeev and Feldstein, 2001; Feldstein et al., 2005).

For the study of the interaction of cosmic rays with the Earth's environment it is important to quantify the cutoff rigidity, which represents roughly the lowest rigidity limit above which cosmic rays can cross the Earth's magnetosphere and reach a specific position from a specific observational direction (Cooke et al., 1991). For the purpose of the study of solar energetic particles observed on Earth during Ground Level Enhancement (GLE) or for the study of cosmic ray anisotropy, it is also important to determine the asymptotic direction of a cosmic ray particle, which represents its direction of motion before entering into the magnetosphere. By approximating the geomagnetic field by a geocentric dipole, the cutoff rigidity is expressed by the Störmer cutoff formula:

$$R_c = \frac{M \cos^4 \lambda}{r^2(1 + (1 - \cos^3 \lambda \cos \epsilon \sin \eta))^2} \tag{52}$$

where M is the dipole moment, r is the distance from the dipole center, λ is the geomagnetic latitude, ϵ is the azimuthal angle measured clockwise from the geomagnetic east direction (for positive particles), and η is the angle from the local magnetic zenith direction (Cooke et al., 1991). Störmer (1950) studied theoretically the motion of charged particles in the geomagnetic dipole. Unfortunately, the Störmer formula gives only a first order approximation of the cutoff rigidity. For more precise estimation of the cutoff rigidity and for computing the asymptotic direction of incidence, backward trajectory tracing codes, which combine the IGRF model and an external magnetospheric model of the Earth, are needed (Flückiger and E., 1990, Smart et al., 2000 and references therein). In these codes the trajectories of cosmic rays with different rigidities, arriving at the same observing position and from the same direction of incidence, are computed backward in time as illustrated in Fig. 30. The curves labeled 1, 2, 3, and 4 represent the trajectories of positively charged particles with a rigidity of 20, 10, 5, and 4.5 GV respectively. In this case all the trajectories are initiated in the vertical direction at 20 km altitude above Jungfraujoch Switzerland. Particles with high rigidities (trajectory 1,2) have small trajectory bending before escaping the Earth's magnetosphere. A particle with 5 GV rigidity is bent stronger but can still escape the Earth's magnetosphere. The trajectory labeled 4 makes several complex loops before reaching another point on the Earth's surface, illustrating that for this specific rigidity a cosmic ray can not reach the Jungfraujoch location. Some trajectories not shown here, which neither go back to the Earth nor leave the magnetosphere, can also be observed. Trajectories that do not leave the Earth's magnetosphere are called forbidden trajectories while those of particles escaping the Earth's magnetosphere are called allowed trajectories. The direction of motion at the position where an allowed trajectory crosses the magnetopause represents the asymptotic direction of incidence.

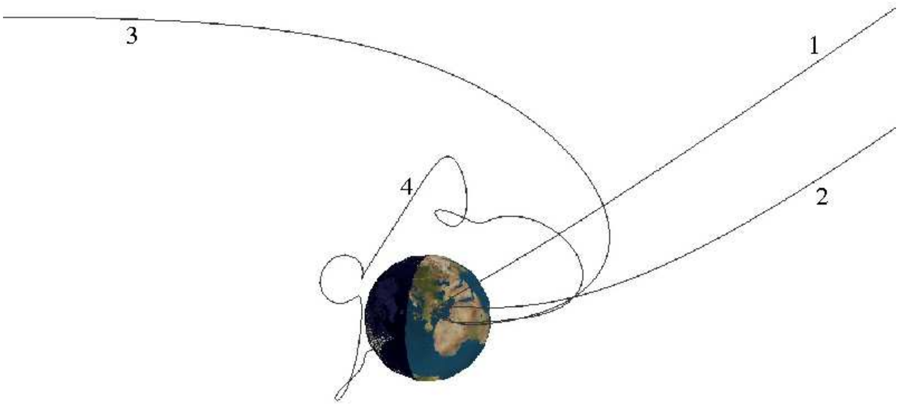

Figure 30. Illustration of the backward trajectory technique used for computing cutoff rigidity and asymptotic direction of incidence. See details in text.

For a specific direction of incidence, backward trajectories are computed generally for a set of rigidities spanning a large range of values with a constant rigidity interval δR (usually 0.01 GV). From these computations three rigidity regions are identified: i) a high rigidity region where all trajectories are allowed, ii) a low rigidity region where all trajectories are forbidden and, iii) an intermediate region called the penumbra where bands of allowed trajectories are separated by bands of forbidden ones. The rigidity of the last allowed computed trajectory before the first forbidden one is called the upper cutoff rigidity R_U. The rigidity of the last allowed trajectory, below which all trajectories are forbidden, is called the lower cut-off rigidity R_L. Finally, the effective cutoff rigidity R_C is given by $R_C = R_U - n\delta R$, where n represents the number of allowed trajectories in the penumbra. The reader will find a complete description of the asymptotic direction computation method and cosmic ray cutoff terminology in Cooke et al. (1991).

Figure 31 displays the vertical effective cutoff rigidity as a function of latitude and longitude on Earth obtained with the MAGNETOCOSMICS code (Desorgher, 2004). This kind of map is periodically published for 20 km and 450 km altitudes, and for different geomagnetic activities (Smart and Shea, 1997; Smart et al., 1999a; Smart et al., 1999b). For the analysis of the measurements of most ground-based cosmic ray experiments, where mostly vertically incident particles contribute to the counting rate, it is sufficient to consider that only cosmic rays with rigidity higher than the vertical effective cutoff rigidity R_C can reach the top of the Earth's atmosphere from all directions of incidence. However at high latitude and for positions with high cutoff rigidity, the contribution of non vertical particles becomes important and the variation of R_C with the direction of incidence must be taken into account (Clem et al., 1997). In the left panel of Fig. 32 we illustrate the difference obtained in the mean solar activity galactic proton flux penetrating the atmosphere at mid-latitude if R_C is considered as being constant (thin solid line) or as varying with the direction of incidence (thick solid line). The dashed line represents the flux outside the magnetosphere. The right panel represents the variation of the flux with the azimuth direction if R_C is considered as varying with the direction of incidence. Note that for each azimuth the flux is integrated over the zenith angle. The well-know east-west asymmetry is clearly observed. Our computation of GCR induced atmospheric ionisation shows that for these specific conditions the ionisation is overestimated by roughly 10 % in the higher part of the atmosphere (depth$<$ 100gcm^{-2}) if the dependence of R_C on the direction is not considered.

When studying the long term influence of cosmic rays on the Earth's environment, it is important to take into account the variation of the geomagnetic field during the past. Barraclough (1974) published spherical harmonic models of the geomagnetic field for eight epochs between 1600 and 1910. By computing vertical cutoff rigidity using these models, (Shea and Smart, 2004) have estimated that the decrease of the geomagnetic field over the last 400 years has probably induced a 10% increase of the cosmic ray flux on Earth. Archeomagnetic data have been used in various studies to quantify the variation of the geomagnetic dipole moment over the last 50 000 years and 12 000 years (McElhinny and Senanayake, 1982; Yang et al., 2000). Laj et al. (2000) and Laj et al. (2002), have used sediments, archeomagnetic and volcanic data for deducing the variation of the geomagnetic dipole over the last 75 000 years. Wagner et al. (2000) and Muscheler et al. (2005a) have deduced from cosmogenic radionuclide data the variation of the geomagnetic dipole moment over the past 60 000 years. In their studies the measured concentration of radionuclides in natural archives is considered to be an indirect proxy of the geomagnetic shielding and therefore of the geomagnetic dipole (see section 13). In all reconstruction methods of the past geomagnetic field over the millennium time scale cited above, the Earth's magnetic field is considered to be a geocentric dipole. As already said it is only a first order approximation and if possible the non dipole component of the geomagnetic field should also be taken into account to quantify the geomagnetic shielding. The importance of

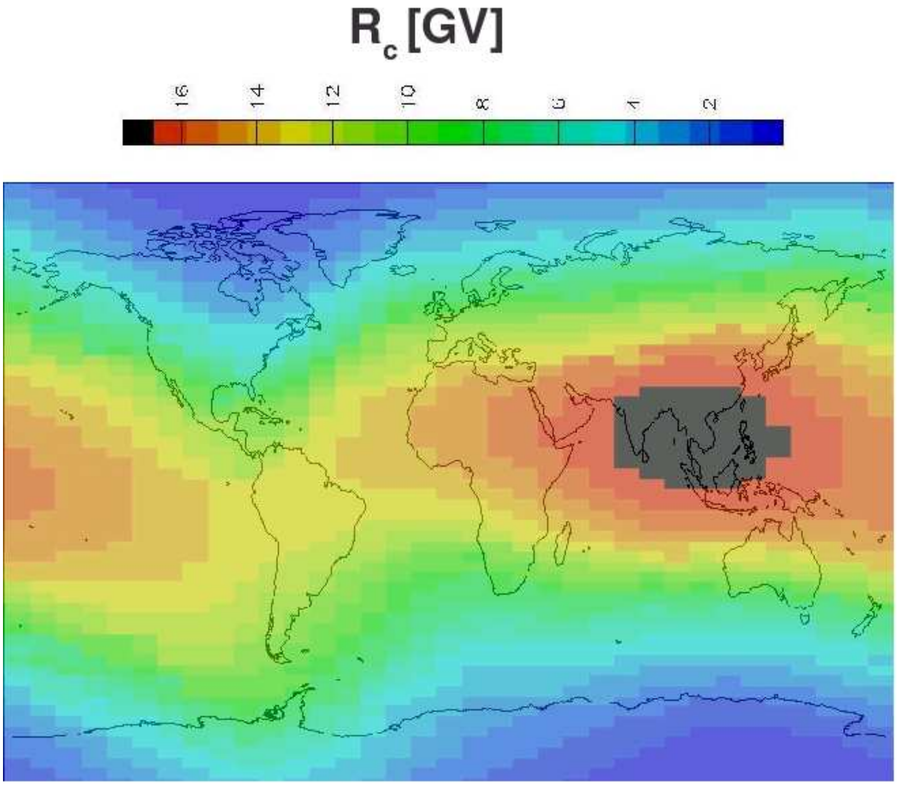

Figure 31. Variation of the vertical effective cutoff rigidity as a function of latitude and longitude of the observer at 20 km altitude and for the time period 1982. The cutoff rigidities were computed with the MAGNETOCOSMICS code and by using the IGRF model. (Desorgher, 2004).

the non-dipole component when quantifying the geomagnetic shielding during the past has been discussed by Flückiger et al. (2003) and Shea and Smart (2004). Very recently, Korte and Constable (2005b) and Korte and Constable (2005a) have released the first spherical harmonic model of the geomagnetic field for the last 7000 years. They have shown that the dipole component of their model follows the same time variation trend but is significantly smaller than the dipole moments obtained by Yang et al. (2000), and McElhinny and Senanayake (1982). No comparison of the geomagnetic shielding obtained with the various past geomagnetic field models has been published yet.

12.2. Cosmic Ray Interaction in the Atmosphere

In addition to the Earth's magnetosphere, the Earth's atmosphere shields us partly against galactic and solar cosmic rays. Experiments in

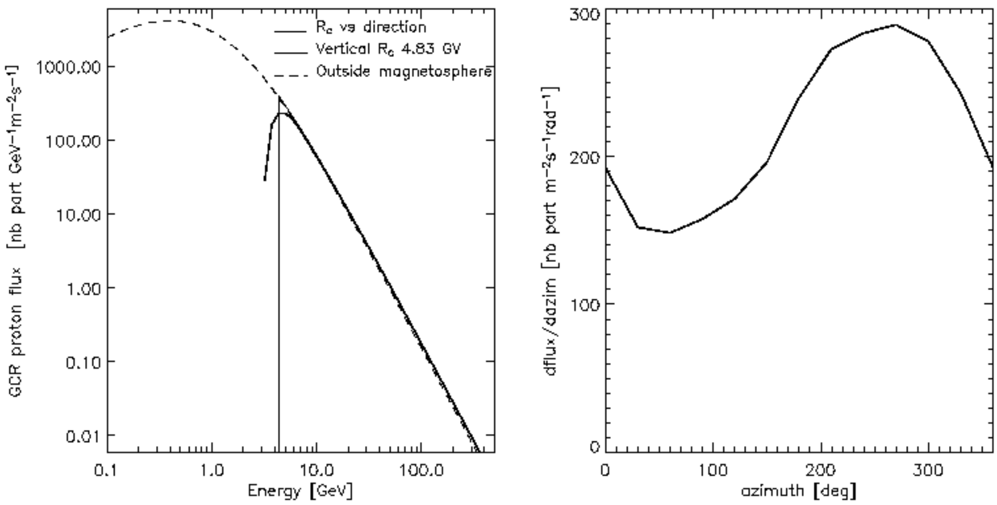

Figure 32. The left panel represents the mean solar activity GCR proton flux at the top of the atmosphere at 45° N latitude and 0° longitude, computed by considering the effective cutoff rigidity R_c either as varying with the direction of incidence (thick solid line) or as being constant for all directions (thin solid line). The dashed line represents the flux of GCR protons outside the magnetosphere. The right panel represents the computed azimuthal variation of the GCR proton flux at the top of the atmosphere that is obtained if the variation of R_C with the direction of incidence is taken into account. The flux at a given azimuth is integrated over the zenith angle. The east and west directions correspond to 90° and 270° azimuth respectively.

space can resolve the individual chemical elements and isotopes of the cosmic radiation over an extended element and energy range. Hydrogen and helium nuclei are the dominant elements, constituting ∼98% of the cosmic ray ions. As an example Fig. 33 sketches typical cosmic ray energy spectra observed in interplanetary space near the Earth (from http://helios.gsfc.nasa.gov/ace/gallery.html).

At energies below a few tenth of keV/nuc and above several GeV the solar wind and the galactic cosmic ray component are dominant. In the intermediate energy range particle intensities can vary by orders of magnitude during the 11 year solar activity cycle. The populations indicated in Fig. 33 by corotating and anomalous cosmic rays are observed around solar minimum and represent particles that are accelerated in corotating interaction regions (Heber et al., 1999, and references therein) and at the termination shock (Fichtner, 2001, and

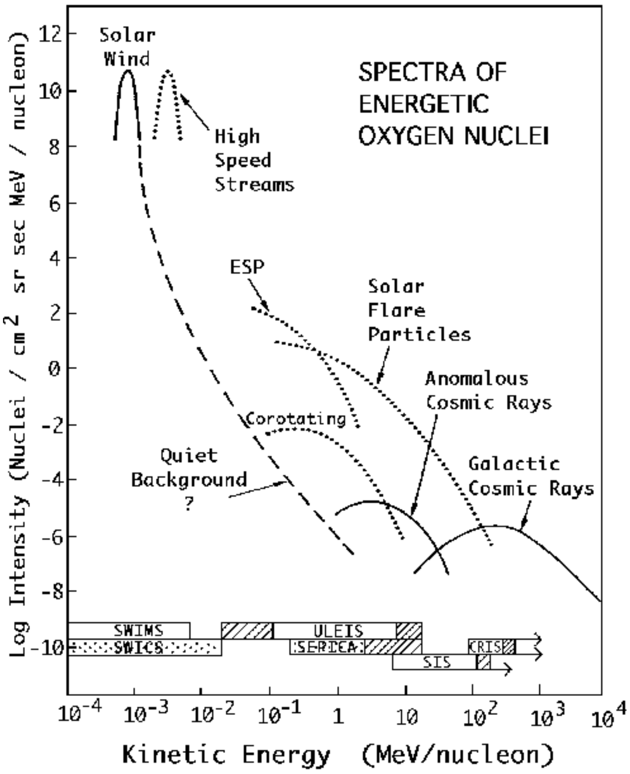

Figure 33. Typical oxygen energy spectra in interplanetary space close to the Earth (from http://helios.gsfc.nasa.gov/ace/gallery.html).

references therein), respectively. Energetic storm particles (ESP) and solar flares particles occur sporadically and most likely around solar maximum. Protons in these solar energetic particle populations have energy spectra that span the region from about 10 keV to above 10 GeV. However, solar events producing protons with energies above 1 GeV are rare. Due to the geomagnetic shielding solar energetic particles with energy < 100 MeV can only reach the Earth's atmosphere over polar regions. When these particles hit the atmosphere they loose their energy mainly due to ionization, leading to the production of different trace gases, as discussed below. While the intensity of solar cosmic rays decreases strongly with energy, the spectra of galactic cosmic ray ions have maxima at several hundred MeV/nuc (Heber, 2001; Heber and Potgieter, 2000, and references therein). A GCR particle that penetrates into the Earth's atmosphere interacts by electromagnetic and nuclear processes with the atoms of the atmosphere, resulting in a cascade of secondary particles also called a cosmic ray shower, as

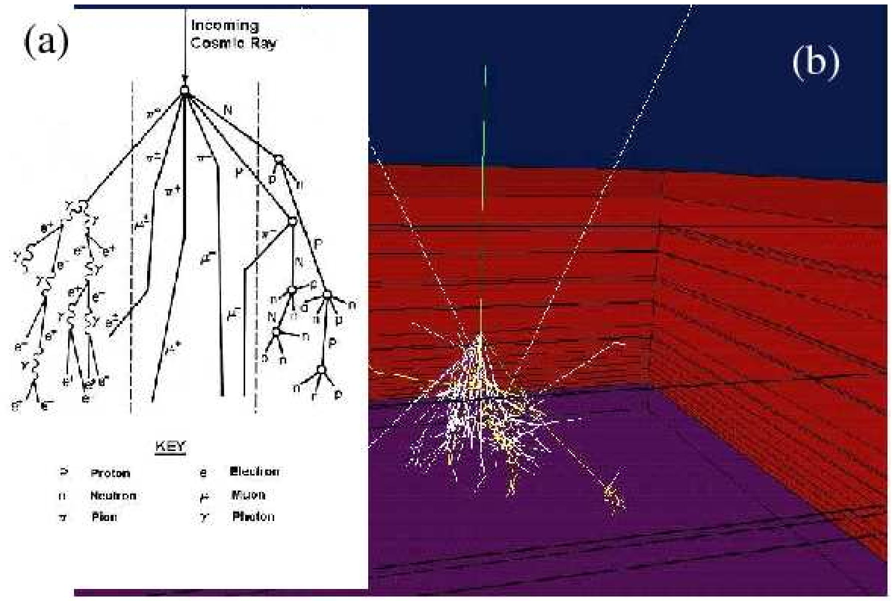

Figure 34. (a) Schematic view of a typical particle shower that develops when a cosmic ray interacts with the Earth's atmosphere. (b) Simulation with the ATMOCOSMICS code of 10 cosmic ray showers resulting from the interaction of 10 protons of 10 GeV energy with the Earth's atmosphere Desorgher et al. (2003).

illustrated in Fig. 34, see also the following section. If the primary cosmic ray has an energy greater than 500 MeV the cosmic ray shower can reach the Earth's surface where the secondary particles may be detected by ground based cosmic ray experiments. A description of the different interactions involved in the development of a cosmic ray shower can be found for example in (Wolfendale, 1973; Stanev, 2004; Grieder, 2001).

The effects of energetic particles on the Earth's environment are various. Some of these effects are listed below:

1. Below 50 km altitude the cosmic ray shower particles are the main source of ionization in the atmosphere. As explained in the previous section, it has been proposed that the galactic cosmic ray induced atmospheric ionization plays a key-role in the formation of clouds in the troposphere and therefore that the cosmic ray flux could represent an important driver to explain the long term variation of the climate on Earth.

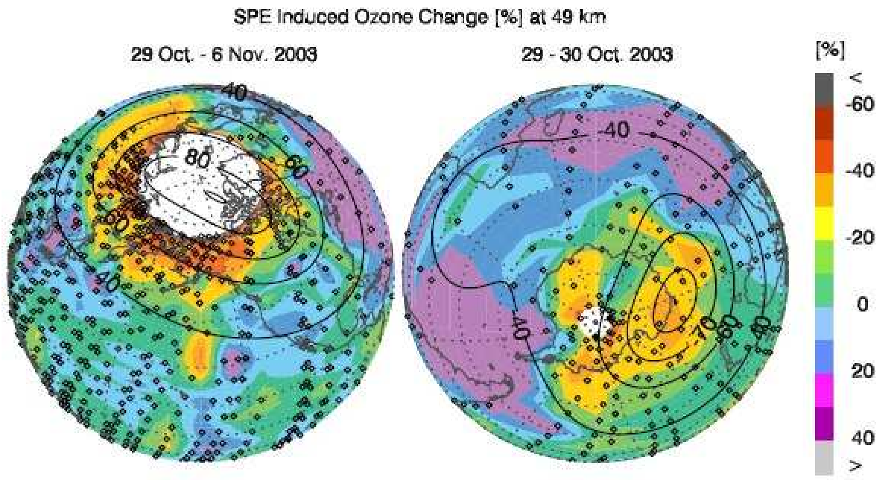

Figure 35. Changes in ozone concentration in the Earth's atmosphere at 49 km altitude during the October-November 2003 solar proton events. For details see Rohen et al. (2005).

2. Solar energetic particles are the sources of ozone loss in the upper atmosphere (Callis et al., 1998; Jackman et al., 2000). The ionization and dissociation of the neutral atmosphere induced by charged particle precipitation leads to the formation of NO_x (N, NO, NO_2) (Crutzen et al., 1975; Porter et al., 1976; Heath et al., 1977) and HO_x (Solomon et al., 1981), which in turn destroy the ozone. Figure 2 shows the change in ozone concentration at 49 km altitude during the October-November 2003 solar proton events in both hemispheres relative to a reference period before the large events occurred. Also shown are isolines of different magnetic latitudes. From that figure it is evident that the solar particles caused a significant ozone loss in both hemispheres. While most authors consider only the interaction of solar energetic protons with the atmosphere, Schröter et al. (2005) computed the atmosphere ionization during the solar particle event on June 14th 1989, including the electron component. Their calculations shows a two times stronger ion pair production at altitudes between 50 km and 90 km.

3. Cosmogenic nuclides are produced in the atmosphere by the interaction of secondary cosmic ray protons and neutrons with atmospheric nuclei. The measurements of their concentrations in natural archives allows in particular to study the variation during the past of the cosmic ray flux and of the Earth's climate (see section 13).

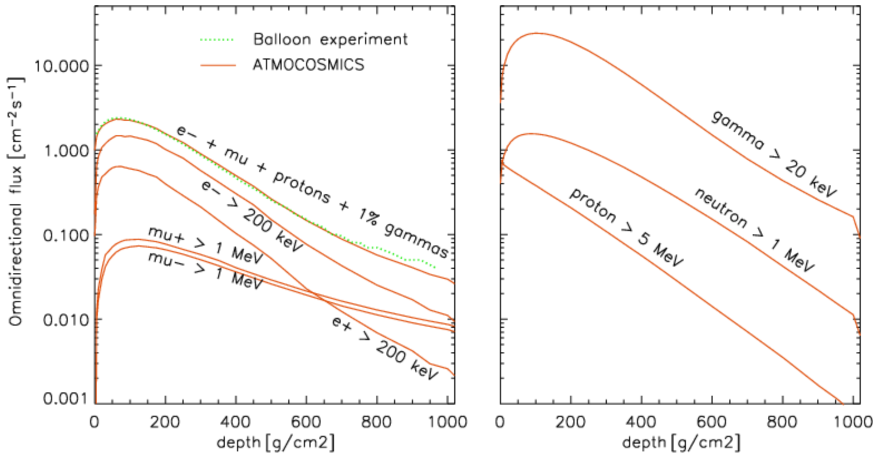

Figure 36. The solid lines represent the ATMOCOSMICS computed flux of cosmic ray shower particles vs atmospheric depth over Moscow during solar maximum activity. The dotted line in the left panel represents the year 2000 averaged flux of cosmic ray measured over Moscow by the balloon experiment from the Lebedev Physical Institute (Bazilevskaya et al., 1991). This experiment is sensitive to fluxes of electrons with energy > 200 keV, protons with energy > 5 MeV, muons, and 1% of gamma rays with energy > 20 keV. The upper most solid line in this panel represents the total flux of these particles computed with ATMOCOSMICS. From (Desorgher et al., 2005)

To quantify the effect of cosmic rays on the Earth's environment it is important to know precisely the flux of cosmic ray shower particles in function of position, atmospheric depth, and time. For this purpose complex codes that simulate the transport of cosmic rays through the Earth's atmosphere have been developed by several groups and validated with experimental data (O'Brien, 1979; Velinov et al., 2001; Zuccon, 2002; Clem et al., 2003; Webber and Higbie, 2003; Lei et al., 2004; Desorgher et al., 2005; Schröter et al., 2005). One of this code is the Monte Carlo ATMOCOSMICS[2] code, based on Geant4 (Geant4 Collaboration et al., 2003), that allows to simulate the hadronic and electromagnetic interaction of energetic particles (< 1 TeV) with the Earth's atmosphere (Desorgher et al., 2003; Desorgher et al., 2005). As an example Fig. 34 displays on the right simulation results of the interaction of 10 GeV protons with the Earth's atmosphere obtained with ATMOCOSMICS.

Desorgher et al. (2005) simulated with ATMOCOSMICS the interaction of galactic cosmic ray protons with energy < 1 TeV with the Earth's atmosphere over Moscow during solar maximum activity. In

[2] It is now part of the PLANETOCOSMICS program which is available from http://cosray.unibe.ch/∼laurent/planetocosmics.

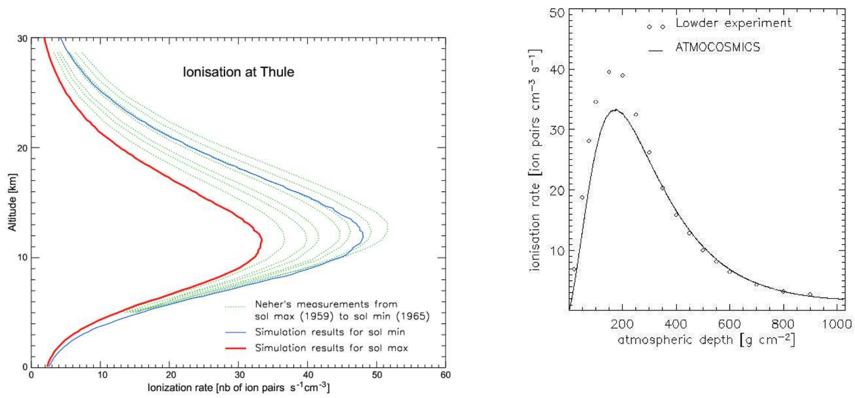

Figure 37. Left: The thin and bold solid lines represent the ATMOCOSMICS computed atmospheric ionization rate induced by galactic cosmic rays (GCR) over Thule during the minimum and maximum of solar activity, respectively (Desorgher et al., 2005). The dotted lines represent the atmospheric ionization rate measured over Thule by Neher (1971) from 1959 to 1965. Right: Atmospheric ionization rate induced by GCR over Durham NH in May 1969 as computed by ATMOCOSMICS (solid line) and measured by (Lowder et al., 1971) (diamonds).

both panels of Fig. 36 the solid lines represent the computed flux of different types of secondary particles versus atmospheric depth.

The dotted line in the left panel of 36 represents the yearly averaged flux of cosmic ray shower particles measured over Moscow by the balloon experiment of the Lebedev Physical Institute (Bazilevskaya et al., 1991). The upper most solid line represents the ATMOCOSMICS computed total flux of particles at which this experiment is sensitive (e.g. electrons with energy $> 200\,\mathrm{keV}$, protons with energy $> 5\,\mathrm{MeV}$, muons, and 1% of gamma rays with energy $> 20\,\mathrm{keV}$). It can be seen that a very good agreement was obtained between the simulation results and the experimental data.

In order to investigate the cosmic ray cloud hypothesis several groups have computed the GCR induced atmospheric ionization by using cosmic ray transport codes (Usoskin et al., 2004a; Pallé et al., 2004; Desorgher et al., 2005). In most of these codes the computed energy deposited by cosmic ray showers in the Earth's atmosphere is converted into an ionization rate by considering a $\sim$35 eV mean ionisation energy. In Fig. 37 the ATMOCOSMICS computed atmospheric ionization rate induced by GCR over Thule (left panel) for minimum and maximum solar activity, and over Durham NH in May 1969 (right panel), are compared to experimental data from Neher (1971) and Lowder et al.

(1971), respectively. A good agreement between the simulation results and the measurements is obtained.

In conclusion complex transport codes like MAGNETOCOSMICS and ATMOCOSMICS simulating the interaction of cosmic rays with the Earth's magnetosphere and atmosphere have to be used to better understand and quantify the effect of cosmic rays on our environment.

13. Cosmic Ray Flux and Cosmogenic Isotopes

Primary cosmic rays are charged particles, which impinge on Earth with relativistic energies (i.e., above 0.1 GeV). Most of these originate from outside the solar system (i.e. GCRs), while the remainder, with lower energies, originate from the Sun (i.e. SEPs), see Masarik and Reedy (1995). Secondary cosmic-rays are produced through the interaction of primary cosmic rays with atmospheric and terrestrial nuclei, and include strongly interacting particles (e.g. neutrons, protons and pions), weakly interacting particles (e.g. muons and neutrinos), electromagnetic radiation (photons), positrons and electrons. Secondary neutrons are responsible for the majority of nuclear transformations in which cosmogenic nuclides are produced (Lal, 1991). Neutrons may be classified by energy according to the types of nuclear reactions in which they are involved (Masarik and Reedy, 1995):

– *High-energy neutrons* are produced through direct reactions of primary and secondary cosmic-ray particles with terrestrial nuclei. They are capable of inducing spallation reactions, and range from primary energies of several GeV down to ca. 10 MeV.

– *Fast neutrons* are produced primarily from the de-excitation of nuclei following compound nucleus reactions produced through interaction with high-energy neutrons. A common mode of de-excitation is nuclear evaporation: the emission of neutrons and protons with kinetic energies in the range 0.1-10 MeV.

– *Slow neutrons* have kinetic energies in the order of 1 keV, and are produced from the slowing down of fast neutrons, through elastic and inelastic collisions with nuclei.

– *Thermal and epithermal neutrons* are produced from the slowing down of fast neutrons to energies similar to the vibrational motion of nearby molecules. An important characteristic is their relatively high probability of being absorbed by some nuclei. Thermal neutrons have an average energy of 0.025 eV at 20° C , while epithermal neutrons have energies between 100 eV and the cadmium cut-off energy for transparency to neutrons of 0.5 eV.

The development of accelerator mass-spectrometry (AMS) has increased the detection sensitivity for long-lived cosmogenic radionuclides, produced in nuclear reactions initiated by cosmic rays, by several orders of magnitude and allows us now to analyse with high resolution natural archives such as ice cores. The concentration of cosmogenic nuclides in these archives is the result of the interplay between three processes: production, transport and deposition. In order to make full use of the information stored in these archives, a detailed knowledge of the source functions of the cosmogenic nuclides is necessary.

Models have been developed that describe the production of nuclides by the interaction of cosmic ray particles with the main target elements of the atmosphere. The first extensive and pioneering work in this field by Lal and Peters (1967) was based on data from direct observations limited to a few years. Subsequently there have been a number of model calculations devoted to particle and cosmogenic nuclide production in the atmosphere (Hess et al., 1961; Newkirk, 1963; Lingenfelter, 1963; Oeschger et al., 1969; Light et al., 1973; O'Brien, 1979; Blinov, 1988; Masarik and Reedy, 1995), see also the previous section.

The good agreement between the calculated and measured ^{14}C production rates proves the reliability of the model approach. However, we have to take into account that the conditions affecting the cosmic ray propagation within the heliosphere are changing with time (quiet-Sun periods like during the Maunder Minimum (1645–1715 AD), low or high geomagnetic field intensity like during the Laschamp event about 40 ky BP).

The production rate of cosmogenic nuclides depends on the CRF. Time-dependent changes of the production rate are caused mainly by variations of the geomagnetic field intensity and the solar activity. From measurements of cosmogenic radionuclides with different half-lives and different irradiation histories in meteorites, the average galactic CRF was inferred to be constant within 10% during the last few million years (Vogt et al., 1990). The incident CRF on Earth is different from that incident on meteorites at least in one respect: the Earth's geomagnetic field prevents most low energetic cosmic-ray particles from interacting with the atmosphere.

Concentrations of cosmogenic nuclides observed in various archives on the Earth's surface are determined by their production, atmospheric mixing, and deposition processes. We concentrate here only on the pro-

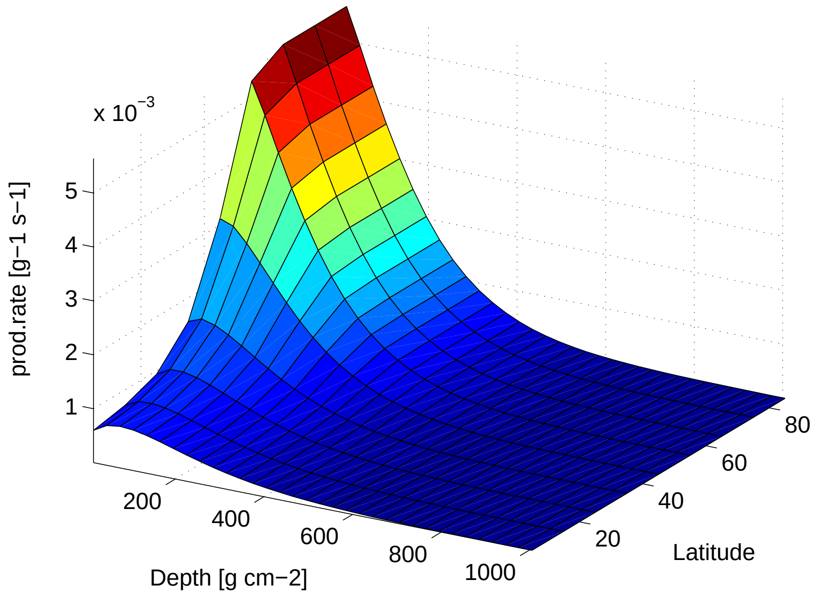

Figure 38. Dependence of the atmospheric ^{10}Be production rate on the depth and the latitude assuming the present magnetic field intensity and a solar activity of $F = 700\,\mathrm{MeV}$. The production rate is largest at high latitude high altitude and decreases with decreasing latitude for all depths in the atmosphere.

duction processes, which depend on both the latitude and the altitude (Fig. 38).

To simulate in detail the development of the secondary particle cascade in the atmosphere and to calculate the corresponding production rates of cosmogenic isotopes in the atmosphere, numerical models were developed. Among the most frequently used models are LCS (Prael and Lichtenstein, 1989), GEANT (Brun et al., 1987) combined with MCNP (Briesmeister, 1993), and MCNPX (Waters, 1999). These codes use only basic physical quantities and parameters, without including any free parameters, to numerically simulate all processes relevant in particle production and transport. This enables us to trace the fate of each individual particle and in doing so to study in detail the effects of various parameters on the production rate such as geomagnetic and solar modulation for a wide range of possible conditions. In spite of the fact that the above mentioned codes differ in the values of some physical parameters used in the simulations of elementary processes, they all represent the involved physics satisfactorily. Within the statistical errors, an equally good agreement between experimental and calculated production rates was obtained.

13.1. Calculation of Cosmogenic Nuclide Production Rates

The production rate of the cosmogenic nuclide j at depth D is

$$P_j(D) = \sum_i N_i \sum_k \int_0^k \sigma_{ijk}(E_k) \dot{J}_k(E_k, D) dE_k \tag{53}$$

where N_i is the number of atoms for target element i per kg material in the sample, $\sigma_{ijk}(E_k)$ is the cross section for the production of nuclide j from the target element i by particles of type k with energy E_k, and $J_k(E_k, D)$ is the total flux of particles of type k with energy E_k at location D inside the atmosphere. In our model, the particle fluxes $J_k(E_k, D)$ are calculated using the numerical codes. The cross sections $\sigma_{ijk}(E_k)$ were those evaluated from many measurements and used in earlier calculations. Some information related to the used cross sections is given below.

The main problem with the calculation of production rates using calculated fluxes and code-independent sets of cross sections for the particular nuclides, is the frequent lack of measured cross sections, especially for neutron-induced reactions.

13.2. Geometrical and Chemical Model of the Earth

All calculations based the Monte Carlo technique use a 3D-model of the Earth assumed as a sphere with a radius of 6378 km, and a surface density of $2\,\mathrm{g\,cm^{-3}}$. The composition of the Earth's atmosphere in weight fractions is: 0.755 N, 0.232 O, and 0.013 Ar. The errors resulting from the assumed average composition of the atmosphere and surface are also not significant because it was found (Masarik and Reedy, 1994) that, except for hydrogen, small changes in the abundance of the elements affect only little the calculated particle fluxes.

The Earth's atmosphere is modeled as a spherical shell with an inner radius of 6378 km and a thickness of 100 km. The atmospheric shell is usually divided into a certain number of concentric subshells of equal thickness ($\mathrm{g\,cm^{-2}}$), in order to get a depth dependence of particle fluxes. Each shell is divided into 9 latitudinal sections corresponding to steps of 10 degrees in magnetic latitude. The atmospheric pressure, density and temperature profiles are approximated by the U.S. Standard Atmosphere 1976, model (Champion et al., 1985) that approximates long-term mean conditions at low-mid latitudes, but cannot represent extremes such as Antarctica, where pressures fall 20–40 hPa below the Standard Atmospheric curve (Warren, 1999).

13.3. Cosmic Ray Particle Fluxes and Cosmogenic Nuclide Production

The simulation of particle production and transport processes in all numerical simulations begins with the choice of the primary particle type and its energy. The primary cosmic ray flux at the Earth's orbit has two components: galactic (GCR) and solar (SEP).

The GCR particles are a mixture of ≈87% protons, ≈12% α-particles and ≈ 1% of heavier nuclei with atomic numbers from 3 to ≈90 (Simpson, 1983). The spectral distributions of all particles look quite similar if they are compared in units of energy per nucleon. The propagation of the GCR particles to the Earth is influenced by many interactions that lead to spatial and temporal variations. The dominant effect is the heliospheric modulation, see part IV. Near the Earth during a typical solar cycle, the low energy part of GCR particle flux ($E <$ 1 GeV/nucleon) varies by an order of magnitude. With increasing energy, the modulation effect becomes weaker (Fig. 39).

Solar modulation is taken into account in the expression for the differential primary GCR proton flux. Most simulations use the Castagnoli and Lal (1980) formula for the differential spectra of GCR primary protons. Later another formula was suggested by Webber and Higbie (2003). The influence of solar modulation on cosmogenic nuclides is illustrated in Fig. 40.

For GCR alpha particles and heavier nuclei, analogous formulae hold with slightly different parameters (Lal, 1988). Since differences in cross sections for neutron and proton emission in reactions of primary GCR protons and alpha particles are very small, only interactions of protons are simulated and results are multiplied by factor of 1.44 to account for heavier nuclei. From the fitting of lunar experimental data (Reedy and Masarik, 1994), the effective long-term average flux of nucleons with energies above 10 MeV at 1 AU was determined to be 4.56 nucleons $\mathrm{cm}^{-2}\mathrm{s}^{-1}$.

Because of their relatively low energies, SEP can cause nuclear reactions in the Earth's atmosphere only at high geomagnetic latitudes (above 60°), and even there the nuclide production is restricted to the very top of the atmosphere. The long-term average production of cosmogenic nuclides by SEP is not expected to be significant. Some huge solar-particle events produce proton fluxes much higher than the average, and they could make a contribution to the production of some

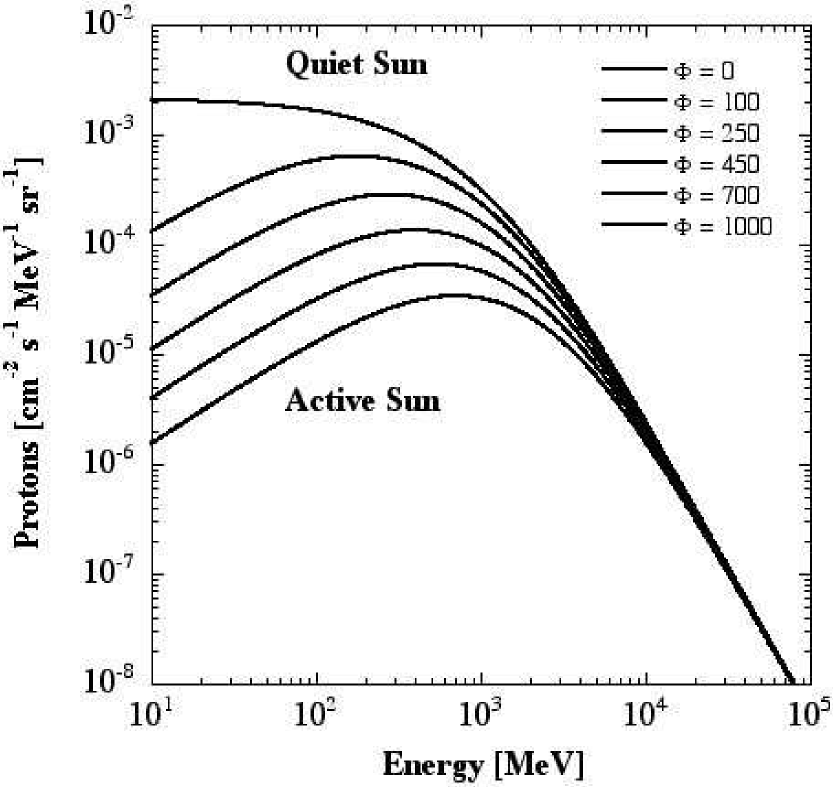

Figure 39. Differential primary proton spectra of the GCRs for different levels of solar activity expressed by the solar modulation parameter Φ.

cosmogenic nuclides (e.g. ^{7}Be and ^{36}Cl) observable in some layers in polar ice (^{36}Cl), such as from Greenland and Antarctica. Calculations confirming these expectations with the analysis of obtained results were published earlier (Masarik and Reedy, 1995).

13.4. The Geomagnetic Field and Cosmogenic Nuclide Production

The geomagnetic field, which is dominated by its dipole component, acts as a shield. It deflects incoming particles depending on their electric charge, energy, and angle of incidence. Depending on the geomagnetic latitude and angle of incidence, there is a critical energy below which cosmic-ray particles cannot penetrate into the Earth's atmosphere. This

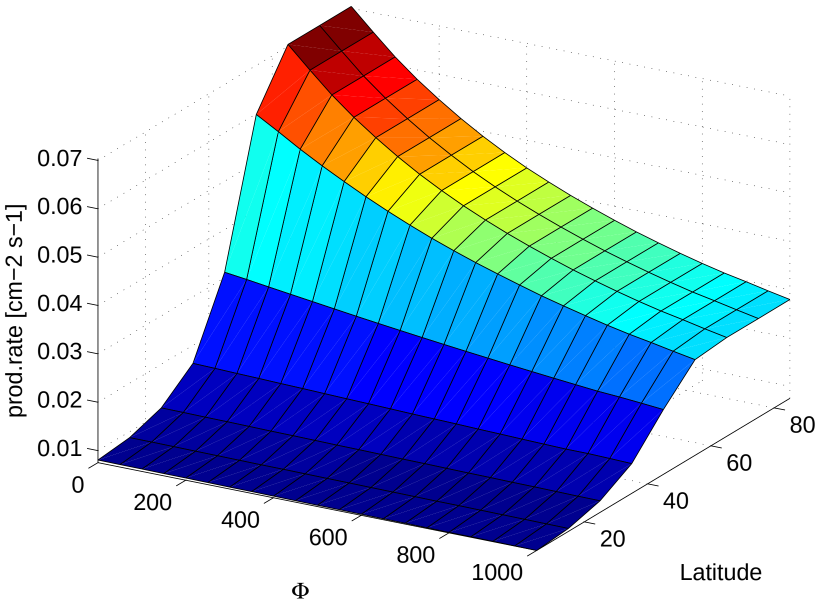

Figure 40. Dependence of the depth integrated atmospheric ^{10}Be production rate on the solar modulation Φ and the latitude. Due to the large cut-off rigidity at low latitudes solar modulation is largest at high latitudes.

leads to a latitudinal dependence of the primary and secondary particle fluxes and consequently also of the production rate of cosmogenic nuclides, with higher values around the magnetic poles and lower values in the equatorial region (Fig. 41). From paleomagnetic records, it is known that the geomagnetic field varied in the past in its intensity, direction, and polarity (Tauxe, 1993; Gosse et al., 1996; Yang et al., 2000).

Two main approaches to the characterization of geomagnetic field effects are used in theoretical estimates of cosmogenic nuclide production. The first is based on the relation between cosmic ray flux and the magnetic inclination and the second is based on the cut-off rigidities corresponding to a particular geomagnetic latitude. The most of theoretical models, especially Monte Carlo models, uses the second approach. The cut-off rigidity (R_c) describes the momentum to charge ratio above which these particles can penetrate the geomagnetic field and interact with the Earth's atmosphere. The value of R_c tends to increase with decreasing latitude, resulting in lower cosmic-ray intensities towards the equator (Graham et al., 2005).

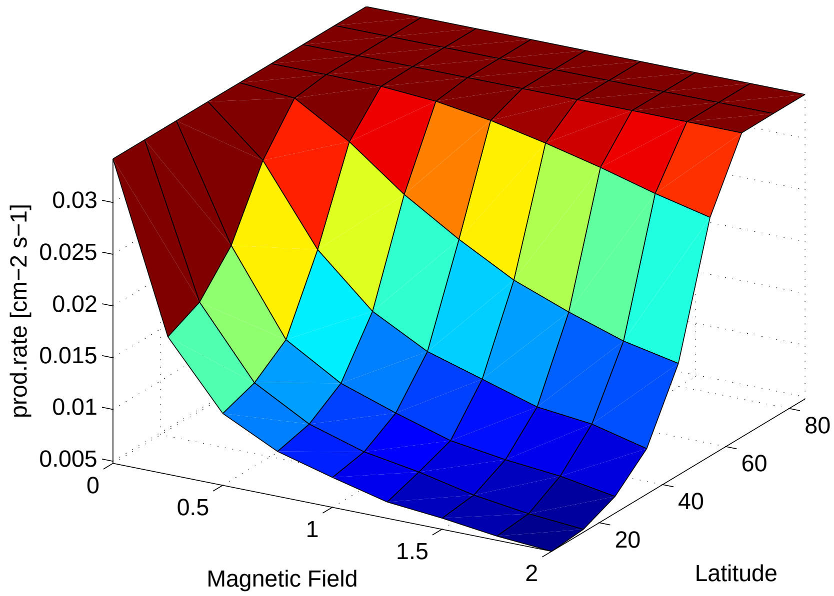

Figure 41. Dependence of the depth integrated atmospheric ^{10}Be production rate on the geomagnetic field intensity and the latitude. The field intensity is expressed in relative units with 1 for the present field intensity. The latitudinal production rates decrease with decreasing latitude for all field intensities larger than zero.

In a magnetic field with substantial non-dipolar components, such as the present geomagnetic field, there is always a “longitude effect” in cosmic-ray intensity. The primary flux is nearly omnidirectional and therefore a complete description of primary cosmic-ray access to the Earth requires calculation of cutoff rigidities for all angles of incidence (Clem et al., 1997). The reliability of R_c has been confirmed by numerous sea level latitude surveys (Moraal et al., 1989; Dorman et al., 2000).

Because direct measurements of the cosmic-ray intensity are collected in the present-day geomagnetic field, they should properly be ordered according to R_c. Unfortunately, R_c cannot be accurately calculated for the past 200–10 000 years because the geomagnetic field parameters are not known. However, if the long-term (>10 000 years) behaviour of the Earth’s magnetic field can be approximated by an axial dipole field, as is often assumed (Fraser-Smith, 1985) then geomagnetic latitude is equivalent to geographic latitude over the long-term and R_c can be estimated (Desilets et al., 2001).

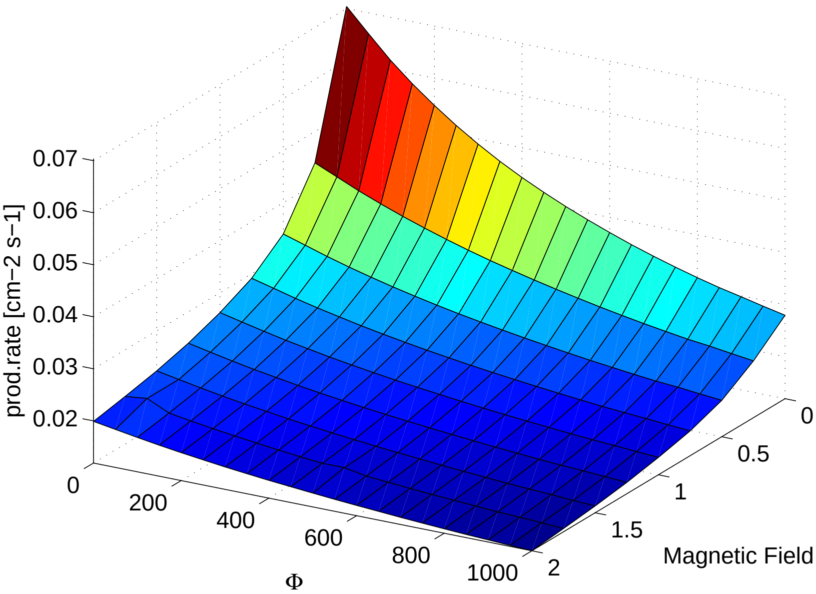

Figure 42. Dependence of the mean global production rate of ^{10}Be in the Earth's atmosphere on the geomagnetic field intensity and solar modulation parameter Φ. The dynamic range of the production rate between extreme situations (no solar modulation, no magnetic field and high solar modulation, doubled magnetic field intensity) is almost an order of magnitude.

In order to adjust our CRF data to a common time line, we need to be able to predict the relative variation in terrestrial cosmic-ray flux with solar modulation. Hence, we have attempted to quantify the variation of production rates as a function of solar modulation and geomagnetic field intensity. In order to investigate the influence of geomagnetic field variations on particle fluxes and cosmogenic nuclide production rates, the relative intensity of the geomagnetic field was varied from 0 to 2 relative to the present field, in steps of 0.25. The shape of the field was left unchanged. The resulting dependence is given in Fig. 42.

13.5. Cross Sections for Cosmogenic Nuclide Production

The main target elements in the atmosphere are nitrogen, oxygen and argon. For reactions on oxygen, the same cross sections were used as in the case of extraterrestrial material (Masarik and Reedy, 1994; Reedy and Masarik, 1994). For nuclear reactions on nitrogen and argon, experimental cross sections were used whenever possible. Otherwise they were estimated from similar reactions on other isotopes. For the tritium production the cross sections of Nir et al. (1966) were applied.

With the development of AMS also the production rates of some other nuclides, like ^{26}Al, ^{22}Na, and ^{32}Si, were measured. We did not calculate their production rates because there are no reliable cross sections available for them. Our calculated particle fluxes are accessible on the Web and can be used to calculate the production of any radionuclide provided the corresponding cross sections are available.

The uncertainties of the cross sections for nitrogen and argon are difficult to estimate because they have not been tested in extraterrestrial materials. The uncertainties of proton cross sections are probably within their measuring errors, which are usually below 10% for the latest data and 20% or even more for older data. The uncertainties in evaluated cross sections for neutron-induced reactions are unknown, but probably less than 50%. The reported uncertainties for the measured neutron cross sections are on the level of 25%. The lack of precise cross sections for the production of different nuclei from the target elements of interest represents the largest contribution to the uncertainty of these calculations.

Part VII

Cosmic Ray Imprints in Terrestrial Archives and Their Implications to Climate

14. Imprints in Earth's archives

Planets and moons are potential archives to store changes of the local interstellar medium over eons, with the Earth as a special archive. A major problem with the terrestrial archives, however, is the multiple influences of the complex geological and climatological processes, which make it hard to disentangle them and interstellar-terrestrial relations. Nonetheless, ice cores, sediments, tree rings, etc. are the only archives accessible without spacecraft. The best studied data sets are provided by the ^{14}C and ^{10}Be isotopes. ^{14}C is produced by the capture of a thermal neutron from the interaction of cosmic rays with the atmosphere (see part VI) in the reaction $^{14}\mathrm{N}(n,p)^{14}\mathrm{C}$, while ^{10}Be is a spallation product from nitrogen and oxygen. Both atoms quickly oxidize to C O $_2$ and Be O. The advantage of archives with these isotopes is their relatively high production rate (2.2 atoms $\mathrm{cm}^{-2}\,\mathrm{s}^{-1}$ for ^{14}C and 0.02 atoms $\mathrm{cm}^{-2}\,\mathrm{s}^{-1}$ for ^{10}Be) and their long half–lives ($^{14}\mathrm{C} \approx 5730$ yr and $^{10}\mathrm{Be} \approx 1.5\,\mathrm{kyr}$).

The two corresponding time series are not directly comparable, because ^{10}Be is bound by aerosols and washed out subsequently by precipitation within about year. In view of this short time scale, it serves as a tracer for a more regional production. The latter is higher over the magnetic poles, because the cosmic rays can deeper penetrate into the atmosphere following the magnetic field lines (see sec. 12). Therefore, ^{10}Be records may be best observed at high geo-magnetic latitudes, i.e. in polar ice-cores. ^{14}C oxidizes into atmospheric CO_2 which is connected to larger reservoirs and is deposited on a global scale due to the longer deposition time scale (Kocharov, 1991; Bard et al., 1997). These differences are shown in Fig. 43.

The solar cycle variations are clearly seen in Fig. 44. The two year delay of the ^{10}Be curve compared to that of the sunspot number is in good agreement with the lag of one year of the CR modulation and the one year atmospheric residence time.

The ^{10}Be records can be extended into the past, but the data analysis becomes more difficult and will not be discussed here see, e.g. (Beer et al., 1991). Nevertheless, the ^{10}Be records have been used to reconstruct the sunspot numbers as proxy for the solar cycle variations in the past, therefore, allow to estimate the CR-fluxes at Earth orbit. This in turn allows a reconstruction of the structure of the heliospheric shield in the past, or in other words, it should be possible to get observational hints on the history of the interstellar environmental changes (Scherer, 2000; Scherer et al., 2001a; Florinski and Zank, 2005).

Additional information can be gained from the ^{14}C records (radiocarbon) sampled from tree rings or other organics. There the problem

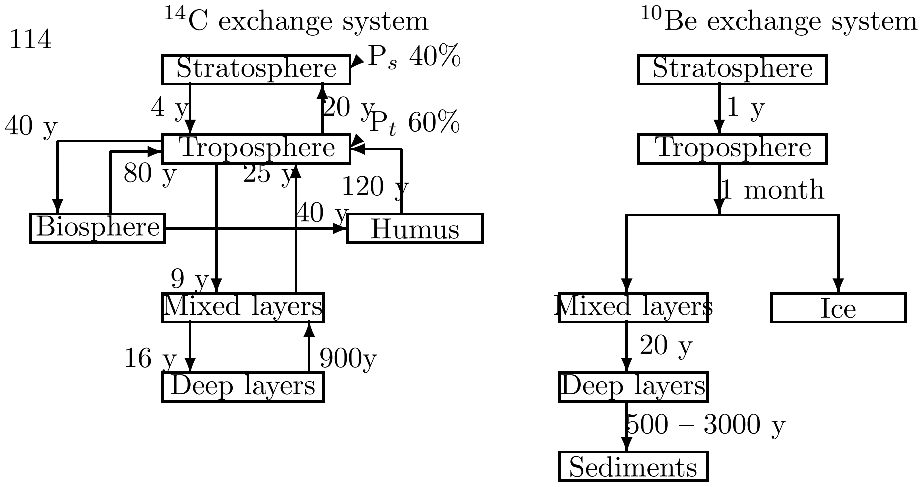

Figure 43. Difference in the ^{14}C and ^{10}Be transport from the atmosphere into archives. The figure gives the transfer times, and in the case of ^{14}C the relative production rates in the stratosphere P_s and in the troposphere P_t are presented.

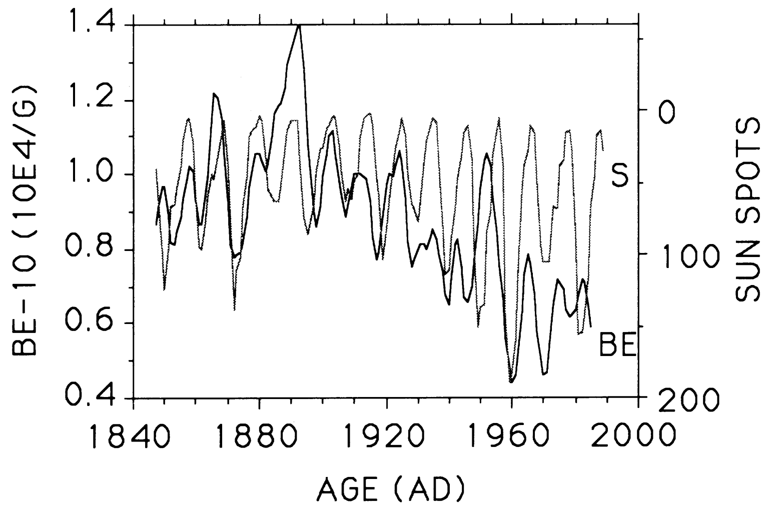

Figure 44. Solar cycle variation of ^{10}Be (thick line). The ^{10}Be data have been shifted by two years. The thin line is the smoothed sunspot number (Beer et al., 1991).

arises that the ^{14}C records are anticorrelated with the magnetic moment of the Earth, as indicated in Fig. 14. The data can be detrended and then show a nearly periodic behavior anticorrelated to the solar activity cycle.

Also for the centennial time scale exist indications of variable cosmic ray fluxes. An example is shown in Fig. 46, where it is evident that during the Maunder Minimum the production of cosmogenic ^{14}C has

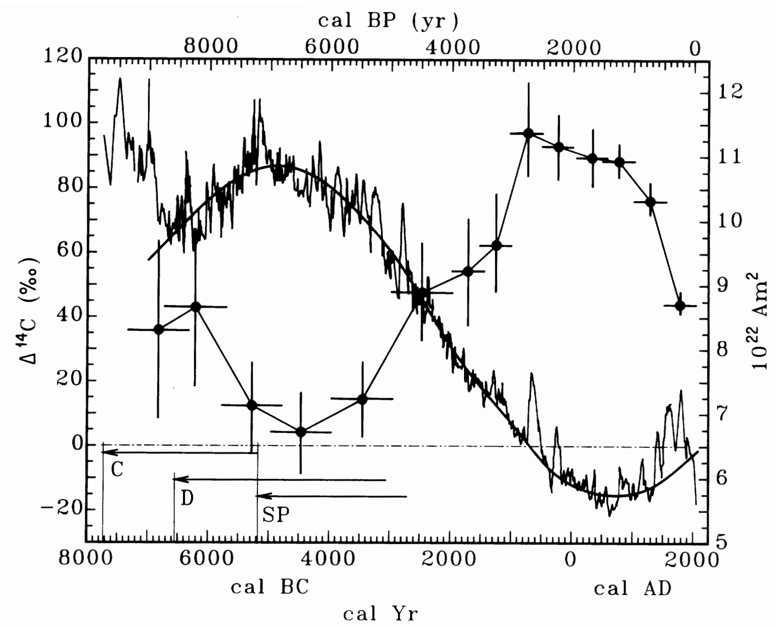

Figure 45. The ^{14}C variation for the last 10 kyr. The crosses indicate the dipole moment (Damon and Sonett, 1991).

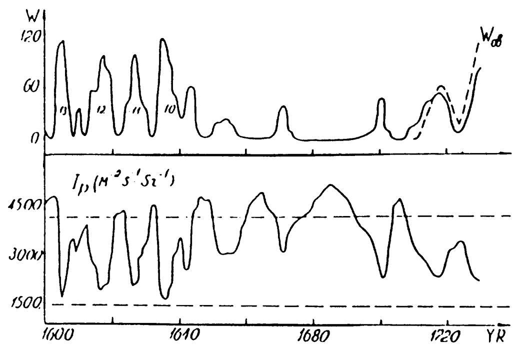

Figure 46. The sunspot number (upper panel) and the cosmic ray intensity (lower panel) during the Maunder Minimum (Kocharov, 1991).

been significantly higher indicating that the cosmic ray fluxes have been much higher, too (McCracken and McDonald, 2001).

During that period the climate was quite cold, which fits into the chain of argumentation, that a higher cosmic ray flux causes a higher cloudiness, which then reflects more radiation back into the space. This kind of climate forcing was also discussed recently by van Geel et al., van Geel et al. (1998, 1999a), who explained a local climate change

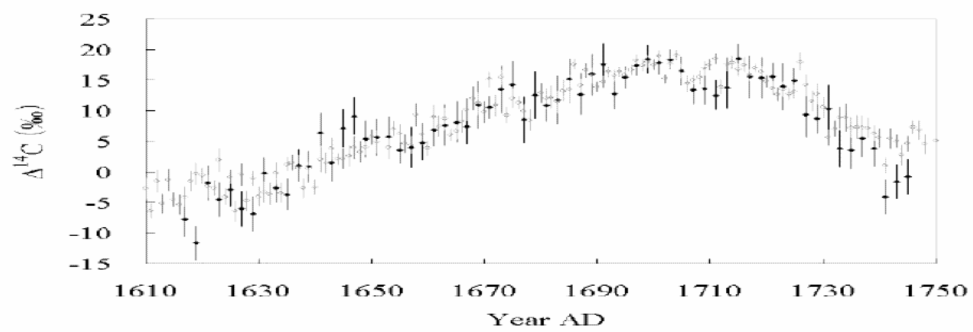

Figure 47. The ^{14}C enhancement during the Maunder Minimum, as consequence of a higher CRF (taken from Miyahara et al. (2005)).

850 calendar years BC and the simultaneous rise in ^{14}C and will be continued in the next section.

First modulation models (see sections 9 and 10) to explain the cosmic ray flux enhancements during the Grand minima have been developed by Scherer and Fichtner (2004) and Caballero-Lopez et al. (2004). It was found, that the spatial structure of the outer heliosphere in the Grand Minima is not so important, but rather the changes in the heliospheric magnetic field, which is the continuation of the solar surface magnetic field.

15. Implications to Climate

The principal source of energy that drives the dynamics of the outer spheres of our planet, including its climate, is unquestionably our Sun, and it is the electromagnetic radiation that overwhelmingly dominates energy exchange between the Earth and its cosmic environment. The equation for global planetary energy equilibrium (Kandel and Viollier, 2005) can be written as:

$$T_s = \left(\frac{(1-A)\frac{S_0}{4r_\odot^2 + P}}{\sigma(1-g)} \right)^{1/4} \tag{54}$$

where T_s is surface temperature, A the Bond albedo, S_0 the solar "constant", $r_\odot$ the distance from the Sun, P the internal planetary energy production (crustal heat flow), σ the Stefan-Boltzmann constant, and g the normalized greenhouse factor. The quantities S_0 and $r_\odot$ are astronomical while the A, T_s, g and P should be regarded as parameters of the planet's global system. The planetary surface temperature T_s is

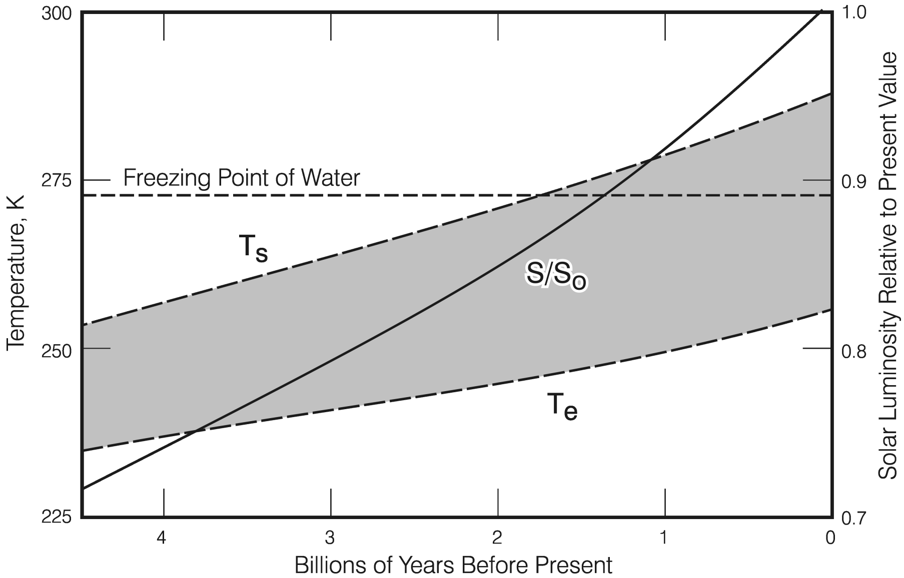

Figure 48. Evolution of solar luminosity ($S/S0$) normalized to today and the respective black body (T_e) and greenhouse augmented (T_s) temperature over geologic history. Adapted from (2005).

controlled essentially by its albedo A and normalized greenhouse factor g (P being negligible at 0.086 $\mathrm{W\,m^{-2}}$), which can be externally forced by natural and/or anthropogenic perturbations.

The short wave energy flux from the Sun that reaches the upper atmosphere is 342 Watts per square meter ($\mathrm{W\,m^{-2}}$), with ≈77 $\mathrm{W\,m^{-2}}$ reflected back into space by the atmosphere and clouds and ≈30 $\mathrm{W\,m^{-2}}$ by the Earth surface (Baede et al., 2001). At a radiative balance of 235 $\mathrm{W\,m^{-2}}$ the Earth would have an average surface temperature of only $-19°$ C, resulting in a perpetually frozen planet (Ruddiman, 2001). Moreover, the standard solar model (Gough, 1981) predicts that the luminosity of the Sun 4.6 billion years (Ga) ago was only ≈70% of the present value and increased ever since due to the advancing conversion of hydrogen to helium in its core (Fig. 48), making the early planet even more inhospitable to life. Yet the geologic record tells us that the planet had running water from at least 3.8 Ga ago (Windley, 1984) and abundant life since at least 3.5 Ga ago (Schopf, 1983). Its climate must have been therefore equable, not that much different from present-day conditions.

The saving grace is the existence of the planetary atmosphere which traps sufficient long wave energy, reradiated by the warm Earth's surface ("natural greenhouse effect"); to raise the surface temperature, today by ≈33° C, to a comfortable average of 14° C. This "natural" greenhouse effect is overwhelmingly due to water vapour, the principal greenhouse gas, and only to a lesser degree to other greenhouse gases (GHG), such as CO_2, CH_4, N_2O or CFCs. The global water cycle plays therefore the dominant role, in some estimates up to 90 – 95% in the magnitude of the "greenhouse" effect. It also is the major player in the global transfer of energy from the equator to the poles, a redistribution that is responsible for vagaries of regional climates. The "anthropogenic" addition of GHG, principally CO_2, since the advent of the industrial revolution, is believed to have enhanced the natural greenhouse effect by $\approx$2.5 W m^{-2} (Ramaswamy et al., 2001). For comparision, satellite data for less than a decade (1995–2002) suggest a decline in the cloud albedo by $\approx$7% (Kandel and Viollier, 2005; their Fig. 3b), consistent with a 2 – 6 W m^{-2} enhancement of the short wave solar energy input into the system (Pallé et al., 2005; Wild et al., 2005). The current scientific and political dispute boils down ultimately to the following: is the additional energy that is responsible for the centennial temperature rise of $\approx$0.6° C due principally to GHG or is it due to some external factor, such as the Sun? Note that we are not dealing with mutually exclusive scenarios. Climate models would respond in a similar way to the addition of energy from any source and it is only the relative importance of these potential "drivers", at a variety of time scales, which is the contentious issue. Note also that, compared to the sizes of the global energy fluxes, and their overall uncertainty of the order $\pm$6 W m^{-2}, the apparent centennial to annual trends are at the limit of detectability (Kandel and Viollier, 2005). It is therefore not likely that the issue of principal climate driver can be resolved by energy balance considerations. Instead, observations based on past climate trends and their compatibility with the celestial vs GHG records may help to resolve their relative contributions.

15.1. Celestial Climate Drivers and Amplifiers

Considering that the "consensus" view (IPCC, 2001) favours CO_2 as the principal climate driver on most (Ruddiman, 2001), or at least the human, time scales, it is important to ask what is the "sensitivity" of climate to doubling of CO_2 from its "pre-industrial" value of $\approx$280 ppm. Direct radiative forcing of 4 W m^{-2}, attributed to CO_2 doubling, should theoretically increase the global temperature by $\approx$1.25° C, short of the predictions by general circulation models (GCMs) of 1.5 – 5.5° C. Similarly, direct empirical surface measurements show a centennial temperature rise of only $\approx$0.6° C (IPCC, 2001), of which $\approx$1/3 is attributed to the observed increase in solar brightness. The "anthropogenic" greenhouse effect, of $\approx$80 – 100 ppm CO_2, should thus account for $\approx 0.4^\circ$ C. An extrapolation of these empirical data to CO_2 doubling would therefore suggest that the real climate sensitivity to CO_2 is closer to, or below, the minimal model predictions of 1.5° C (Shaviv, 2005), consistent with the direct satellite and balloon observations for the mid-lower troposphere (Sherwood et al., 2005; Mears and Wentz, 2005; Pinker et al., 2005). The amplification of temperatures in GCMs is thus mostly due to the "positive feedback" of higher atmospheric water vapour concentrations, and the large spread in their predictions reflects essentially the differences in model parameterization of clouds.

The attribution of only $\approx 1/3$ of the centennial temperature rise to solar forcing (Mitchell et al., 2001), despite very good correlation, is based on the empirical observation that averaged over the 11-year solar cycle the Total Solar Irradiance (TSI) variability is only 0.1% (1.5 $\mathrm{W\,m^{-2}}$) per 11-year solar cycle (Lean, 2005), insufficient to account for the 0.6° C centennial temperature rise in the GCMs. An amplifier related to solar dynamics would therefore be required to explain the entire magnitude of the trend and the 1980–2002 satellite data (Scafetta and West, 2005; Scafetta and West, 2006) indeed show that the response to the 11-year TSI cycle is $1.5-3$ times larger than in the GCM predictions. The galactic cosmic ray (GCR) flux was briefly considered to be such an amplifier, but dismissed because of the lack of understanding of physical processes, particularly cloud formation, that could point to a climate connection (Ramaswamy et al., 2001).

Recently, however, a spate of empirical observations demonstrates that the "Sun-climate connection is apparent in a plethora of high-fidelity climate indicators" (Lean, 2005), such as surface temperatures, cloud cover, drought, rainfall, cyclones, forest fires ... This does suggest the existence of an amplifier related to the muted changes in the solar luminosity "constant". That observational evidence supports the presence of the 11-year solar signal in the dynamics of the stratosphere and troposphere is confirmed also in the Hadley Centre review of Gray et al. (2005). In the stratosphere, it modulates the temperature and ozone levels. In the troposphere, during the solar maximum, the subtropical jets are weakened and shifted polewards and the pattern of the North Atlantic Oscillation index (NAO) extends over Eurasia. While the impact of direct solar radiative forcing relative to amplification of TSI by indirect mechanisms is still a subject of debate, the detection/attribution assessments of climate models "suggest that the solar influence on climate is greater than would be anticipated from radiative forcing estimates. This implies that either the radiative forcing is underestimated or there are some processes inadequately represented in those models" (Gray et al., 2005). If so, climate modulation by indirect amplifying mechanisms may play an important role.

Ozone and temperature anomalies in the stratosphere, generated by the UV spectral portion of the TSI flux (Haigh, 1994; Shindell et al., 1999; Labitzke et al., 2002), were proposed as such potential indirect mechanisms. However, the existing models apparently do not simulate well the propagation of these anomalies into the troposphere (Gray et al., 2005).

Considering that the aa index of geomagnetic activity (Prestes et al., 2006) and the GCR flux (sections 8, 12; Sabbah and Rybanský, 2006) also reflect the 11-year solar cycle, scenarios that implicate magnetic fields and electrical circuitries of the Sun and the Earth in climate modulation appear to be more promising amplifying candidates, because high-energy particles, such as GCR and solar protons, during their passage through the Earth's atmosphere and magnetosphere can trigger processes that affect the planetary radiative balance. The most likely pathway for translation of the high energy particle flux into a climate variable involves the role of clouds (Marsh and Svensmark, 2000a; Usoskin et al., 2004a; Harrison and Stephenson, 2006), since the "GCR have been shown to be closely correlated with continuous satellite (ISCCP) retrieval of low cloud cover from 1983-1994, and possibly to 2001" (Gray et al., 2005). Considering that solar radiation reflected by the atmosphere (and albedo of clouds) accounts for $\approx$77 $\mathrm{W\,m^{-2}}$, that climate models may underestimate the tropospheric short wave absorption by up to 30 – 40 $\mathrm{W\,m^{-2}}$, and that evapotranspiration and precipitation each account for 78 $\mathrm{W\,m^{-2}}$ (Baede et al., 2001; Stocker et al., 2001), a change in cloudiness of only a few percent could potentially alter the planetary energy balance by as much as the proposed anthropogenic GHG effect (2.5 $\mathrm{W\,m^{-2}}$).

Despite the fact that "modeling and observation now support atmospheric production of ultra-fine aerosols from cosmic ray produced ions" (Gray et al., 2005) and despite the ´theory (that) shows that charged aerosols are preferentially removed by cloud droplets, presenting the possibility of a long-range influence (on climate) through the global electrical circuit¡, the physics of the processes resulting in cloud nucleation is still a hotly debated issue. The proposed mechanisms may involve (1) aerosol microphysics, such as particle nucleation, coagulation and scavenging (Yu, 2002) in response to GCR flux, (2) charging of aerosol particles and droplets at particle and cloud boundaries related to the global electrical circuit and their removal to cloud droplets (electrofreezing, electroscavenging) (Tinsley and Yu, 2004), and (3) other potential mechanisms or any combination of the above (see Gray et al., 2005 for a review). The growth of charged molecular clusters from ultrafine aerosols, essential as an intermediate step in the formation of cloud condensation nuclei (CCN), is likely catalyzed by hygroscopic H_2SO_4 aerosols (Carslaw et al., 2002; Lee, 2003). Cloud formation by this scenario may therefore require spatial convergence of all these variables (GCR, water vapour, and natural as well as anthropogenic aerosols) in the troposphere.

15.2. Terrestrial Archives

Accepting that celestial and GHG forcings of climate are not mutually exclusive, but complementary drivers, addition of energy from either source would lead to a quasi-similar model outcome. Note that it is not the actual CO_2 that is embedded in most GCMs, but its assumed energy equivalent, the "prescribed CO_2". Unfortunately, both alternatives, celestial as well as GHG, suffer from the same deficiency, poorly understood physics of clouds that hampers modeling of the water cycle, even so it is this cycle acts as a major thermostat n climate regulation. In an effort to shed some light on the issue by empirical observations, the subsequent sections will juxtapose the signals of these complementary drivers, as presently known from terrestrial archives across the entire terrestrial time/space hierarchy, from resolution of billions of years to human time scales.

The direct instrumental record of global temperature is known for only about a century and satellite measurements of TSI, cloud parameters and atmospheric GHG concentrations are available for only a few decades. For longer time scales, we have to rely on proxies. These include concentrations of GHGs occluded in, and oxygen/hydrogen isotope paleotemperatures calculated from, the polar ice caps which enables observation of the climate/GHG relationship over the past $\approx$ 400 000 (and potentially 650 000) years (Siegenthaler et al., 2005). In contrast, apart from sunspot numbers that are known for several centuries, we have no direct proxies for TSI and no record of clouds. Fortunately, the energetic particles of the GCR during their interaction with the atmosphere produce the so-called cosmogenic nuclides, such as ^{10}Be, ^{14}C, ^{36}Cl (sections 12, 13), and these can be measured in terrestrial archives such as ice, trees, and sediments. Because the GCR flux reaching the Earth is inversely proportional to the intensity of the sun (and the intensity of the heliospheric shield), the concentration of these radioisotopes can be utilised as a proxy for TSI and potentially cloudiness. Note that the utility of the ^{14}C and ^{10}Be records peters out at $\approx$ 40 000 and $\approx$ 300 000 years, respectively (Frank, 2000). The utility of cosmogenic nuclides as proxies for TSI is further complicated by the fact that on time scales exceeding the decadal solar cycles, the GCR flux is attenuated also by the geomagnetic field that varies in intensity. Its variation is relatively well known for the last 800 000 years (Guyodo and Valet, 1999) and less so for the last 2 million years (Valet et al., 2005). Thus, unless the geomagnetic and heliomagnetic fields are somehow coupled, the extraction of TSI from these proxy signals may require correction for GCR attenuation by the geomagnetic field (section 13). In that case, the TSI/climate (or global temperature) scaling parameter over longer time scales may also vary (Gray et al., 2005).

The complementary oceanic temperature record for centennial to millennial and low million-year (Tertiary) time scales is available from numerous studies on calcitic shells of foraminifera that were the outcome of the Deep Sea Drilling Programme (e.g. Ruddiman, 2001). Potentially, this approach can yield a record even for the entire Phanerozoic (Veizer et al., 2000), albeit constrained by the limitations of geochronology and biostratigraphy. A comparable record for GCR flux can eventually also be quantified via data on exposure ages in meteorites (section 6).

15.3. Paleoclimate on Billion Year Time Scales

Accepting the validity of the standard solar model, the Earth − even with the contribution from the greenhouse − should have been a frozen body until about 1 Ga ago (Fig. 48). Yet, the sedimentary record (Windley, 1984) demonstrates convincingly the existence of open water bodies and streams, hence at least benign climate, during the entire Precambrian. Some authors (e.g. Knauth and Lowe, 2003) even argued that the declining δ^{18}O values in ancient cherts and carbonates (Fig. 49) indicates that the Archean oceans may have been as warm as $\approx 70 \pm 15°$ C, but the clear evidence for ice ages at ≈2.9 Ga, 2.2–2.4 Ga and since ≈0.7 Ga ago (Frakes et al., 1992; Young et al., 1998) rules out such an interpretation. Ice ages may have coexisted with temperate oceans, but not with the hot ones.

In order to resolve the "faint young Sun" conundrum, it was argued that the benign planetary surface temperatures were maintained by a supergreenhouse of CO_2, NH_3 or CH_4. Unfortunately, the atmospheric CO_2 levels required to counter the lower solar luminosity are up to 104 times higher than the modern values (Kasting, 1993) and this would result in a pH of the oceans ≈2-3 units lower than today. Temperature and pH both affect the δ^{18}O of marine carbonate minerals, but have opposing effects of similar magnitude, essentially canceling each other. The downward δ^{18}O trend (Fig. 49) is therefore unlikely to be an outcome of the hot "CO_2 greenhouse" oceans, but rather of the changing oxygen isotopic composition of seawater (Veizer and et al.,

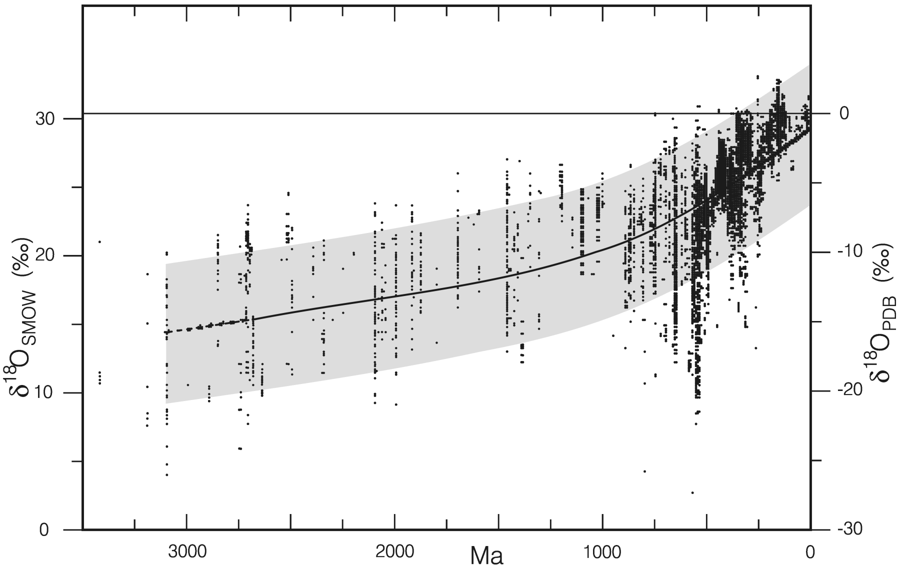

Figure 49. Oxygen isotope record of Ca C O $_3$ shells and sediments over geologic history (n = 9957). The upper envelope is the best approximation of the original signal. Most post-depositional processes tend to shift the δ^{18}O to more negative values and the bulk of the observed spread is due to this cause. Adapted from Shields and Veizer (2002).

1999; Veizer and Mackenzie, 2004). The alternative proposition of a CH_4 or NH_3 greenhouse (Sagan and Chyba, 1997; Kasting and Ono, 2005) faces the problem that such greenhouses could have been sustained only in an oxygen-free ocean/atmosphere system. This may have been theoretically feasible for the young Earth, up to ≈2.4 Ga ago, but not subsequently because the surficial environments were sufficiently oxidized (Holland, 1984).

In an alternative explanation Shaviv (2003b) invoked the impact of a stronger solar wind from the young Sun, coupled with the changing galactic star formation rates, to vary the intensity of the CRF into the terrestrial atmosphere. His model calculations, based on the acceptance of the CRF/climate causation, suggest that the celestial scenario could explain ≈2/3 of the dim Sun anomaly, with the remainder ameliorated perhaps by modestly higher GHG levels. Moreover, star formation rates in the Milky Way galaxy are believed to have been high ≈3 − 2 Ga ago and during the last 1 Ga , but muted in the intervening 2 − 1 Ga interval (section 6). This would have been mirrored in the temporal evolution of the GCR flux, and cloud albedo, resulting in cooling ≈3 − 2 and < 1 Ga ago and warming during the 2 − 1 Ga interval. The enigmatic absence of any indication of cold climate during this protracted 2 − 1 Ga warm interval, preceded and followed by planetary glaciations, is consistent with such a scenario.

15.4. Paleoclimate on Million Year Time Scales

The geological record of the Phanerozoic, the last 545 million years, is replete with shelly fossils. Utilising biostratigraphy, it has better temporal resolution than the Precambrian, particularly for the younger time intervals. However, as a unit, its average resolution is somewhere between 1 and 5 Ma , due mostly to difficulties in correlating the highly incomplete sedimentary sequences across the globe. The record, integrated over the $1-5$ Ma bins, shows intervals of 10^7-year duration with predominantly, but not exclusively, warm and cold climates, called greenhouses and icehouses, respectively (Frakes et al., 1992). Evaluation of the temporal and spatial distribution of climate sensitive sediments and fossil assemblages, as recorded in paleogeographic maps, shows a structure of 4 greenhouse/icehouse intervals (Fig. 50), alternating with $\approx$140 Ma periodicity. This paleoclimate trend coincides, in phase and amplitude, with the detrended δ^{18}O signal of the paleotemperature (based on the calcitic shells of marine fossils), as well as with the variations in the intensity of the GCR-flux (Shaviv and Veizer, 2003; de la Fuente Marcos and de la Fuente Marcos, 2004; Gies and Helsel, 2005). All these observations are consistent with the proposition that celestial forcing is the primary climate driver on multimillion-year time scales, the icehouses coincident with the passages of the heliosphere through the arms of the Milky Way galaxy. The dense population of young stars in galactic arms, hence enhanced GCR-flux and cloud albedo, are postulated to have been the causes of planetary cooling (Shaviv, 2002 and see part III).

In contrast to the celestial scenario, the model and proxy based estimates of atmospheric CO_2 levels for the Phanerozoic (Fig. 50) do not show any correlation with the paleoclimate picture that emerged from geological criteria (Veizer, 2005). While a correlation may exist for some partial intervals (e.g. Pagani et al., 2005), this is not the case for the Phanerozoic as a unit. Note also that any translation of proxy signals into Phanerozoic atmospheric CO_2 levels is beset by large uncertainties (Royer et al., 2001). Similarly, no convincing correlation exists between tectonic phenomena, such as the dispersal/reassembly of continents or seafloor spreading rates. Neither the GHG nor tectonic forcing is therefore likely to have been the primary climate driver on Phanerozoic time scales.

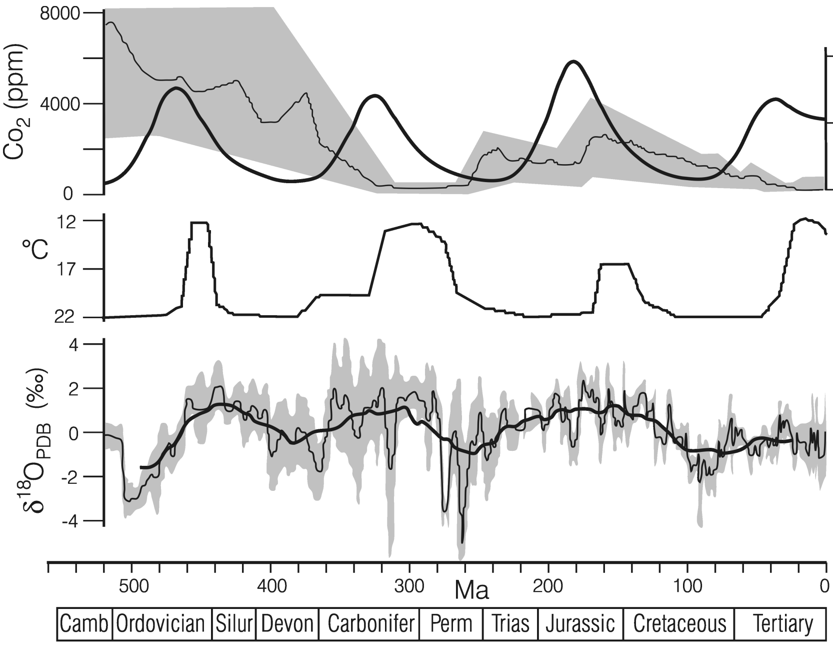

Figure 50. Phanerozoic climate history. Top: Thin line and shading: atmospheric CO_2 and the estimated ranges for the GEOCARB III model (Berner and Kothval, 2001); thick line: normalized cosmic ray flux (Shaviv and Veizer, 2003); Middle: Paleoclimate interpretation based on the paleogeographic distribution of climate sensitive sediments and fossils (www.scotese.com/climate.htm; figure 1 in Boucot and Gray (2001)); Bottom: Brachiopod, belemnite and planktonic foraminifera δ^{18}O isotope time-series ($N = 4775$) plotted in the Harland et al. (1990) time scale. The data are Gaussian filtered with $\pm 1\sigma$ uncertainty (dashed lines) and the linear trend (Veizer and et al., 1999) is removed. The thick line marks the moving average for 50 Ma window.

15.5. Paleoclimate on Multimillenial Time Scales

The time scales in the $10^4 - 10^5$ year range fall into the band of Milankovitch frequencies. The response of terrestrial climate to orbital parameters is assumed to have been proportional at any instant to the magnitude of summer insolation at 65°N, with ≈413 000 and ≈100 000 year frequencies due to eccentricity, ≈41 000 years to tilt and ≈23 000 years to precession. Assuming near-constant TSI, this orbital modulation (±12%) of insulation at the top of Earth's near-polar atmosphere, would not have been sufficient to cause the observed amplitudes of climate variability at high latitudes, and even less so in the equatorial regions. Amplifications by ice sheet dynamics in cold regions and by monsoon dynamics at low latitudes are therefore invoked as solutions (Ruddiman, 2001). The records of such climate oscillations are preserved in marine sediments, ice cores, cave stalagmites, lake and bog sediments, pollen data and similar archives. The most comprehensive record, based δ^{18}O measured in shells of marine foraminifera, resolves about 50 discrete cycles from $\approx$2.75 Ma, the presumed onset of northern glaciation (but see (Mudelsee and Raymo, 2005), to 0.9 Ma ago (Fig. 51b), consistent with the tilt as the driving parameter. However, from 0.9 Ga onwards the $\approx$100 000-year oscillation becomes the dominant one (Fig. 51a). The overall agreement of the δ^{18}O signal with the orbital parameters is indeed impressive. Note, nevertheless, that the outstanding fit is to some extent due also to the fact that the records were "tuned" to these parameters. This is permissible because of uncertainties in the δ^{18}O chronology of $\pm$5 000 years (Martinson et al., 1987), or more for the pre-300 000-year datasets (Imbrie et al., 1984). Another perplexing aspect is the appearance of the 100 000-year quasi-periodicity at $\approx$0.9 Ma ago, because the insolation forcing by eccentricity (<1%; Berger et al., 2005) is negligible. Moreover, its communication to low-latitudes is not understood, but this is a problem that plagues, to some extent, all orbital frequencies (Ruddiman, 2001). Could it be that the signals, or at least the quasi-100 000-year component, are not driven by orbital parameters? Could internal terrestrial phenomena (e.g. GHG) or external celestial causes (e.g. varying solar activity and/or cosmic ray flux) be the ultimate climate drivers on at least some of these time scales?

At first glance, the GHG proposition squares well with the Antarctic (Petit et al., 1999; Siegenthaler et al., 2005; Spahni et al., 2005) ice core data. The correlations between δ^{18}O and δD of ice (climate proxies) and the concentrations of CO_2 and CH_4 in enclosed air bubbles are impressive (Fig. 52). However, these correlations are discernible only if viewed at resolutions in excess of 1 000 years. Higher resolution records for all seven glacial terminations studied to this day show that the rise in CO_2 postdates the warming by several hundred to 2 800 years (Fischer et al., 1999; Monnin et al., 2001; Mudelsee, 2001; Caillon et al., 2003; Vakulenko et al., 2004; Siegenthaler et al., 2005). Consequently, CO_2 is likely a product of the $\approx$100 000-year climate oscillations, not their cause.

Could it be, therefore, as argued by Muller and MacDonald (1997), that the $\approx$100 000-year spectral peak is of astronomical origin, albeit forced by celestial driver(s) rather than by planetary orbital parameters? Could varying solar intensity or GCR-flux be the culprit? Such a proposition can be tested because at these time scales we do have preserved records of their proxies, the cosmogenic nuclides, such as ^{10}Be, ^{14}C and ^{36}Cl. These cosmogenic nuclides are generated in the terrestrial atmosphere by GCR-flux that, in turn, is inversely proportional to the strength of the heliospheric and magnetospheric shields, the

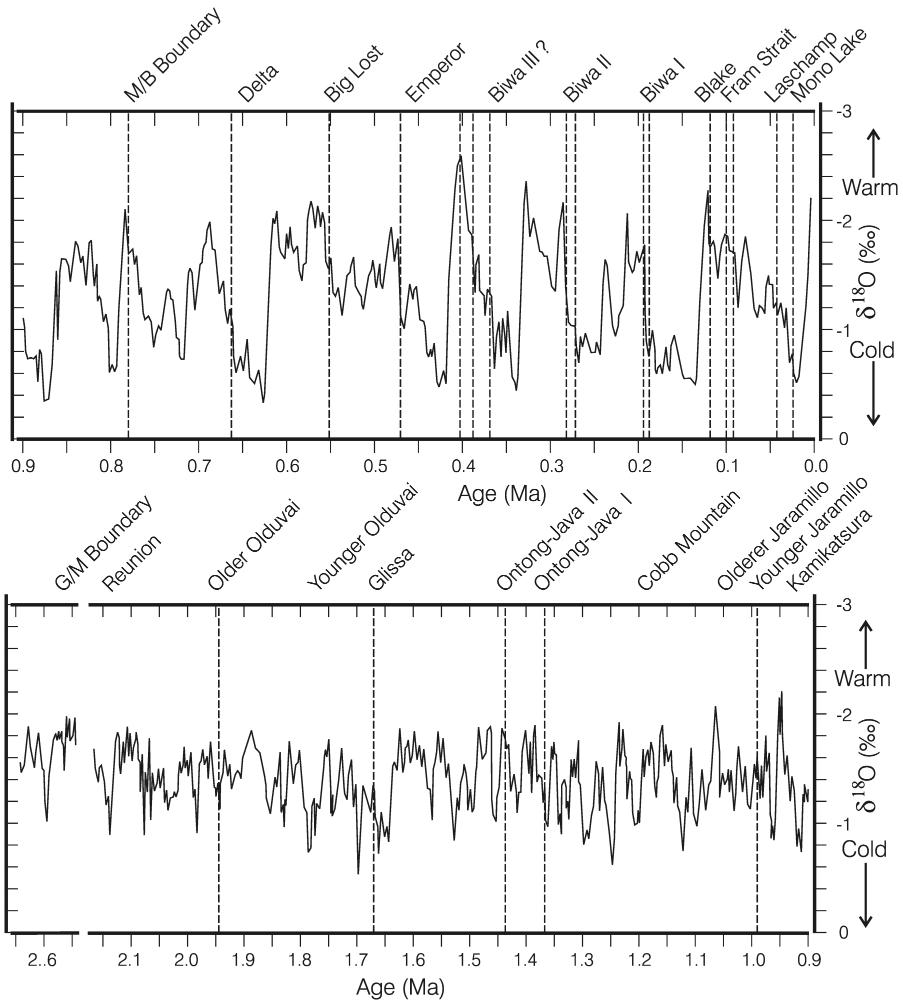

Figure 51. Marine oxygen isotope record of the 0 – 0.9 Ma (top) and 0.9 – 2.6 Ma (bottom) intervals, with geomagnetic events and polarity reversal listed at the top. Adapted from Worm (1997).

latter being the dominant modulation on multimillenial time scales (see part VI). For the last 200 000 years the geomagnetic intensity indeed shows minima at the 100 000-year frequency that coincide with the ^{10}Be production maxima (Fig. 53). Overall, the two trends mimic each other, as well as the stacked δ^{18}O climate trend. While the ^{10}Be record for earlier Quaternary times is not available, the stacked geomagnetic field paleointensity curve does extend to ≈800 000 years (Guyodo and Valet, 1999) and shows some resemblance to the contemporary δ^{18}O pattern, including intensity dips at quasi-100 000-year periodicity. The degree of this apparent correlation is presently a matter of dispute, with some

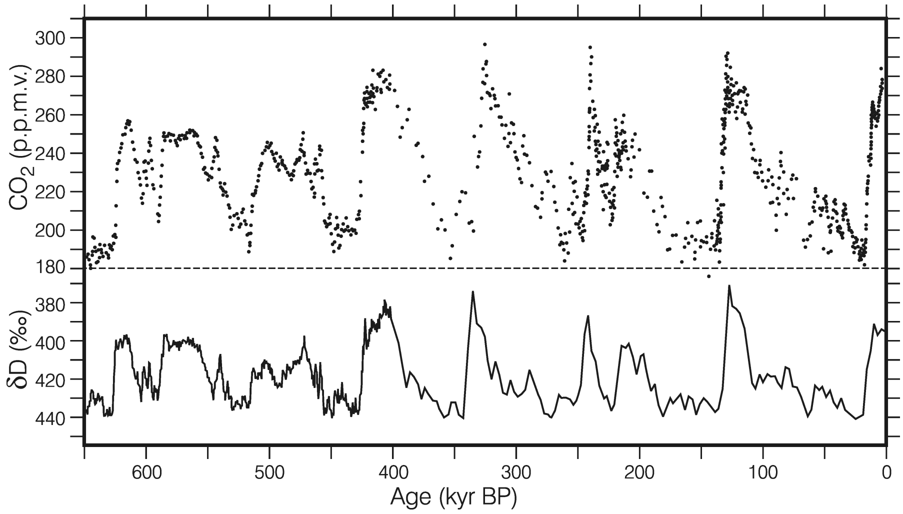

Figure 52. Antarctic ice core data for the last 650 000 years (650 kyr). Isotopic composition of hydrogen isotopes in ice (δD) is a proxy for temperature, with temperature increasing with declining δD. CO_2 concentrations were measured in frozen air bubbles. Adapted from Siegenthaler et al. (2005).

authors claiming high significance (Worm, 1997; Channell et al., 1998), others disputing it (Guyodo and Valet, 1999), and still others (Frank, 2000), despite stated preferences, reserving their definitive judgment.

A direct comparison of various proxies and of their lags/leads on shorter, 10^4–10^3-year, time scales is at present difficult because it is hampered by limitations of geochronology, correlation uncertainties, and by dampened amplitudes of the stacked records. The presumably best resolved signals are those of the last 50 000 years, and here the δ^{18}O minimum appears to have lagged by $\approx$15 000 $\pm$10 000 years behind the minimum of geomagnetic paleointensity (Frank, 2000), a lag that approaches the uncertainty limits of the orbitally based chronology. While some of this mismatch may indeed be due to correlation problems, a more likely explanation is that the discrepancy is real, potentially due to superimposed variation in heliomagnetic shield intensity modulated by the Sun. Assuming this to be the case, one can subtract the portion of the ^{10}Be signal that is due to geomagnetic paleointensity and view the superimposed higher order oscillations as an indirect measure of solar irradiance (Masarik and Beer, 1999). Utilising this conceptual framework, Sharma (2002) reproduced a 200 000 year solar irradiance trend that fits surprisingly well with the normalized δ^{18}O record for coeval oceans (Fig. 54). This, the advocated correlations of ^{10}Be with δ^{18}O (cold phases of the Dansgaard-Oeschger events) in the Greenland GISP2 ice core for the 40 000 – 11 000 years BP interval (van Geel et al.,

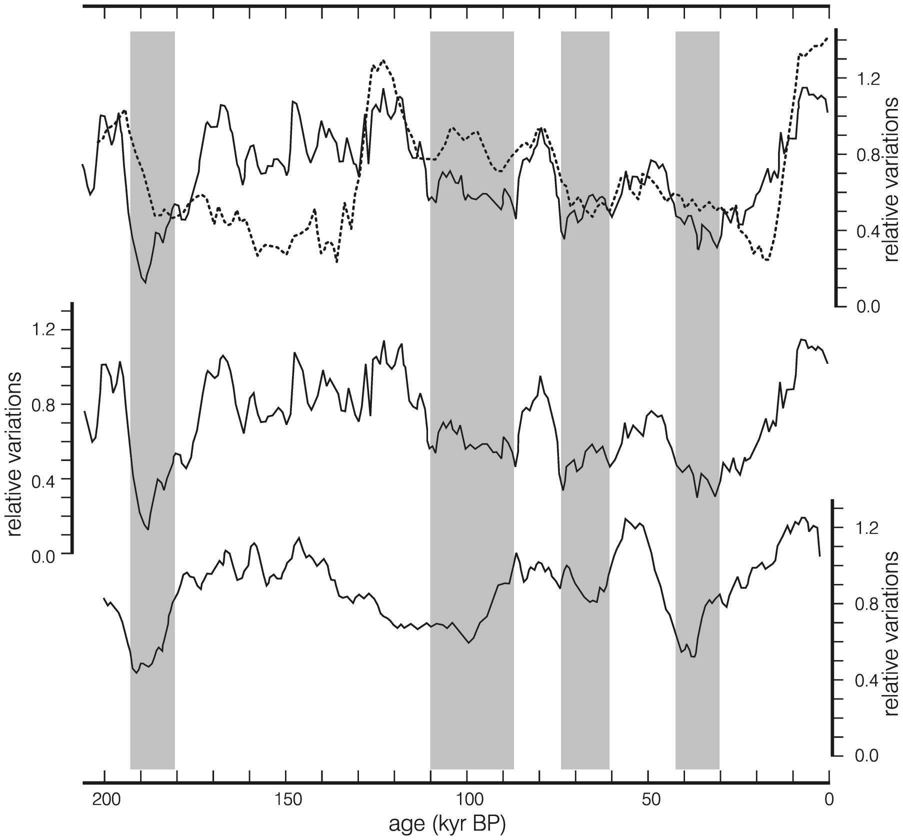

Figure 53. Relative variations of the geomagnetic field paleointensity for the last 200 000 years as derived (bottom) from global stacked paleomagnetic record (Guyodo and Valet, 1999) and (middle) from reconstruction based on ^{10}Be production rate. Top figure is a comparison of the ^{10}Be trend (full line) with the global δ^{18}O stacked record (dotted line) (Martinson et al., 1987). Shaded – intervals of low paleomagnetic intensities. Adapted from Frank (2000).

1999b), along with the monsoonal patterns in the Arabian Sea area for the last 65 000 years (Higginson et al., 2004), all argue for solar forcing of climate via GCR-flux modulation on time scales of $\leq 10^4$ years. However, the issue is complicated by the fact that a terrestrial record based on a single cosmogenic isotope is equivocal. For example, the ^{10}Be record can reflect either a variable GCR-flux (production) or a changing depositional rate of the hosting phase (redistribution) (Christl et al., 2003), both potentially related to climate, but with opposite cause/effect interpretations. Fortunately, at least for the last $\approx$45 000 years, the opposing propositions can be tested because for this time span we also have a record of an additional cosmogenic tracer, ^{14}C. While the uncertainties in the Δ^{14}C signal for the inter-

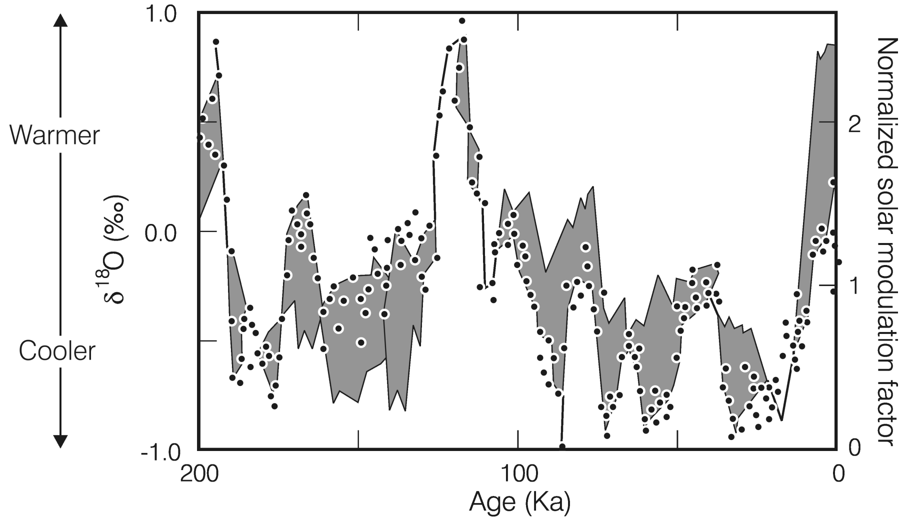

Figure 54. Calculated intensity of solar irradiance (dots) during the past 200 000 years juxtaposed with the normalized δ^{18}O record of the oceans (shading). Note that the magnitude of uncertainties in the derived curve are a matter of debate, but this would not necessarily impact the causation which could be only from Sun to Earth. Adapted from Sharma (2002).

vals older than ≈25 000 years are still relatively large, the subsequent record, particularly during the Holocene, is well constrained (Bard, 1998; Frank, 2000) and will be discussed in the next section. Having these parallel records of ^{10}Be and ^{14}C enables us to resolve the production/redistribution dichotomy because cosmogenic nuclides, despite their common production (GCR-flux), have entirely different terrestrial dispersal pathways (see section 13). ^{10}Be "rains" directly onto the surface of the planet where it is deposited in the ice or sediments, while ^{14}C becomes first part of the atmospheric CO_2 pool and is only later (≈20 years) sequestered by photosynthetic activity into plants. Hence, any covariant trend of ^{10}Be and ^{14}C can only be due to the production term. Moreover, the issues of lags and leads become less critical than for the purely terrestrial parameters (e.g. CO_2/δ^{18}O correlations), because any potential causation can only be from space to Earth, and not the other way around.

15.6. Postglacial Climate on Millenial to Centennial Time Scales

The retreat of large ice sheets in the northern hemisphere commenced ≈15 000 years ago, reached a maximum ≈10 000 years ago, and ended ≈6 000 years ago (Ruddiman, 2001). This retreat also marks the termination of the last 100 000-year cooling oscillation (Termination I) that, as argued above, may have been potentially a response to geomagnetic modulation of the cosmic ray flux.

Bond et al. (2001) showed convincingly that “over the last 12 000 years virtually every centennial time scale increase in drift ice in (their) North Atlantic record was tied to a distinct interval of variable and, overall, reduced solar output”, as read from ^{10}Be and ^{14}C proxies (Fig. 55). Most of these 200 − 500 year climatic oscillations may be a response to heliospheric modulation of GCR-flux by the HMF. In a somewhat nuanced view, (Gallet et al., 2005; see also St-Onge et al., 2003) argued, nevertheless, that at least some of the cooling intervals in the last 3 000 years do reflect short-term spikes in geomagnetic field intensity, as measured on French faience potsherds.

The coherency of the Bond et al. (2001) marine signal with complementary records from marine sediments (Christl et al., 2003; St-Onge et al., 2003; Poore et al., 2004; Jiang et al., 2005), lacustrine settings (Björck et al., 1991; Magny, 1993; Verschuren et al., 2000; Snowball and Sandgren, 2002; Hu et al., 2003; Lim et al., 2005), speleothems (Neff et al., 2001; Niggemann et al., 2003; Mangini et al., 2005; Fleitmann et al., 2003; Wang et al., 2005), polar ice sheets (Stuiver et al., 1997; Laj et al., 2000), Alaskan glaciers (Wiles et al., 2004), bogs (Chambers et al., 1999; Blaauw et al., 2004; Xu et al., 2006), intensity of monsoonal or wet/dry cycles (Hodell et al., 2001; Wang et al., 2001; Cruz et al., 2005; Gupta et al., 2005) and pollen records (Viau et al., 2002; Willard et al., 2005), suggests that we are indeed dealing with a global record of climate. The ultimate driver was likely the variable solar activity, the more so that the CO_2 levels (Fig. 55) during this entire time span were relatively flat (Fig. 55), at the “pre-industrial” levels of $\approx$270 $\pm$10 ppm (Indermühle et al., 1999).

The Medieval Climate Optimum (MCO) at $\approx$800 − 1300 AD and the Little Ice Age (LIA) at $\approx$1400 − 1850 AD are a portion of this oscillating climate pattern that deserves more thorough consideration because of the much debated “hockey stick” temperature reconstruction of Mann et al. (1999). In contrast to the claim of these authors for their local significance, the MCO and LIA were features that were recorded across the globe (Soon and Baliunas, 2003). Moreover, the amplitude of these climate swings must have exceeded the global temperature gradients of the last century because of the existence of farms in Greenland and vineyards in England during the MCO, juxtaposed to frozen Baltic Sea and canals in Europe during the LIA. Neither climate mode was a commonality during the last century and the composite proxy record of Mann et al. (1999) must therefore underestimate the magnitude of short term climate oscillations (von Storch et al., 2004; Esper et al.,

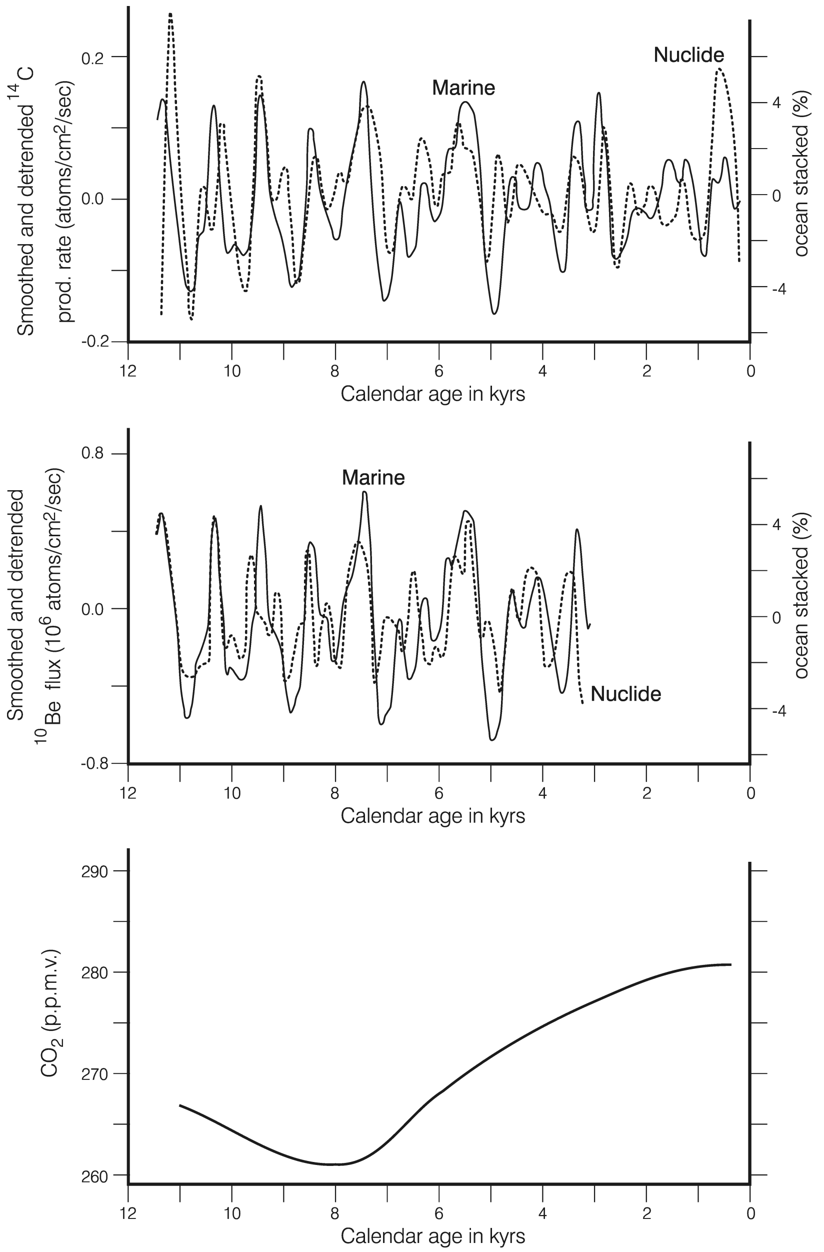

Figure 55. Comparison of the detrended and smoothed production rates for ^{14}C (top) and ^{10}Be (middle) with changes in proxies of drift ice ("marine") in North Atlantic deep-sea sediments (Bond et al., 2001). The "pre-industrial" ice core CO_2 concentrations from Indermühle et al. (1999).

2005; Moberg et al., 2005). In contrast to the "hockey stick" reconstruction, the stalagmite record from a cave in the Alps (Mangini et al.,

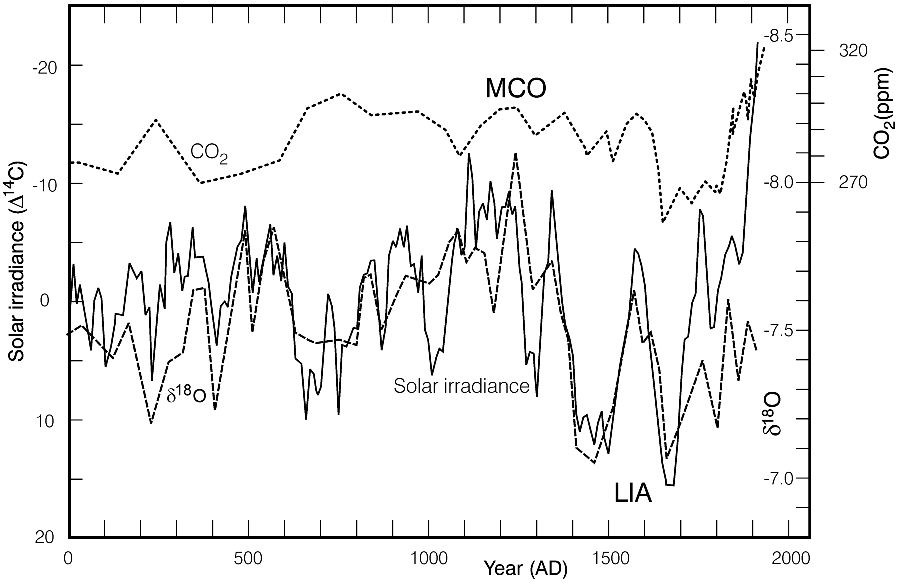

Figure 56. The $\delta^{18}O$ record of a stalagmite from the Spannagel cave in the central Alps (dashed line) covering the last 2000 years, compared to ^{14}C production rate ($\Delta^{14}C$) (full line with reversed scale) that is a proxy for solar irradiance (Mangini et al., 2005). CO_2 concentration from ice cores and instrumental measurements from Indermühle et al. (1999) and IPCC (2001). MCO is the warm Medieval Climate Optimum and LIA stands for Little Ice Age.

2005), covering the time span from 2000 years BP to the early 20th century, clearly shows both the MCO and LIA (Fig. 56). Note also the exceptionally good inverse correlation with the ^{14}C record, the latter a function of the intensity of solar radiation. A comparison to solar irradiance based on ^{10}Be would yield a similar outcome. In fact, the ^{10}Be and ^{14}C records are coherent for the last 9 000 years (Solanki et al., 2004). Note again, that all these marked climate shifts happened when the atmospheric CO_2 levels were marooned at their "pre-industrial" value of $\approx$280 ppm (Fig. 56).

15.7. Post Little Ice Age Climate on Decadal Time Scales

The end of the LIA, in the last decades of the 19th century, coincided with the advent of the industrial revolution and it is this time interval that is the centerpiece of intense scientific and political debates. The instrumental centennial global temperature record (IPCC, 2001) shows an overall warming of $\approx 0.6^\circ$ C, in two spurts, at $\approx$1880 – 1940 and 1976 – 2000, with almost three decades of temperature decline in the intervening interval. In contrast, atmospheric CO_2 increased exponentially to today (Fig. 57). A general consensus accepts that the pre-

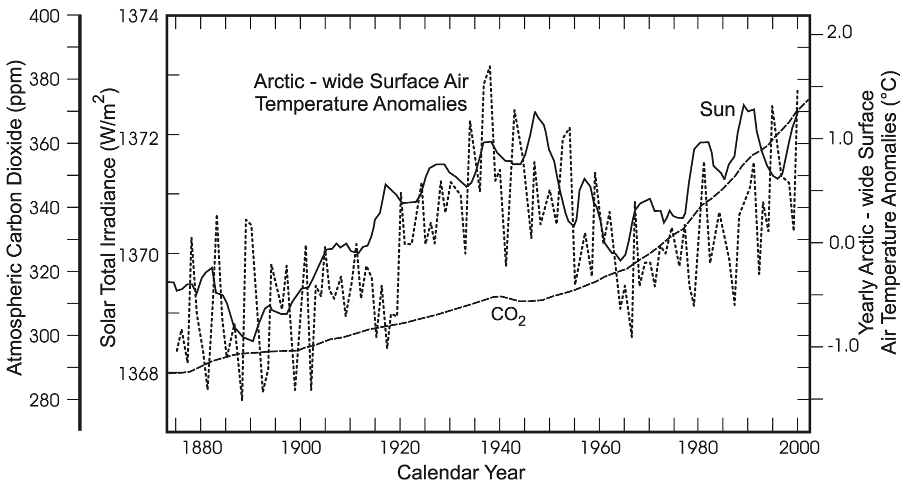

Figure 57. Decadally smoothed annual mean Arctic-wide air temperature anomaly time series (dotted) compared to the estimated TSI (Sun, full line) and to atmospheric CO_2 levels from 1875 to 2000 (dashed line). Adapted from Soon (2005).

1940's temperature rise, because of only a slight increase in atmospheric CO_2 levels, could not have been caused by GHGs, and this warming is thus attributed mostly to increased solar activity (Mitchell et al., 2001). The subsequent evolution, however, is a bone of contention. Solanki et al. (2004), reconstructing solar evolution from observational and proxy data, showed that the Sun's intensity over the second half of the 20th century was higher than at any time over the last 8 000 years (but see Muscheler et al., 2005b vs. Solanki et al., 2005. Their solar trend and the IPCC temperature trend are almost identical, except for the last 2 to 3 decades, when the temperature rise exceeded that of the solar index. Solanki and coauthors attributed this to the emergence of the anthropogenic CO_2 signal from the background of natural variability, while the "consensus" IPCC interpretation attributes even the entire post-1940's temperature trend mostly to anthropogenic causes, with cooling to 1976 due to emissions of sulphur aerosols and the subsequent warming to GHGs (Mitchell et al., 2001).

The largest impact of climate modulation by GHG should be evident in polar regions. Yet, the decadally smoothed Arctic observational data (Soon, 2005) show almost a perfect correlation with TSI, even for the last decades (Fig. 57). Note, also, that the GCMs' do not take into account the possible amplification of TSI, likely via GCR-flux and cloud albedo, and this may lead to an underestimate of their climate sensitivity to solar forcing (Scafetta and West, 2005) and to simultaneous overestimate of the GHG impact. While the models assume that the relative GHG/solar impact on centennial climate evolution was ≈2:1

(Mitchell et al., 2001), statistical evaluation of empirical centennial trends shows that the decadally smoothed solar modulator (Fig. 57) can explain $\geq 48-80\%$ of the regional and global temperature variances (Foukal, 2002; Soon, 2005; Kilcik, 2005). Observational data therefore argue of a reversal of significance, making the case for existence of a TSI amplifier. Is there any empirical support for this proposition? If amplification by GCR-flux exists, whatever the actual pathway, it has to be modulated by the magnetosphere. The convincing correlations (Le Mouël et al., 2005; Veretenenko et al., 2005) of decadally smoothed TSI, temperature, "magnetic indices" (Fig. 58), cyclonic activity and ^{10}Be clearly support the existence of such an amplifier. In view of these data, the potential discrepancy of the last $2-3$ decades may require re-examination. It may be that we are only dealing with a problem of a long-term persistence (Cohn and Lins, 2005) or with an "edge effect" of a time series and final judgment should therefore be deferred until a longer time series is acquired. This cautionary note is supported further by complementary observational data. In contrast to GCM models that hold the Earth's albedo roughly constant (≈ 0.3), the observational data by several approaches and groups (Pallé et al., 2005; Wild et al., 2005) show a significant decadal variability in albedo, mostly, although not exclusively, attributed to cloudiness. For the $1985-2000$ (or 2002) interval alone, the impact of such forcings on the planetary energy balance is claimed to have been $+2$ to $6\ \mathrm{W\,m^{-2}}$, coincident with a decline of the Bond albedo of $\approx 7\%$ (Kandel and Viollier, 2005), while for the combined GHG + aerosol it was only $+0.6\ \mathrm{W\,m^{-2}}$. For the $2000-2004$ period, the somewhat inconclusive data indicate a comparable relative importance. For comparison, the cumulative radiative forcing of all anthropogenic GHGs combined that is estimated at $\approx 2.5\ \mathrm{W\,m^{-2}}$ (IPCC, 2001). These observations suggest that celestial phenomena may have been the dominant forcing factor even during the most recent past.

Further observational support for the claim that solar activity plays a decisive role on climate on (sub)decadal time scales comes from a multitude of direct empirical observations. Alexander (2005) documented 21-year solar cycle periodicity in South African annual rainfall, river flow, floods, lake and groundwater levels, and in the Southern Oscillation index. The intensity and variability of Schwabe, Hale and Gleissberg solar cycles was shown to correlate with the monsoonal dynamics (Higginson et al., 2004; van Loon et al., 2004; Bhattacharyya and Narasimha, 2005), Pacific SSTs (Weng, 2005), Siberian climate (Raspopov et al., 2004), Northern Atlantic cyclogenesis, geomagnetic activity and galactic GCR-flux (Veretenenko et al., 2005), atmospheric Southern Annual Mode (Kuroda and Kodera, 2005), Southern Oscillation Index (Higginson et al., 2004), North Atlantic Oscillation (Pozo-

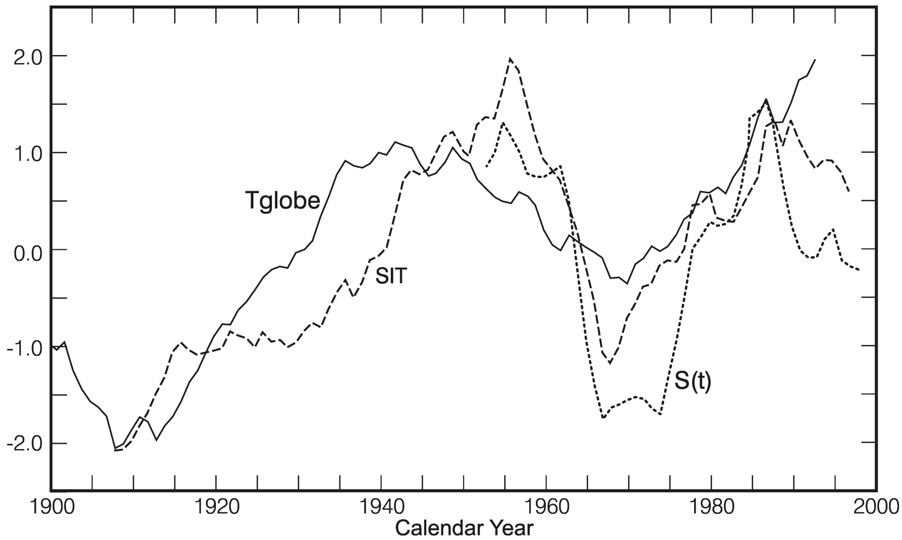

Figure 58. Normalised time evolution of the 11-year running mean for magnetic indices (SIT) at Sitka, normalized solar irradiance (St) and global temperature (Tglobe) during the last century. Adapted from Le Mouël et al. (2005).

Vázquez et al., 2004), tropospheric temperatures, water vapour distribution and global circulation regime (Gleisner et al., 2005) and latitudinal and temporal cloud distribution (Usoskin et al., 2004c), the latter postulated as due to cosmic ray induced ionization. Variations in the interplanetary magnetic/electric field are also linked to tropospheric temperature patterns at Vostok (Troshichev et al., 2003). For many additional examples see the publication lists of the articles quoted in this review.

Part VIII

Resume

16. Where do we stand?

In this review the evolution of the cosmic ray flux from its origin into the Earth atmosphere is presented. The consequences of variable cosmic ray fluxes for the Earth environment, i.e. the production of cosmogenic isotopes and the interpretation of the related archives as well as the influence on climate is discussed. Although many of the physical processes seem to be understood and others are actively researched, many open questions remain. As the explicit formulation of such questions depends on the research field, it seems better to identify the most obvious tasks for future research:

Galaxy: It is evident, that in different regions of the solar orbit around the galactic center the cosmic ray flux is different. The physical processes of the acceleration of a single cosmic ray particle and at its source, at least below 1 TeV, seem to be understood. To determine the spectra and total flux of the cosmic rays, it is necessary to know the number and strength of the sources and their distribution in space and time. In view of the apparent lack of in-situ data (e.g. the local interstellar spectra), more sophisticated modeling is required until an Interstellar Probe will provide us with direct observations of the local interstellar medium.

Heliosphere: The acceleration and propagation of cosmic rays at the termination shock and beyond is presently studied in much detail. The modulation of cosmic rays including charge, space and time dependence is observed with numerous spacecraft as well as Earth bound observatories. Nevertheless, the acceleration of cosmic rays at dynamic shock waves, like the termination shock needs further research. A crucial question is how varies the heliospheric modulation volume with time? It is evident that the Sun encounters different interstellar environments during its passage through the galaxy, and hence the outer heliospheric structure will change. For example, relatively small changes in the interstellar number density will cause the termination shock to migrate inward into the planetary system. The possible consequences of such a migration have been studied only poorly and need further development.

Archives: The cosmogenic isotopes are produced in the atmosphere and are then stored in sediments, ice-cores, or meteorites. In many studies the cosmic ray flux at the top of the atmosphere is derived using the force-field approximation, which neglects charge sign dependence. The latter, however, is well recorded with Earth bound observatories, like neutron monitors. Therefore, it is evident that these effects should be taken into account interpreting cosmogenic data.

Climate: Empirical evidence for an influence of "space weather and climate" on planetary environments, especially on the terrestrial climate, exists for time scales, reaching from decades up to billion years. As shown in this review it makes sense to distinguish between solar-terrestrial and interstellar-terrestrial relations, i.e. to distinguish between an internal solar and external interstellar trigger for influence on Earth and its environment. In contrast to the solar forcing the cosmic ray forcing operates, in principle, on all time scales. For both forcings the processes relevant for an influence on climate are unclear. Nonetheless, the evidence for the cosmic ray forcing is increasing as is the understanding of its physical principles. Cosmic rays which, despite their negligible energy compared to that of solar irradiance, are the main source of ionization in the troposphere. The detailed chain of processes connecting the variable cosmic ray flux with the terrestrial climate (i.e. via cloud formation) has still to be identified.

Anomalous cosmic rays: Due to potential massive changes in the structure of the heliosphere along its path around the galactic center, it is likely that not only galactic but also the anomalous cosmic rays are a mediator of the interstellar-terrestrial relations. The investigation of this problem has only recently started.

The complexity of the topic "interstellar-terrestrial relations" evidently requires an interdisciplinary cooperation. This alone already has a great potential to lead the scientists to new frontiers.

Acknowledgements

We thank the International Space Science Institute (ISSI) for their financial support and hospitality.

H.-J.F. and K.S. are grateful for financial support granted to them by the Deutsche Forschungsgemeinschaft (DFG) in the frame of the project "Heliotrigger" (Fa 97/28-1) as well as H.F., B.H. and again K.S. in the project "HelioCAWSES" (FI[redacted], B[redacted])

U.W.L. wishes to thank the Claude Leon Foundation for financial support for his post-doctoral research and the DFG within the project "[redacted]" (SCHL 201/14-3).

M.S.P., S.E.S.F. and U.W.L. acknowledge the partial support of the South African National Research Foundation under grant number 2053475.

J.V. was supported financially by the Natural Sciences and Engineering Research Council of Canada and the Canadian Institute for Advanced Research. P. Wickham and E. Hearn provided technical support.

L.D. and E.F. were supported by the Swiss National Science Foundation, grant 200020-105435/1, and by the Swiss State Secretariat for Education and Research, SER, grant COST-724/C05.0034.

References

Alexander, W.: 2005, 'Linkages Between Solar Activity and Climatic Responses'. *Energy & Environment* **16**, 239–254.

Alexeev, I. I. and Y. I. Feldstein: 2001, 'Modeling of geomagnetic field during magnetic storms and comparison with observations'. *Journal of Atmospheric and Terrestrial Physics* **63**, 431–440.

Amaral, L. H. and J. R. D. Lepine: 1997, 'A self-consistent model of the spiral structure of the Galaxy'. *Mon. Not. Roy. Astron. Soc.* **286**, 885–894.

Axford, W. I.: 1981, 'Late paper: Acceleration of cosmic rays by shock waves'. In: *Workshop on Plasma Astrophysics*. pp. 425–+.

Aylmer, D., V. Bonanno, G. F. Herzog, H. Weber, J. Klein, and R. Middleton: 1988, '^{26}Al and ^{10}Be production in iron meteorites'. *Earth Planet. Sci. Lett.* **88**, 107–118.

Baede, A., E. Ahlonsou, Y. Ding, and D. Schimel: 2001, 'The Climate System: an Overview'. In: J. Houghton, Y. Ding, D. Griggs, M. Noguer, P. van der Linden, X. Dai, K. Maskell, and C. Johnson (eds.): *Climate Change 2001: The Scientific Basis: Contribution of Working Group I to the Third Assessment Report of the Intergovernmental Panel on Climate Change (Ch. 1)*. pp. 85–98, Cambridge University Press, Cambridge, U.K.

Baranov, V. B. and Y. G. Malama: 1993, 'Model of the solar wind interaction with the local interstellar medium - Numerical solution of self-consistent problem'. *J. Geophys. Res.* **98**, 15157–+.

Bard, E.: 1998, 'Geochemical and geophysical implications of the radiocarbon calibration'. *GCA* **62**, 2025–2038.

Bard, E., G. M. Raisbeck, F. Yiou, and J. Jouzel: 1997, 'Solar modulation of cosmogenic nuclide production over the last millennium: comparison between ^{14}C and ^{10}Be records'. *Earth and Planetary Science Letters* **150**, 453–462.

Barraclough, D.: 1974, 'Spherical harmonic analyses of the geomagnetic field for eight epochs between 1600 and 1910'. *Geophys. J. R. Astron. Soc.* **36**, 497–513.

Barry, D. C.: 1988, 'The chromospheric age dependence of the birthrate, composition, motions, and rotation of late F and G dwarfs within 25 parsecs of the sun'. *Astrophys. J.* **334**, 436–448.

Bazilevskaya, G. A., M. Krainev, Y. I. Stozhkov, A. Svirzhevskaya, and N. Svirhevsky: 1991, 'Long-term Soviet Program for the Measurements of Ionizing Radiation in the Stratosphere'. *J. Geomag. Geoelectr. Japan* **43**, 893–.

Beer, J., A. Blinov, G. Bonani, H. J. Hofmann, and R. C. Finkel: 1990, 'Use of Be-10 in polar ice to trace the 11-year cycle of solar activity'. *Nature* **347**, 164–166.

Beer, J., G. M. Raisbeck, and F. Yiou: 1991, 'Time variations of Be-10 and solar activity'. In: C. Sonett, M. Giampapa, and M. Mathews (eds.): *The Sun in Time*. pp. 343–359, Univ. Ariz. Press.

Begelman, M. C. and M. J. Rees: 1976, 'Can cosmic clouds cause climatic catastrophes'. *Nature* **261**, 298–+.

Berezinskiĭ, V. S., S. V. Bulanov, V. A. Dogiel, and V. S. Ptuskin: 1990, *Astrophysics of cosmic rays*. Amsterdam: North-Holland, 1990, edited by Ginzburg, V.L.

Berger, A.: 1991, *Long-term history of climate ice ages and Milankovitch periodicity*, pp. 498–510. The Sun in Time.

Berger, A., J. L. Mélice, and M. F. Loutre: 2005, 'On the origin of the 100-kyr cycles in the astronomical forcing'. *Paleoceanography* **20**(4), PA4019.

Berner, R. and Z. Kothval: 2001, 'GEOCARBIII: A revised model of atmopsheric C O $_2$ over Phanerozoic time'. *Am. J. Sci.* **301**, 182–204.

Bhattacharyya, S. and R. Narasimha: 2005, 'Possible association between Indian monsoon rainfall and solar activity'. *Geophys. Res. Lett.* **32**, 5813–+.

Bieber, J. W., W. H. Matthaeus, A. Shalchi, and G. Qin: 2004, 'Nonlinear guiding center theory of perpendicular diffusion: General properties and comparison with observation'. *Geophys. Res. Lett.* **31**, L10805:p1–4.

Binney, J. and S. Tremaine: 1987, *Galactic dynamics*. Princeton, NJ, Princeton University Press, 747 p.

Björck, S., M. Malmer, C. Hjort, P. Sandgren, O. Ingólfsson, B. Wallén, R. Smith, and B. Jónsson: 1991, 'Stratigraphic and paleoclimatic studies of a 5,500 years old moss bank on Elephant Island'. *Antarctica Arctic Alpine Res.* **23**, 361–374.

Blaauw, M., B. van Geel, and J. van der Plicht: 2004, 'Solar forcing of climatic change during the mid-Holocene: indications from raised bogs in The Netherlands.'. *The Holocene* **14**(1), 35–44.

Blinov, A.: 1988, 'The dependence of cosmogenic isotope production rate on solar activity and geomagnetic field variations'. In: F. R. Stephenson and A. W. Wolfendale (eds.): *Secular Solar and Geomagnetic Variations in the last 10,000 Years*. pp. 329–340, Kluver, Dordrecht.

Blitz, L., M. Fich, and S. Kulkarni: 1983, 'The new Milky Way'. *Science* **220**, 1233–1240.

Bond, G., B. Kromer, J. Beer, R. Muscheler, M. N. Evans, W. Showers, S. Hoffmann, R. Lotti-Bond, I. Hajdas, and G. Bonani: 2001, 'Persistent Solar Influence on North Atlantic Climate During the Holocene'. *Science* **294**, 2130–2136.

Borrmann, T.: 2005, 'Ein hydrodynamisches 3D-Mehrkomponentenmodell der Heliosphäre und ihrer Wechselwirkung mit kosmischer Strahlung'. Ph.D. thesis, Ruhr-Universität Bochum, Germany.

Borrmann, T. and H. Fichtner: 2005, 'On the dynamics of the heliosphere on intermediate and long time-scales'. In: *COSPAR, Plenary Meeting*. pp. 1186–+.

Boucot, A. J. and J. Gray: 2001, 'A critique of Phanerozoic climatic models involving changes in the CO_2 content of the atmosphere'. *Earth Science Reviews* **56**, 1–4.

Briesmeister, J. F. e.: 1993, 'MCNP - A general Monte Carlo N-particle transport code version 4A, LA-12625-M'. Technical report, LANL, Los Alamos.

Brun, R., F. Bruyant, M. Maire, A. McPherson, and P. Zanarini: 1987, 'GEANT3 User's guid'. Technical report, CERN.

Burger, R. A. and M. Hattingh: 1998, 'Toward a Realistic Diffusion Tensor for Galactic Cosmic Rays'. *Astrophys. J.* **505**, 244–251.

Burger, R. A. and M. Hitge: 2004, 'The Effect of a Fisk-Type Heliospheric Magnetic Field on Cosmic-Ray Modulation'. *Astrophys. J. Lett.* **617**, L73–L76.

Burlaga, L. F., F. B. McDonald, and N. F. Ness: 1993, 'Cosmic ray modulation and the distant heliospheric magnetic field - Voyager 1 and 2 observations from 1986 to 1989'. *J. Geophys. Res.* **98**(17), 1–11.

Burlaga, L. F., N. F. Ness, M. H. Acuña, R. P. Lepping, J. E. P. Connerney, E. C. Stone, and F. B. McDonald: 2005, 'Crossing the Termination Shock into the Heliosheath: Magnetic Fields'. *Science* **309**, 2027–2029.

Büsching, I., A. Kopp, M. Pohl, R. Schlickeiser, C. Perrot, and I. Grenier: 2005, 'Cosmic-Ray Propagation Properties for an Origin in Supernova Remnants'. *Astrophys. J.* **619**, 314–326.

Bzowski, M., H. J. Fahr, and D. Rucinski: 1996, 'Interplanetary Neutral Particle Fluxes Influencing the Earth's Atmosphere and the Terrestrial Environment'. *Icarus* **124**, 209–219.

Caballero-Lopez, R. A. and H. Moraal: 2004, 'Limitations of the force field equation to describe cosmic ray modulation'. *Journal of Geophysical Research (Space Physics)* **109**, 1101–+.

Caballero-Lopez, R. A., H. Moraal, K. G. McCracken, and F. B. McDonald: 2004, 'The heliospheric magnetic field from 850 to 2000 AD inferred from ^{10}Be records'. *Journal of Geophysical Research (Space Physics)* **109**, A12102:p.1–15.

Caillon, N., J. P. Severinghaus, J. Jouzel, J.-M. Barnola, J. Kang, and V. Y. Lipenkov: 2003, 'Timing of Atmospheric CO_2 and Antarctic Temperature Changes Across Termination III'. *Science* **299**, 1728–1731.

Callis, L. B., M. Natarajan, D. S. Evans, and J. D. Lambeth: 1998, 'Solar atmospheric coupling by electrons (SOLACE) 1. Effects of the May 12, 1997 solar event on the middle atmosphere'. *J. Geophys. Res.* **103**, 28405–28420.

Cane, H. V., G. Wibberenz, I. G. Richardson, and T. T. von Rosenvinge: 1999, 'Cosmic ray modulation and the solar magnetic field'. *Geophys. Res. Lett.* **26**, 565–568.

Carslaw, K. S., R. G. Harrison, and J. Kirkby: 2002, 'Cosmic Rays, Clouds, and Climate'. *Science* **298**, 1732–1737.

Castagnoli, G. C. and D. Lal: 1980, 'Solar modulation effects in terrestrial production of carbon 14'. *Radiocarbon* **22**, 133–158.

Chalov, S. V. and H. J. Fahr: 1995, 'Entropy generation at the multi-fluid solar wind termination shock producing anomalous cosmic ray particles'. *Planet. Space Sci.* **43**, 1035–1043.

Chalov, S. V. and H. J. Fahr: 2000, 'Pick-up ion acceleration at the termination shock and the post-shock pick-up ion energy distribution'. *Astron. & Astrophys.* **360**, 381–390.

Chambers, F., M. Ogle, and J. Blackford: 1999, 'Paleoenvironmental evidenc for solar forcing of Holocene climate: Linkages to solar science'. *Progress Phys. Geogr.* **23**, 181–201.

Champion, K. S. W., A. E. Cole, and A. J. Kantor: 1985, 'Handbook of Geophysics and the Space Environment'. In: A. S. Jursa (ed.): *Standard and reference atmosphere, in Handbook of Geophysics and the Space Environment.* pp. 14–1 – 14–43, Air Force Geophys. Lab., U.S. Air Force.

Channell, J. E. T., D. A. Hodell, J. McManus, and C. Lehman: 1998, 'Orbital modulation of the Earth's magnetic field intensity'. *Nature* **394**, 464–469.

Charvatova, I.: 1990, 'The relations between solar motion and solar variability'. *Bulletin of the Astronomical Institutes of Czechoslovakia* **41**, 56–59.

Christl, M., C. Strobl, and A. Mangini: 2003, 'Beryllium-10 in deep-sea sediments: a tracer for the Earth's magnetic field intensity during the last 200,000 years.'. *Quatern. Sci. Rev.* **22**, 725–739.

Clem, J. M., J. W. Bieber, P. Evenson, D. Hall, J. E. Humble, and M. Duldig: 1997, 'Contribution of obliquely incident particles to neutron monitor counting rate'. *J. Geophys. Res.* **102**, 26919–26926.

Clem, J. M., G. de Angelis, P. Goldhagen, and J. W. Wilson: 2003, 'Preliminary validation of computational procedures for a new atmospheric ionizing radiation (air) model'. *Advances in Space Research* **32**, 27–33.

Cohn, T. A. and H. F. Lins: 2005, 'Nature's style: Naturally trendy'. *Geophys. Res. Lett.* **32**(23), L23402.

Cooke, D. J., J. E. Humble, M. A. Shea, D. F. Smart, and N. Lund: 1991, 'On cosmic-ray cut-off terminology'. *Nuovo Cimento C Geophysics Space Physics C* **14**, 213–234.

Crutzen, P. J., I. S. A. Isaksen, and G. C. Reid: 1975, 'Solar Proton Events: Stratospheric Sources of Nitric Oxide'. *Science* **189**, 457–459.

Cruz, F. W., J., S. J. Burns, I. Karmann, W. D. a. V. M. Sharp, A. D. Cardoso, J. A. Ferrari, P. L. Silva Dias, and O. J. Viana: 2005, 'Insolation-driven changes in atmospheric circulation over the past 116,000 years in subtropical Brazil'. *Nature* **434**, 63–66.

Cummings, A. C. and E. C. Stone: 2001, 'Onset of Solar Modulation in the Outer Heliosphere as Seen in Anomalous Cosmic Rays'. *Proc. 27th Int. Cosmic Ray Conf.* **27**, 4251–+.

Dame, T. M., D. Hartmann, and P. Thaddeus: 2001, 'The Milky Way in Molecular Clouds: A New Complete CO Survey'. *Astrophys. J.* **547**, 792–813.

Damon, P. E. and C. P. Sonett: 1991, *Solar and terrestrial components of the atmospheric C-14 variation spectrum*, pp. 360–388. The Sun in Time.

de La Fuente Marcos, R. and C. de La Fuente Marcos: 2004, 'On the recent star formation history of the Milky Way disk'. *New Astronomy* **9**, 475–502.

de la Fuente Marcos, R. and C. de la Fuente Marcos: 2004, 'On the recent star formation history of the Milky Way disk'. *New Astronomy* **9**, 475–502.

Dennison, B. and V. N. Mansfield: 1976, 'Glaciations and dense interstellar clouds'. *Nature* **261**, 32–34.

Desilets, D., M. Zreda, and N. A. Lifton: 2001, 'Comment on 'Scaling factors for production rates of in situ produced cosmogenic nuclides: a critical reevaluation' by Tibor J. Dunai'. *Earth Planet. Sci. Lett.* **188**, 283–287.

Desorgher, L.: 2004, 'The MAGNETOCOSMICS code'. Technical report, http::cosray.unibe.ch/~laurent/magnetoscosmics.

Desorgher, L., E. O. Flückiger, M. Gurtner, M. R. Moser, and R. Bütikofer: 2005, 'Atmocosmics:. a Geant 4 Code for Computing the Interaction of Cosmic Rays with the Earth's Atmosphere'. *International Journal of Modern Physics A* **20**, 6802–6804.

Desorgher, L. E. O. F., M. R. Moser, and R. Bütikofer: 2003, 'Geant4 Simulation of the Propagation of Cosmic Rays through the Earth's Atmosphere'. In: *Proceedings of the 28th International Cosmic Ray Conference*, Vol. 7. pp. 4277–4280.

Dorman, L. I., G. Villoresi, N. Iucci, M. Parisi, M. I. Tyasto, O. A. Danilova, and N. G. Ptitsyna: 2000, 'Cosmic ray survey to Antarctica and coupling functions for neutron component near solar minimum (1996-1997) 3. Geomagnetic effects and coupling functions'. *J. Geophys. Res.* **105**, 21047–21056.

Eddy, J. A.: 1976, 'The Maunder Minimum'. *Science* **192**, 1189–1202.

Eichkorn, S., S. Wilhelm, H. Aufmhoff, K. H. Wohlfrom, and F. Arnold: 2002, 'Cosmic ray-induced aerosol-formation: First observational evidence from aircraft-based ion mass spectrometer measurements in the upper troposphere'. *Geophys. Res. Lett.* **29**, 43–1.

Esper, J., R. Wilson, D. Frank, A. Moberg, H. Wanner, and J. Luterbachner: 2005, 'Climate: past ranges and future changes'. *Quatern. Sci. Rev.* **24**, 2164–2166.

Fahr, H. J.: 1990, 'The Maxwellian alternative to the dark matter problem in galaxies'. *Astron. & Astrophys.* **236**, 86–94.

Fahr, H.-J.: 2004, 'Global structure of the heliosphere and interaction with the local interstellar medium: three decades of growing knowledge'. *Advances in Space Research* **34**, 3–13.

Fahr, H. J., T. Kausch, and H. Scherer: 2000, 'A 5-fluid hydrodynamic approach to model the solar system-interstellar medium interaction'. *Astron. & Astrophys.* **357**, 268–282.

Feldstein, Y. I., A. E. Levitin, J. U. Kozyra, B. T. Tsurutani, A. Prigancova, L. Alperovich, W. D. Gonzalez, U. Mall, I. I. Alexeev, L. I. Gromova, and L. A. Dremukhina: 2005, 'Self-consistent modeling of the large-scale distortions in the geomagnetic field during the 24-27 September 1998 major magnetic storm'. *Journal of Geophysical Research (Space Physics)* **110**(A9), 11214–+.

Ferreira, S. E. S.: 2002, 'The Heliospheric Transport of Galactic Cosmic Rays and Jovian Electrons'. Ph.D. thesis, Potchefstroomse Universiteit , South Africa.

Ferreira, S. E. S. and M. S. Potgieter: 2004, 'Long-Term Cosmic-Ray Modulation in the Heliosphere'. *Astrophys. J.* **603**, 744–752.

Ferreira, S. E. S., M. S. Potgieter, R. A. Burger, B. Heber, and H. Fichtner: 2001, 'Modulation of Jovian and galactic electrons in the heliosphere: 1. Latitudinal transport of a few MeV electrons'. *J. Geophys. Res.* **106**, 24979–24988.

Ferreira, S. E. S. and K. Scherer: 2004, 'Modulation of Cosmic-Ray Electrons in the Outer Heliosphere'. *Astrophys. J.* **616**, 1215–1223.

Ferreira, S. E. S. and K. Scherer: 2005, 'Time evolution of galactic and anomalous cosmic ray spectra in a dynamic heliosphere'. *Astrophys. J.* **submitted**, ???–???

Fichtner, H.: 2001, 'Anomalous Cosmic Rays: Messengers from the Outer Heliosphere'. *Space Science Reviews* **95**, 639–754.

Fichtner, H.: 2005, 'Cosmic rays in the heliosphere: progress in the modelling during the past 10 years'. *Advances in Space Research* **35**, 512–517.

Fichtner, H., M. Potgieter, S. Ferreira, and A. Burger: 2000, 'On the propagation of Jovian electrons in the heliosphere: transport modelling in 4-D phase space'. *Geophys. Res. Lett.* **27**, 1611–+.

Fichtner, H., K. Scherer, and B. Heber: 2006, 'A criterion to discriminate between solar and cosmic ray forcing of the terrestrial climate'. *J. Atmos. Terr. Phys.* **submitted**, 00.

Fichtner, H., S. R. Sreenivasan, and H. J. Fahr: 1996, 'Cosmic ray modulation and a non-spherical heliospheric shock.'. *Astron. & Astrophys.* **308**, 248–260.

Fischer, H., M. Wahlen, J. Smith, D. Mastroianni, and B. Deck: 1999, 'Ice Core Records of Atmospheric CO2 Around the Last Three Glacial Terminations'. *Science* **283**, 1712–1714.

Fisk, L. A.: 1996, 'Motion of the footpoints of heliospheric magnetic field lines at the Sun: Implications for recurrent energetic particle events at high heliographic latitudes'. *J. Geophys. Res.* **101**, 15547–15553.

Fleitmann, D., S. J. Burns, M. Mudelsee, J. Neff, U. Kramers, A. Mangini, and A. Matter: 2003, 'Holocene Forcing of the Indian Monsoon Recorded in a Stalagmite from Southern Oman'. *Science* **300**, 1737–1739.

Florinski, V. and G. Zank: 2005, 'Galactic cosmic ray response to heliospheric environment changes and implications for cosmogenic isotope records'. In: *Proc. Int. Cosmic Ray Conf., Pune, Aug 3-10.* p. in press.

Florinski, V., G. P. Zank, J. R. Jokipii, E. C. Stone, and A. C. Cummings: 2004, 'Do Anomalous Cosmic Rays Modify the Termination Shock?'. *Astrophys. J.* **610**, 1169–1181.

Flückiger, E. O., R. Bütikofer, L. Desorgher, and M. R. Moser: 2003, 'Global Cosmic Ray Cutoff Rigidities Over the Past 2000 Years'. In: *Proc. 28th Int. Cosmic Ray Conf.*, Vol. 7. p. 4229.

Flückiger, E. O. and K. E.: 1990, 'Aspects of Combining Models of the Earth's Internal and External Magnetic Fields'. *J. Geomag. Geoelectr.* **42**, 1123–1136.

Foukal, P.: 2002, 'A comparison of variable solar total and ultraviolet irradiance outputs in the 20th century'. *Geophys. Res. Lett.* **29**, 4–1.

Frakes, L., E. Francis, and J. Syktus: 1992, *Climate modes of the Phanerozoic; The history of the Earth's climate over the past 600 million years.* Cambridge University Press, Cambridge (U.K.).

Frank, M.: 2000, 'Comparison of cosmogenic radionuclide production and geomagnetic field intensity over the last 200 000 years'. *Phil. Trans. R. Soc. Lond. A* **358**, 1089–1107.

Fraser-Smith, A.: 1985, 'Centered and eccentric geomagnetic dipoles and their poles 1600-1985'. *Rev. geophys.* **25**, 1–16.

Frisch, P. C.: 2000, 'The galactic environment of the Sun'. *J. Geophys. Res.* **105**, 10279–10290.

Gallet, Y., A. Genevey, and F. Fluteau: 2005, 'Does Earth's magnetic field secular variation control centennial climate change? [rapid communication]'. *Earth Planet. Sci. Lett.* **236**, 339–347.

Gardiner, L. T., T. Sawa, and M. Fujimoto: 1994, 'Numerical Simulations of the Magellanic System - Part One - Orbits of the Magellanic Clouds and the Global Gas Distribution'. *Mon. Not. Roy. Astron. Soc.* **266**, 567–582.

Geant4 Collaboration, S. Agostinelli, J. Allison, K. Amako, J. Apostolakis, H. Araujo, P. Arce, M. Asai, D. Axen, S. Banerjee, G. Barrand, F. Behner, L. Bellagamba, J. Boudreau, L. Broglia, A. Brunengo, H. Burkhardt, S. Chauvie, J. Chuma, R. Chytracek, G. Cooperman, G. Cosmo, P. Degtyarenko, A. dell'Acqua, G. Depaola, D. Dietrich, R. Enami, A. Feliciello, C. Ferguson, H. Fesefeldt, G.

Folger, F. Foppiano, A. Forti, S. Garelli, S. Giani, R. Giannitrapani, D. Gibin, J. J. Gómez Cadenas, I. González, G. Gracia Abril, G. Greeniaus, W. Greiner, V. Grichine, A. Grossheim, S. Guatelli, P. Gumplinger, R. Hamatsu, K. Hashimoto, H. Hasui, A. Heikkinen, A. Howard, V. Ivanchenko, A. Johnson, F. W. Jones, J. Kallenbach, N. Kanaya, M. Kawabata, Y. Kawabata, M. Kawaguti, S. Kelner, P. Kent, A. Kimura, T. Kodama, R. Kokoulin, M. Kossov, H. Kurashige, E. Lamanna, T. Lampén, V. Lara, V. Lefebure, F. Lei, M. Liendl, W. Lockman, F. Longo, S. Magni, M. Maire, E. Medernach, K. Minamimoto, P. Mora de Freitas, Y. Morita, K. Murakami, M. Nagamatu, R. Nartallo, P. Nieminen, T. Nishimura, K. Ohtsubo, M. Okamura, S. O'Neale, Y. Oohata, K. Paech, J. Perl, A. Pfeiffer, M. G. Pia, F. Ranjard, A. Rybin, S. Sadilov, E. di Salvo, G. Santin, T. Sasaki, N. Savvas, Y. Sawada, S. Scherer, S. Sei, V. Sirotenko, D. Smith, N. Starkov, H. Stoecker, J. Sulkimo, M. Takahata, S. Tanaka, E. Tcherniaev, E. Safai Tehrani, M. Tropeano, P. Truscott, H. Uno, L. Urban, P. Urban, M. Verderi, A. Walkden, W. Wander, H. Weber, J. P. Wellisch, T. Wenaus, D. C. Williams, D. Wright, T. Yamada, H. Yoshida, and D. Zschiesche: 2003, 'Geant4-a simulation toolkit'. *Nuclear Instruments and Methods in Physics Research A* **506**, 250–303.

Gierens, K. and M. Ponater: 1999, 'Comment on "Variation of cosmic ray flux and global cloud coverage - a missing link in solar-climate relationships" by H. Svensmark and E. Friis-Christensen (1997)'. *Journal of Atmospheric and Terrestrial Physics* **61**, 795–797.

Gies, D. R. and J. W. Helsel: 2005, 'Ice Age Epochs and the Sun's Path through the Galaxy'. *Astrophys. J.* **626**, 844–848.

Gleeson, L. J. and W. I. Axford: 1968, 'Solar Modulation of Galactic Cosmic Rays'. *Astrophys. J.* **154**, 1011–+.

Gleisner, H., P. Thejll, M. Stendel, E. Kaas, and B. Machenhauer: 2005, 'Solar signals in tropospheric re-analysis data: Comparing NCEP/NCAR and ERA40'. *J. Atm. Solar-Terrestrial Phys.* **67**, 785–791.

Gosse, J. C., R. C. Reedy, C. D. Harrington, and J. Poths: 1996, 'Overview of the workshop on secular variations in production rates of cosmogenic nuclides on Earth'. *Radiocarbon* **38**, 135–147.

Gough, D. O.: 1981, 'Solar interior structure and luminosity variations'. *Solar Phys.* **74**, 21–34.

Graham, I. J., B. J. Barry, R. G. Ditchburn, and A. Zondervan: 2005, 'Validation of cosmogenic nuclide production rate scaling factors through direct measurement. Part 2 - Production of ^{7}Beand ^{10}Be in water targets deployed in the Southern Hemisphere, 1997-2001'. *GNS Science Report* pp. 1–23.

Gray, L., J. Haigh, and R. Harrison: 2005, 'The influence of solar changes on the earth's climate'. Technical report, Hadley Centre technical note 62. www.met-office.gov.UK/research/hadleycentre/pubs/HCTN/HCTN_62.pdf.

Grieder, P. K. F.: 2001, *Cosmic rays at Earth, Researcher's reference manual and data book*. Elsevier.

Grove, J. M.: 1988, *The Little Ice Age*. Routledge.

Gupta, A. K., M. Das, and D. M. Anderson: 2005, 'Solar influence on the Indian summer monsoon during the Holocene'. *Geophys. Res. Lett.* **32**, 17703–+.

Guyodo, Y. and J.-P. Valet: 1999, 'Global changes in intensity of the Earth's magnetic field during the past 800 kyr 249'. *Nature* **399**, 249–251.

Haigh, J. D.: 1994, 'The Role of Stratospheric Ozone in Modulating the Solar Radiative Forcing of Climate'. *Nature* **370**, 544–+.

Hampel, W. and O. A. Schaeffer: 1979, 'Al-26 in iron meteorites and the constancy of cosmic ray intensity in the past'. *Earth Planet. Sci. Lett.* **42**, 348–358.

Harland, W., R. Armstrong, A. Cox, L. Craig, A. Smith, and D. Smith: 1990, *A Geologic Time Scale 1989*. Cambridge University Press, Cambridge, UK.

Harrison, R. G. and D. B. Stephenson: 2006, 'Empirical evidence for nonlinear effect of galactic cosmic rays on clouds'. *Proc. R. Soc. A* pp. 1–13.

Hartquist, T. W. and G. E. Morfill: 1983, 'Evidence for the stochastic acceleration of cosmic rays in supernova remnants'. *Astrophys. J.* **266**, 271–275.

Heath, D. F., A. J. Krueger, and P. J. Crutzen: 1977, 'Solar Proton Event: Influence on Stratospheric Ozone'. *Science* **197**, 886–889.

Heber, B.: 2001, 'Modulation of galactic and anomalous cosmic rays in the inner heliosphere'. *Advances in Space Research* **27**, 451–460.

Heber, B., J. M. Clem, R. Müller-Mellin, H. Kunow, S. E. S. Ferreira, and M. S. Potgieter: 2003, 'Evolution of the galactic cosmic ray electron to proton ratio: Ulysses COSPIN/KET observations'. *Geophys. Res. Lett.* **30**, 6–1.

Heber, B. and M. S. Potgieter: 2000, 'Galactic Cosmic Ray Observations at Different Heliospheric Latitudes'. *Advances in Space Research* **26**, 839–852.

Heber, B., T. R. Sanderson, and M. Zhang: 1999, 'Corotating interaction regions'. *Advances in Space Research* **23**, 567–579.

Heerikhuisen, J., V. Florinski, and G. P. Zank: 2006, 'Interaction between the solar wind and interstellar gas: a comparison between Monte-Carlo and fluid approaches'. *submitted* , .

Hess, W. N., E. H. Canfield, and R. E. Lingenfelter: 1961, 'Cosmic-Ray Neutron Demography'. *J. Geophys. Res.* **66**, 665–+.

Higginson, M. J., M. A. Altabet, L. Wincze, T. D. Herbert, and D. W. Murray: 2004, 'A solar (irradiance) trigger for millennial-scale abrupt changes in the southwest monsoon?'. *Paleoceanography* **19**, 3015–+.

Hodell, D. A., M. Brenner, J. H. Curtis, and T. Guilderson: 2001, 'Solar Forcing of Drought Frequency in the Maya Lowlands'. *Science* **292**, 1367–1370.

Hoeksema, J. T.: 1992, 'Large-scale structure of the heliospheric magnetic field - 1976-1991'. In: *Solar Wind Seven Colloquium*. pp. 191–196.

Holland, H. D.: 1984, *Chemical Evolution of the Atmosphere and Oceans*. Princeton University Press, Princeton, U.S.A.

Hoyle, F.: 1984, 'On the Causes of Ice-Ages'. *Earth Moon and Planets* **31**, 229–+.

Hoyle, F. and R. A. Lyttleton: 1939, 'The effect of interstellar matter on climatic variation'. In: *Proceedings of the Cambridge Philisophical Society*. pp. 405–+.

Hu, F. S., D. Kaufman, S. Yoneji, D. Nelson, A. Shemesh, Y. Huang, J. Tian, G. Bond, B. Clegg, and T. Brown: 2003, 'Cyclic Variation and Solar Forcing of Holocene Climate in the Alaskan Subarctic'. *Science* **301**, 1890–1893.

Imbrie, J., J. Hays, D. Martinson, A. McIntyre, A. Mix, J. Morley, N. Pisias, W. Prell, and N. Shackleton: 1984, 'The orbital theory of Pleistocene climate: support from a revised chronology of the marine square 18O record'. In: N. S. A.L. Berger, J. Imbrie (ed.): *Milankovitch and Climate, Part 1*. pp. 269–305, Reidel.

Indermühle, A., T. Stocker, F. Joos, H. Fischer, H. Smith, M. Wahlen, B. Deck, D. Mastroianni, J. Tschumi, T. Blunier, R. Meyer, and B. Stauffer: 1999, 'Holocene carbon-cycle dynamics based on $C\,O_2$ trapped in ice at Taylor Dome, Antarctica 121'. *Nature* **398**, 121–127.

IPCC (ed.): 2001, 'Intergovernmental Panel on Climate Change: 2001, Climate Change 2001: The Scientific Basis'. Cambridge University Press, Cambridge, U.K.

Izmodenov, V.: 2001, 'Velocity Distribution of Interstellar H Atoms in the Heliospheric Interface'. *Space Science Reviews* **97**, 385–388.

Izmodenov, V. V.: 2004, 'The Heliospheric Interface: Models and Observations'. In: *ASSL Vol. 317: The Sun and the Heliosphere as an Integrated System*. pp. 23–+.

Jackman, C. H., E. L. Fleming, and F. M. Vitt: 2000, 'Influence of extremely large solar proton events in a changing stratosphere'. *J. Geophys. Res.* **105**, 11659–11670.

Jiang, H., J. Eiríksson, M. Schulz, K.-L. Knudsen, and M.-S. Seidenkrantz: 2005, 'Evidence for solar forcing of sea-surface temperature on the North Icelandic Shelf during the late Holocene'. *Geology* **33**, 73–76.

Jokipii, J. R.: 1971, 'Propagation of cosmic rays in the solar wind'. *Rev. Geophys. Space Phys.* **9**(1), 27–87.

Jokipii, J. R. and J. Kota: 1989, 'The polar heliospheric magnetic field'. *Geophys. Res. Lett.* **16**, 1–4.

Jokipii, J. R., E. H. Levy, and W. B. Hubbard: 1977, 'Effects of particle drift on cosmic-ray transport. I. General properties, application to solar modulation'. *Astrophys. J.* **213**(3), 861–868.

Kandel, R. and M. Viollier: 2005, 'Planetary Radiation Budgets'. *Space Science Reviews* **120**, 1–2.

Kasting, J. and S. Ono: 2005, '[redacted]'. *in press, Proc. Roy. Soc. London.*[redacted].

Kasting, J. F.: 1993, 'Earth's early atmosphere'. *Science* **259**, 920–926.

Kernthaler, S. C., R. Toumi, and J. D. Haigh: 1999, 'Some doubts concerning a link between cosmic ray fluxes and global cloudiness'. *Geophys. Res. Lett.* **26**, 863–866.

Kilcik, A.: 2005, 'Regional sun–climate interaction'. *J. Atmos. Solar-Terr. Phys.* **67**, 1573–1579.

Knauth, L. and D. Lowe: 2003, 'High Archean climatic temperature inferred from oxygen isotope geochemistry of cherts in the 3.5 Ga Swaziland Supergroup, South Africa.'. *Geol. Soc. Am. Bull.* **115**, 566–580.

Kocharov, G.: 1991, 'Cosmic rays in the past'. *Nuclear Physics B Proceedings Supplements* **22**, 153–164.

Korte, M. and C. G. Constable: 2005a, 'Continuous geomagnetic field models for the past 7 millennia: 2. CALS7K'. *Geochemistry, Geophysics, Geosystems* **6**, 2–+.

Korte, M. and C. G. Constable: 2005b, 'The geomagnetic dipole moment over the last 7000 years-new results from a global model [rapid communication]'. *Earth and Planetary Science Letters* **236**, 348–358.

Kristjánsson, J. E., J. Kristiansen, and E. Kaas: 2004, 'Solar activity, cosmic rays, clouds and climate - an update'. *Advances in Space Research* **34**, 407–415.

Krymskii, G. F.: 1977a, 'A regular mechanism for accelerating charged particles at the shock front'. *Akademiia Nauk SSSR Doklady* **234**, 1306–1308.

Krymskii, G. F.: 1977b, 'A regular mechanism for the acceleration of charged particles on the front of a shock wave'. *Akademiia Nauk SSSR Doklady* **234**, 1306–1308.

Kuroda, Y. and K. Kodera: 2005, 'Solar cycle modulation of the Southern Annular Mode'. *Geophys. Res. Lett.* **32**, L13802.

Labitzke, K., J. Austin, N. Butchart, J. Knight, M. Takahashi, M. Nakamoto, T. Nagashima, J. Haigh, and V. Williams: 2002, 'The global signal of the 11-year solar cycle in the stratosphere: observations and models'. *Journal of Atmospheric and Terrestrial Physics* **64**, 203–210.

Laj, C., C. Kissel, A. Mazaud, J. Channell, and J. Beer: 2000, 'North Atlantic Paleointensity Stack Since 75 kal (NAPIS-75) and The Duration of the Laschamp Event'. *Phil. Trans. Royal Soc. of London* **358**, 1009–1025.

Laj, C., C. Kissel, A. Mazaud, E. Michel, R. Muscheler, and J. Beer: 2002, 'Geomagnetic field intensity, North Atlantic Deep Water circulation and atmospheric Δ^{14}C during the last 50 kyr'. *Earth and Planetary Science Letters* **200**, 177–190.

Lal, D.: 1988, 'Theoretically expected variations in the terrestrial cosmic-ray production rates of isotopes'. In: *Solar-Terrestrial Relationships and the Earth Environment in the last Millennia*. pp. 216–+.

Lal, D.: 1991, 'Cosmic ray labeling of erosion surfaces - In situ nuclide production rates and erosion models'. *Earth Planet. Sci. Lett.* **104**, 424–439.

Lal, D. and B. Peters: 1967, 'Cosmic ray produced radioactivity on the Earth'. In: *Handbuch der Physik*, Vol. XLVI/2. Springer, Berlin, pp. 551–612.

Langel, R. A.: 1992, 'International Geomagnetic Reference Field: The sixth generation'. *J. Geomagn. Geoelectr.* **44**, 679.

Langner, U. W. and M. S. Potgieter: 2004, 'Effects of the solar wind termination shock and heliosheath on the heliospheric modulation of galactic and anomalous Helium'. *Annales Geophysicae* **22**, 3063–3072.

Langner, U. W. and M. S. Potgieter: 2005a, 'Effects of the position of the solar wind termination shock and the heliopause on the heliospheric modulation of cosmic rays'. *Advances in Space Research* **35**, 2084–2090.

Langner, U. W. and M. S. Potgieter: 2005b, 'The heliospheric modulation of cosmic ray protons during increased solar activity: effects of the position of the solar wind termination shock and of the heliopause'. *Annales Geophysicae* **23**, 1499–1504.

Langner, U. W. and M. S. Potgieter: 2005c, 'Modulation of Galactic Protons in an Asymmetrical Heliosphere'. *Astrophys. J.* **630**, 1114–1124.

Langner, U. W., M. S. Potgieter, T. Borrmann, and H. Fichtner: 2005a, 'Effects of different solar wind speed profiles in the heliosheath on the modulation of cosmic ray protons,'. *Astrophys. J.* **in press**.

Langner, U. W., M. S. Potgieter, T. Borrmann, and H. Fichtner: 2005b, 'Modulation of anomalous protons: Effects of different solar wind speed profiles in the heliosheath,'. *J. Geophys. Res.* **in press**.

Langner, U. W., M. S. Potgieter, and W. R. Webber: 2003, 'Modulation of cosmic ray protons in the heliosheath'. *Journal of Geophysical Research (Space Physics)* **108**, 14–+.

Lanzerotti, L. J. and C. G. Maclennan: 2000, 'Low-Energy Anomalous Cosmic Rays in the Ecliptic Plane: 1-5 AU'. *Astrophys. J. Lett.* **534**, L109–L112.

Lassen, K. and E. Friis-Christensen: 1995, 'Variability of the solar cycle length during the past five centuries and the apparent association with terrestrial climate'. *Journal of Atmospheric and Terrestrial Physics* **57**, 835–845.

Lavielle, B., K. Marti, J.-P. Jeannot, K. Nishiizumi, and M. Caffee: 1999, 'The ^{36}Cl-^{36}Ar-^{40}K- ^{41}K records and cosmic ray production rates in iron meteorites'. *Earth Planet. Sci. Lett.* **170**, 93–104.

Le Mouël, J.-L., V. Kossobokov, and V. Courtillot: 2005, 'On long-term variations of simple geomagnetic indices and slow changes in magnetospheric currents: The emergence of anthropogenic global warming after 1990?'. *Earth Planet. Sci. Lett.* **232**, 273–286.

le Roux, J. A. and M. S. Potgieter: 1989, 'Episodic cosmic-ray modulation in the heliosphere'. *Advances in Space Research* **9**, 225–228.

le Roux, J. A. and M. S. Potgieter: 1995, 'The simulation of complete 11 and 12 year modulation cycles for cosmic rays in the heliosphere using a drift model with global merged interaction regions'. *Astrophys. J.* **442**, 847–851.

Lean, J.: 2005, 'Living with a Variable Sun'. *Physics Today* **58**, 32–38.

Lee, s.: 2003, '[redacted]'. [redacted] **0**(0), 0.

Lei, F. S. C., C. Dyer, and P. Truscott: 2004, ‘An atmospheric radiation model based on response matrices generated by detailed Monte Carlo simulations of cosmic ray interactions’. *IEEE Trans Nucl Sci* **51**(6), 3442–3451.

Leitch, E. M. and G. Vasisht: 1998, ‘Mass extinctions and the sun’s encounters with spiral arms’. *New Astronomy* **3**, 51–56.

Lerche, I. and R. Schlickeiser: 1982a, ‘On the transport and propagation of cosmic rays in galaxies. I - Solution of the steady-state transport equation for cosmic ray nucleons, momentum spectra and heating of the interstellar medium’. *Mon. Not. Roy. Astron. Soc.* **201**, 1041–1072.

Lerche, I. and R. Schlickeiser: 1982b, ‘On the transport and propagation of relativistic electrons in galaxies The effect of adiabatic deceleration in a galactic wind for the steady state case’. *Astron. & Astrophys.* **107**, 148–160.

Lerche, I. and R. Schlickeiser: 1982c, ‘Transport and propagation of cosmic rays in galaxies. II - The effect of a galactic wind on the mean lifetime and age distribution of non-decaying cosmic rays’. *Astron. & Astrophys.* **116**, 10–26.

Light, E. S., M. Merker, H. J. Vershell, R. B. Mendel, and S. A. Korff: 1973, ‘Time dependent worldwide distribution of atmospheric neutrons and of their products, 2, Calculations’. *J. Geophys. Res.* **78**, 2741–2762.

Lim, J., E. Matsumoto, and H. Kitagawa: 2005, ‘Eolian quartz flux variations in Cheju Island, Korea, during the last 6500 yr and a possible Sun–monsoon linkage’. *Quatern. Res.* **64**, 12–20.

Lin, C. C. and F. H. Shu: 1964, ‘On the Spiral Structure of Disk Galaxies.’. *Astrophys. J.* **140**, 646–655.

Lin, D. N. C., B. F. Jones, and A. R. Klemola: 1995, ‘The motion of the Magellanic clouds, origin of the Magellanic Stream, and the mass of the Milky Way’. *Astrophys. J.* **439**, 652–671.

Lingenfelter, R. E.: 1963, ‘Production of carbon-14 by cosmic-ray neutrons’. *Rev. Geophys* **1**, 35–55.

Lipatov, A. S., G. P. Zank, and H. L. Pauls: 1998, ‘The interaction of neutral interstellar H with the heliosphere: A 2.5-D particle-mesh Boltzmann simulation’. *J. Geophys. Res.* **103**, 20631–20642.

Lisenfeld, U., P. Alexander, G. G. Pooley, and T. Wilding: 1996, ‘Constraints on cosmic ray propagation from radio continuum data of NGC 2146.’. *Mon. Not. Roy. Astron. Soc.* **281**, 301–310.

Loktin, A. V., N. V. Matkin, and T. P. Gerasimenko: 1994, ‘Catalogue of open cluster parameters from UBV-data.’. *Astronomical and Astrophysical Transactions* **4**, 153.

Longair, M. S.: 1994, *High energy astrophysics. Vol.2: Stars, the galaxy and the interstellar medium.* Cambridge: Cambridge University Press, 1994, 2nd ed.

Lowder, W., P. D. Raft, and H. Beck: 1971, ‘Experimental determination of cosmic-ray charged particle intensity profiles in the atmosphere’. In: E. A. Warman (ed.): *Proceedings of the national symposium of natural and manmade radiation in space.* pp. 908–913.

Lukasiak, A., P. Ferrando, F. B. McDonald, and W. R. Webber: 1994, ‘The isotopic composition of cosmic-ray beryllium and its implication for the cosmic ray’s age’. *Astrophys. J.* **423**, 426–431.

Magny, M.: 1993, ‘Solar Influences on Holocene Climatic Changes Illustrated by Correlations between Past Lake-Level Fluctuations and the Atmospheric ^{1}4C Record’. *Quatern. Res.* **40**, 1–9.

Malkov, M. A. and L. O’C Drury: 2001, ‘Nonlinear theory of diffusive acceleration of particles by shock waves ’. *Reports of Progress in Physics* **64**, 429–481.

Mangini, A., C. Spötl, and P. Verdes: 2005, 'Reconstruction of temperature in the Central Alps during the past 2000 yr from a @dˆ1ˆ8O stalagmite record [rapid communication]'. *Earth Planet. Sci. Lett.* **235**, 741–751.

Mann, M. E., R. S. Bradley, and M. K. Hughes: 1999, 'Northern hemisphere temperatures during the past millennium: Inferences, uncertainties, and limitations'. *Geophys. Res. Lett.* **26**, 759–762.

Marsh, N. and H. Svensmark: 2000a, 'Cosmic Rays, Clouds, and Climate'. *Space Science Reviews* **94**, 215–230.

Marsh, N. D. and H. Svensmark: 2000b, 'Low Cloud Properties Influenced by Cosmic Rays'. *Physical Review Letters* **85**, 5004–5007.

Martinson, D., N. Pisias, J. Hays, J. Imbrie, T. J. Moore, and N. Shackleton: 1987, 'Age dating and the orbital theory of the ice ages: Development of a high-resolution 0 to 300,000-year chronostratigraphy'. *Quatern. Res.* **27**, 1–29.

Masarik, J. and J. Beer: 1999, 'Simulation of particle fluxes and cosmogenic nuclide production in the Earth's atmosphere'. *J. Geophys. Res.* **104**, 12099–12112.

Masarik, J. and R. C. Reedy: 1994, 'Effects of bulk chemical composition on nuclide production processes in meteorites'. *Geochim. Cosmochim. Acta* **58**, 5307–5317.

Masarik, J. and R. C. Reedy: 1995, 'Terrestrial cosmogenic-nuclide production systematics calculated from numerical simulations'. *Earth Planet. Sci. Lett.* **136**, 381–395.

Matthaeus, W. H., G. Qin, J. W. Bieber, and G. P. Zank: 2003, 'Nonlinear collisionless perpendicular diffusion of charged particles'. *Astrophys. J. Lett.* **590**(1), L53–L56.

McComas, D. J., R. Goldstein, J. T. Gosling, and R. M. Skoug: 2001, 'Ulysses' Second Orbit: Remarkably Different Solar Wind'. *Space Science Reviews* **97**, 99–103.

McCracken, K. and F. McDonald: 2001, 'The Long Term Modulation of the Galactic Cosmic Radiation, 1100-2000 AD'. In: *International Cosmic Ray Conference*. pp. 3753–+.

McCracken, K. G., J. Beer, and F. B. McDonald: 2002, 'A five-year variability in the modulation of the galactic cosmic radiation over epochs of low solar activity'. *Geophys. Res. Lett.* **29**, 14–1.

McCracken, K. G., F. B. McDonald, J. Beer, G. Raisbeck, and F. Yiou: 2004, 'A phenomenological study of the long-term cosmic ray modulation, 850-1958 AD'. *Journal of Geophysical Research (Space Physics)* **109**, 12103–+.

McCrea, W. H.: 1975, 'Ice ages and the Galaxy'. *Nature* **255**, 607–609.

McCrea, W. H.: 1981, 'Long time–scale fluctuations in the evolution of the Earth'. *Proc. R. Soc. Lond. A* **375**, 1–41,.

McDonald, F. B., J. H. Trainor, N. Lal, M. A. I. van Hollebeke, and W. R. Webber: 1981, 'The solar modulation of galactic cosmic rays in the outer heliosphere'. *Astrophys. J. Lett.* **249**, L71–L75.

McElhinny, M. W. and W. Senanayake: 1982, 'Variations in the Geomagnetic Dipole, I: the past 50 000 years'. *J. Geomagn. Geoelectr.* **34**, 38–51.

McKay, C. P. and G. E. Thomas: 1978, 'Consequences of a past encounter of the earth with an interstellar cloud'. *Geophys. Res. Lett.* **5**, 215–218.

McPherron, R. L.: 1995, 'Magnetospheric dynamics'. In: M. G. Kivelson and C. T. Russel (eds.): *ntroduction to Space Physics*. Cambridge university press.

Mears, C. A. and F. J. Wentz: 2005, 'The Effect of Diurnal Correction on Satellite-Derived Lower Tropospheric Temperature'. *Science* **309**, 1548–1551.

Milankovitch, M.: 1941, 'Kanon der Erdbestrahlung und seine Anwendung auf das Eiszeitproblem'. *Roy. Serb. Acad. Spec. Publ.* **133**, 1–633. (Translation by.

israel Progr. For Scientific Translation, and published for U.S. Department of Commerce and Nat. Sci. Found.), 1974.

Mitchell, J., D. Karoly, G. Hegerl, F. Zwiers, M. Allen, and J. Marengo: 2001, ‘Detection of climate change and attribution of causes. Contribution of Working Group I to the Third Assessment Report of the Intergovernmental Panel on Climate Change (Ch. 1)’. In: J. Houghton, Y. Ding, D. Griggs, M. Noguer, P. van der Linden, X. Dai, K. Maskell, and C. Johnson (eds.): *Climate Change 2001: The Scientific Basis:*. pp. 695–738, Cambridge University Press, Cambridge, U.K.

Mitchell, J. J.: 1976, ‘An Overview of Climatic Variability and Its Causal Mechanism’. *Quaternary Res.* **6**, 481–493.

Miyahara, H., K. Masudaa, H. Menjoa, K. Kuwanaa, Y. Murakia, and T. Nakamurab: 2005, ‘Variation of the cosmic ray intensity during the Maunder Minimum deduced from carbon-14 content in treerings’. In: *Proc. 29th Int. Cosmic Ray Conf. Aug 2-10, Pune, India, paper in SH 3.4*.

Moberg, A., D. Sonechkin, K. Holmgren, N. Datsenko, and K. Wibjörn: 2005, ‘Highly variable Northern Hemisphere temperatures reconstructed from low- and high-resolution proxy data’. *Nature* **433**, 613–617.

Monnin, E., A. Indermühle, A. Dällenbach, J. Flückiger, B. Stauffer, T. F. Stocker, D. Raynaud, and J.-M. Barnola: 2001, ‘Atmospheric CO_2 Concentrations over the Last Glacial Termination’. *Science* **291**, 112–114.

Moraal, H., M. S. Potgieter, P. H. Stoker, and A. J. van der Walt: 1989, ‘Neutron monitor latitude survey of cosmic ray intensity during the 1986/1987 solar minimum’. *J. Geophys. Res.* **94**, 1459–1464.

Moskalenko, I. V., A. W. Strong, S. G. Mashnik, and J. F. Ormes: 2003, ‘Challenging Cosmic-Ray Propagation with Antiprotons: Evidence for a “Fresh” Nuclei Component?’. *Astrophys. J.* **586**, 1050–1066.

Moskalenko, I. V., A. W. Strong, J. F. Ormes, and M. S. Potgieter: 2002, ‘Secondary Antiprotons and Propagation of Cosmic Rays in the Galaxy and Heliosphere’. *Astrophys. J.* **565**, 280–296.

Mudelsee, M.: 2001, ‘he phase relations among atmospheric CO_2 content, temperature and global ice volume over the past 420 ka’. *Quat. Sci. Rev.* **20**, 583–589.

Mudelsee, M. and M. Raymo: 2005, ‘Slow dynamics of the Northern Hemisphere glaciation’. *Paleoceanography* **20**, PA4022.

Müller, H.-R., G. P. Zank, and A. S. Lipatov: 2000, ‘Self-consistent hybrid simulations of the interaction of the heliosphere with the local interstellar medium’. *J. Geophys. Res.* **105**, 27419–27438.

Muller, R. A. and G. J. MacDonald: 1997, ‘Glacial cycles and astronomical forcing’. *Science* **277**, 215–218.

Muscheler, R., J. Beer, P. W. Kubik, and H. A. Synal: 2005a, ‘Geomagnetic field intensity during the last 60,000 years based on ˆ1ˆ0Be and ˆ3ˆ6Cl from the Summit ice cores and ˆ1ˆ4C’. *Quaternary Science Reviews* **24**, 1849–1860.

Muscheler, R., F. Joos, S. Müller, and I. Snowball: 2005b, ‘Climate: How unusual is today’s solar activity?’. *Nature* **436**, E3–E4.

Naoz, S. and N. J. Shaviv: 2004, ‘Open Star Clusters and the Milky Way’s Spiral Arm Dynamics’. Submitted to New Astronomy.

Ndiitwani, D. C., S. E. S. Ferreira, M. S. Potgieter, and B. Heber: 2005, ‘Modelling cosmic ray intensities along the Ulysses trajectory’. *Annales Geophysicae* **23**, 1061–1070.

Neff, U., S. J. Burns, A. Mangini, M. Mudelsee, D. Fleitmann, and A. Matter: 2001, 'Strong coherence between solar variability and the monsoon in Oman between 9 and 6kyr ago'. *Nature* **411**, 290–293.

Neher, H. V.: 1971, 'Cosmic rays at high latitudes and altitudes covering four solar maxima'. *J. Geophys. Res.* **76**, 1637–1651.

Newkirk, L. L.: 1963, 'Calculation of Low-Energy Neutron Flux in the Atmosphere by the S_n Method'. *J. Geophys. Res.* **68**, 1825–+.

Ney, E. P.: 1959, 'Cosmic Radiation and Weather'. *Nature* **183**, 451.

Niggemann, S., A. Mangini, M. Mudelsee, D. K. Richter, and G. Wurth: 2003, 'Sub-Milankovitch climatic cycles in Holocene stalagmites from Sauerland, Germany'. *Earth Planet. Sci. Lett.* **216**, 539–547.

Nir, A., S. T. Kruger, R. E. Lingenfelter, and E. J. Flamm: 1966, 'Natural tritium'. *Rev. Geophys.* **4**, 441–456.

O'Brien, K.: 1979, 'Secular variations in the production of cosmogenic isotopes in the earth's atmosphere'. *J. Geophys. Res.* **84**, 423–431.

O'Brien, K., L. A., de la Zerda, M. Shea, and D. Smart: 1991, 'The production of cosmogenic isotopes in the Earth's atmosphere and their invent ories,'. In: M. M. C.P. Sonett, M.S. Giampapa (ed.): *The sun in time,*. pp. 317–342, Univ. Ariz. Press.

O'C Drury, L.: 1983, 'On particle acceleration in supernova remnants'. *Space Science Reviews* **36**, 57–60.

Oeschger, H., J. Houtermann, H. Loosli, and M. Wahlen: 1969, 'The constancy of cosmic radiation from isotope studies in meteorites and on the Earth'. In: I. U. Olsen (ed.): *Radiocarbon Variations and Absolute Chronology, Nobel symposium,*. John Wiley.

Olson, W. P. and K. A. Pfitzer: 1982, 'A dynamic model of the magnetospheric magnetic and electric fields for July 29, 1977'. *J. Geophys. Res.* **87**, 5943–5948.

Opher, M., P. C. Liewer, M. Velli, L. Bettarini, T. I. Gombosi, W. Manchester, D. L. DeZeeuw, G. Toth, and I. Sokolov: 2004, 'Magnetic Effects at the Edge of the Solar System: MHD Instabilities, the de Laval Nozzle Effect, and an Extended Jet'. *Astrophys. J.* **611**, 575–586.

Ostapenko, A. A. and Y. P. Maltsev: 2000, 'Storm time variation in the magnetospheric magnetic field'. *J. Geophys. Res.* **105**, 311–316.

Pagani, M., J. C. Zachos, K. H. Freeman, B. Tipple, and S. Bohaty: 2005, 'Marked Decline in Atmospheric Carbon Dioxide Concentrations During the Paleogene'. *Science* **309**, 600–603.

Pallé, E., C. J. Butler, and K. O'Brien: 2004, 'The possible connection between ionization in the atmosphere by cosmic rays and low level clouds'. *Journal of Atmospheric and Terrestrial Physics* **66**, 1779–1790.

Pallé, E., P. Montañés-Rodriguez, P. R. Goode, S. E. Koonin, M. Wild, and S. Casadio: 2005, 'A multi-data comparison of shortwave climate forcing changes'. *Geophys. Res. Lett.* **32**, 21702–+.

Palle Bago, E. and J. Butler: 2000, 'The influence of cosmic terrestrial clouds and global warming'. *Astronomy & Geophysics* **41**, 18–22.

Palous, J., J. Ruprecht, O. B. Dluzhnevskaia, and T. Piskunov: 1977, 'Places of formation of 24 open clusters'. *Astron. & Astrophys.* **61**, 27–37.

Parker, E. N.: 1958, 'Dynamics of the Interplanetary Gas and Magnetic Fields.'. *Astrophys. J.* **128**, 664–+.

Parker, E. N.: 1965, 'The passage of energetic charged particles through interplanetary space'. *Planet. Space Sci.* **13**, 9–49.

Perko, J. S. and L. A. Fisk: 1983, 'Solar modulation of galactic cosmic rays. V - Time-dependent modulation'. *J. Geophys. Res.* **88**, 9033–9036.

Petit, J. R., J. Jouzel, D. Raynaud, N. I. Barkov, J.-M. Barnola, I. Basile, M. Bender, J. Chappellaz, M. Davis, G. Delaygue, M. Delmotte, V. M. Kotlyakov, M. Legrand, V. Y. Lipenkov, C. Lorius, L. Pépin, C. Ritz, E. Saltzman, and M. Stievenard: 1999, 'Climate and atmospheric history of the past 420,000 years from the Vostok ice core, Antarctica'. *Nature* **399**, 429–437.

Pinker, R. T., B. Zhang, and E. G. Dutton: 2005, 'Do Satellites Detect Trends in Surface Solar Radiation?'. *Science* **308**, 850–854.

Pogorelov, N. V.: 2004, 'Three-dimensional structure of the outer heliosphere in the presence of the interstellar and interplanetary magnetic fields'. In: *AIP Conf. Proc. 719: Physics of the Outer Heliosphere.* pp. 39–46.

Pogorelov, N. V. and G. P. Zank: 2005, 'Coupling of the interstellar and interplanetary magnetic fields at the heliospheric interface: The effect of neutral hydrogen atoms'. *Advances in Space Research* **35**, 2055–2060.

Pogorelov, N. V., G. P. Zank, and T. Ogino: 2004, 'Three-dimensional Features of the Outer Heliosphere Due to Coupling between the Interstellar and Interplanetary Magnetic Fields. I. Magnetohydrodynamic Model: Interstellar Perspective'. *Astrophys. J.* **614**, 1007–1021.

Poore, R. Z., T. M. Quinn, and S. Verardo: 2004, 'Century-scale movement of the Atlantic Intertropical Convergence Zone linked to solar variability'. *Geophys. Res. Lett.* **31**, 12214–+.

Porter, H. S., C. H. Jackman, and A. E. S. Green: 1976, 'Efficiencies for production of atomic nitrogen and oxygen by relativistic proton impact in air'. *J. Comp. Phys.* **65**, 154–167.

Potgieter, M. S.: 1995, 'The long-term modulation of galactic cosmic rays in the heliosphere'. *Advances in Space Research* **16**, 191–.

Potgieter, M. S.: 1998, 'The Modulation of Galactic Cosmic Rays in the Heliosphere: Theory and Models'. *Space Science Reviews* **83**, 147–158.

Potgieter, M. S., R. A. Burger, and S. E. S. Ferreira: 2001, 'Modulation of Cosmic Rays in the Heliosphere From Solar Minimum to Maximum: a Theoretical Perspective'. *Space Science Reviews* **97**, 295–307.

Potgieter, M. S. and S. E. S. Ferreira: 2001, 'Modulation of cosmic rays in the heliosphere over 11 and 22 year cycles: a modelling perspective'. *Advances in Space Research* **27**, 481–492.

Potgieter, M. S. and U. W. Langner: 2004, 'Heliospheric Modulation of Cosmic-Ray Positrons and Electrons: Effects of the Heliosheath and the Solar Wind Termination Shock'. *Astrophys. J.* **602**, 993–1001.

Potgieter, M. S. and H. Moraal: 1985, 'A drift model for the modulation of galactic cosmic rays'. *Astrophys. J.* **294**, 425–440.

Pozo-Vázquez, D., J. Tovar-Pescador, S. R. Gámiz-Fortis, M. J. Esteban-Parra, and Y. Castro-Díez: 2004, 'NAO and solar radiation variability in the European North Atlantic region'. *Geophys. Res. Lett.* **31**, 5201–+.

Prael, R. E. and H. Lichtenstein: 1989, 'User guide to LCS: The LAHET Code System'. Technical report, Los Alamos National Laboratory report.

Prestes, A., N. R. Rigozo, E. Echer, and L. E. A. Vieira: 2006, 'Spectral analysis of sunspot number and geomagnetic indices (1868 2001)'. *Journal of Atmospheric and Terrestrial Physics* **68**, 182–190.

Ramaswamy, V., O. Boucher, J. Haigh, D. Hauglustaine, J. Haywood, G. Myhre, T. Nakajima, G. Shi, and S. Solomon: 2001, 'Radiative Forcing of Climate Change'. In: J. Houghton, V. Ding, D. Griggs, M. Noguer, P. van der Linden, X. Dai, K.

Maskell, and C. Johnson (eds.): *Climate Change 2001: The Scientific Basis*. pp. 340–416, Cambridge University Press, Cambridge.

Rampino, M.: 1998, 'The galactic history of mass extinctions: An update'. *Cel. Mec.* **69**, 49–58.

Rampino, M., B. Haggerty, and T. Pagano: 1997, 'A Unified Theory of Impact Crises and Mass Extinctions: Quantitative Tests'. *Annals New York Acad. Sci.* **822**, 403–431.

Raspopov, O., V. Dergachev, and T. Kolström: 2004, 'Periodicity of climate conditions and solar variability derived from dendrochronological and other palaeoclimatic data in high latitudes'. *Palaeogeogr. Palaeoclim. Palaeoecol.* **209**, 127–139.

Ratkiewicz, R., A. Barnes, G. A. Molvik, J. R. Spreiter, S. S. Stahara, M. Vinokur, and S. Venkateswaran: 1998, 'Effect of varying strength and orientation of local interstellar magnetic field on configuration of exterior heliosphere: 3D MHD simulations'. *Astron. & Astrophys.* **335**, 363–369.

Reames, D. V. and F. B. McDonald: 2003, 'Wind Observations of Anomalous Cosmic Rays from Solar Minimum to Maximum'. *Astrophys. J. Lett.* **586**, L99–L101.

Reedy, R. C. and J. Masarik: 1994, 'Cosmogenic-Nuclide Depth Profiles in the Lunar Surface'. In: *Lunar and Planetary Institute Conference Abstracts*. pp. 1119–+.

Reinecke, J. P. L., H. Moraal, and F. B. McDonald: 1993, 'The cosmic radiation in the heliosphere at successive solar minima - Steady state no-drift solutions of the transport equation'. *J. Geophys. Res.* **98**(17), 9417–9431.

Reinecke, J. P. L. and M. S. Potgieter: 1994, 'An explanation for the difference in cosmic ray modulation at low and neutron monitor energies during consecutive solar minimum periods'. *J. Geophys. Res.* **99**, 14761–+.

Rocha-Pinto, H. J., J. Scalo, W. J. Maciel, and C. Flynn: 2000, 'Chemical enrichment and star formation in the Milky Way disk. II. Star formation history'. *Astron. & Astrophys.* **358**, 869–885.

Rohen, G., C. von Savigny, M. Sinnhuber, E. J. Llewellyn, J. W. Kaiser, C. H. Jackman, M.-B. Kallenrode, J. Schröter, K.-U. Eichmann, H. Bovensmann, and J. P. Burrows: 2005, 'Ozone depletion during the solar proton events of October/November 2003 as seen by SCIAMACHY'. *Journal of Geophysical Research (Space Physics)* **110**, 9–+.

Royer, D. L., R. A. Berner, and D. J. Beerling: 2001, 'Phanerozoic atmospheric CO_2 change: evaluating geochemical and paleobiological approaches'. *Earth Science Reviews* **54**, 349–92.

Ruddiman, W.: 2001, *Earth's Climate: Past and Future*. W.H. Freeman and Co., New York.

Ruddiman, W. F.: 2006, 'Ice-driven CO_2 feedback on ice volume'. *Climate of the Past Discussions* **2**, 43–78.

Ruderman, M. A.: 1974, 'Possible Consequences of Nearby Supernova Explosions for Atmospheric Ozone and Terrestrial Life'. *Science* **184**, 1079–1081.

Sabbah, I. and M. Rybanský: 2006, 'Galactic cosmic ray modulation during the last five solar cycles'. *Journal of Geophysical Research (Space Physics)* **111**, 1105–+.

Sagan, C. and C. Chyba: 1997, 'The early faint sun paradox: Organic shielding of ultraviolet-labile greenhouse gases'. *Science* **276**, 1217–1221.

Scafetta, N. and B. West: 2005, 'Estimated solar contribution to the global surface warming using the ACRIM TSI satellite composite'. *Geophys. Res. Lett.* **32**, L18713.

Scafetta, N. and B. J. West: 2006, 'Phenomenological solar contribution to the 1900-2000 global surface warming'. *Geophys. Res. Lett.* **33**, 5708–+.

Scalo, J. M.: 1987, ‘The initial mass function, starbursts, and the Milky Way’. In: *Starbursts and Galaxy Evolution*. pp. 445–465.

Schaeffer, O. A., K. Nagel, H. Fechtig, and G. Neukum: 1981, ‘Space erosion of meteorites and the secular variation of cosmic rays /over 10 to the 9th years/’. *Planet. Space Sci.* **29**, 1109–1118.

Scherer, K.: 2000, ‘Drag forces on interplanetary dust grains induced by the interstellar neutral gas’. *J. Geophys. Res.* **105**, 10329–10342.

Scherer, K. and H. J. Fahr: 2003, ‘Breathing of heliospheric structures triggered by the solar-cycle activity’. *Annales Geophysicae* **21**, 1303–1313.

Scherer, K., H.-J. Fahr, H. Fichtner, and B. Heber: 2004, ‘Long-Term Modulation of Cosmic Rays in the Heliosphere and its Influence at Earth’. *Solar Phys.* **224**, 305–316.

Scherer, K. and S. E. S. Ferreira: 2005a, ‘A heliospheric hybrid model: hydrodynamic plasma flow and kinetic cosmic ray transport’. *Astrophysics and Space Sciences Transactions* **1**, 17–27.

Scherer, K. and S. E. S. Ferreira: 2005b, ‘The heliomagnetic and solar-cycle related variations of the cosmic ray flux modeled with the BoPo-hybrid code’. *å* **442**, L11–L14.

Scherer, K. and H. Fichtner: 2004, ‘Constraints on the heliospheric magnetic field variation during the Maunder Minimum from cosmic ray modulation modelling’. *Astron. & Astrophys.* **413**, L11–L14.

Scherer, K., H. Fichtner, and O. Stawicki: 2002, ‘Shielded by the wind: the influence of the interstellar medium on the environment of Earth’. *Journal of Atmospheric and Terrestrial Physics* **64**, 795–804.

Scherer, K., H. Fichtner, O. Stawicki, and H. Fahr: 2001a, ‘Cosmogenic element production in meteorites the influence of long-term variation in heliospheric structure’. In: *International Cosmic Ray Conference*. pp. 4031–+.

Scherer, K., E. Marsch, R. Schwenn, and H. Rosenbauer: 2001b, ‘Long-term variations of the flow direction and angular momentum of the solar wind observed by Helios’. *Astron. & Astrophys.* **366**, 331–338.

Schopf, J.: 1983, *Earth’s Earliest Biosphere: Its Origin and Evolution*. Princeton University Press, Princeton, N.J.

Schröter, J., B. Heber, M.-B. Kallenrode, and F. Steinhilber: 2005, ‘Energetic particles in the atmosphere: A Monte-Carlo simulation’. *Adv. Space Res.* **35**, in press.

Schwartz and James: 1984, ‘Periodic mass extinctions and the sun’s oscillation about the galactic plane’. *Nature* **308**, 712–713.

Sedov, L. I.: 1946, ‘The motion of air in a strong explosion’. *Dokl. Akad. Nauk SSSR* **42**, 17–+.

Shalchi, A. and R. Schlickeiser: 2004, ‘Quasilinear perpendicular diffusion of cosmic rays in weak dynamical turbulence’. *Astron. & Astrophys.* **420**, 821–832.

Shapley, H.: 1921, ‘ ’. *J. Geology* **29**, 502–504.

Sharma, M.: 2002, ‘Variations in solar magnetic activity during the last 200000 years: is there a Sun-climate connection?’. *Earth Planet. Sci. Lett.* **199**, 459–472.

Shaviv, N. and J. Veizer: 2003, ‘Celestial driver of Phanerozoic climate? GSA’. *GSA Today* **13**(7), 4–10.

Shaviv, N. J.: 2002, ‘Cosmic Ray Diffusion from the Galactic Spiral Arms, Iron Meteorites, and a Possible Climatic Connection’. *Phys. Rev. Lett.* **89**(5), 051102–+.

Shaviv, N. J.: 2003a, ‘The spiral structure of the Milky Way, cosmic rays, and ice age epochs on Earth’. *New Astronomy* **8**, 39–77.

Shaviv, N. J.: 2003b, 'Toward a solution to the early faint Sun paradox: A lower cosmic ray flux from a stronger solar wind'. *J. Geophys. Res.* **108**(A12), 3–1.

Shaviv, N. J.: 2005, 'On climate response to changes in the cosmic ray flux and radiative budget'. *Journal of Geophysical Research (Space Physics)* **110**(A9), 8105–+.

Shea, M. A., D. Smart, and G. A. M. Dreschhoff: 1999, 'Identification of major proton fluence events from nitrates in polar ice cores'. *Radiat. Meas.* **30**, 309–316.

Shea, M. A. and D. F. Smart: 2004, 'Preliminary study of cosmic rays, geomagnetic field changes and possible climate changes'. *Advances in Space Research* **34**, 420–425.

Sherwood, S. C., J. R. Lanzante, and C. L. Meyer: 2005, 'Radiosonde Daytime Biases and Late-20th Century Warming'. *Science* **309**, 1556–1559.

Shields, G. and J. Veizer: 2002, 'Precambrian marine carbonate isotope database: Version 1.1'. *Geochemistry, Geophysics, Geosystems* pp. 1–+.

Shindell, D., D. Rind, N. Balachandran, J. Lean, and P. Lonergan: 1999, 'Solar Cycle Variability, Ozone, and Climate'. *Science* **284**, 305–+.

Siegenthaler, U., T. F. Stocker, E. Monnin, D. Lüthi, J. Schwander, B. Stauffer, D. Raynaud, J.-M. Barnola, H. Fischer, V. Masson-Delmotte, and J. Jouzel: 2005, 'Stable Carbon Cycle-Climate Relationship During the Late Pleistocene'. *Science* **310**, 1313–1317.

Simpson, J.: 1983, 'Elemental and isotopic composition of the galactic cosmic rays'. *Annu. Rev. Nucl. Part. Sci.* **33**, 323–381.

Simpson, J. A.: 1951, 'Neutrons Produced in the Atmosphere by the Cosmic Radiations'. *Physical Review* **83**, 1175–1188.

Simpson, J. A.: 2000, 'The Cosmic Ray Nucleonic Component: The Invention and Scientific Uses of the Neutron Monitor - (Keynote Lecture)'. *Space Science Reviews* **93**, 11–32.

Smart, D. F. and M. A. Shea: 1997, 'World Grid of Calculated Cosmic Ray Vertical Cutof f Rigidities for Epoch 1990,'. In: *Proc. 25th Int. Cosmic Ray Conf.*, Vol. 2. pp. 401–404.

Smart, D. F., M. A. Shea, and E. O. Flückiger: 1999a, 'Calculated Vertical Cutoff Rigidities for the International Space Station During Magnetically Quiet Times'. In: *Proc. 26th Int. Cosmic Ray Conf.*, Vol. 7. pp. 394–397.

Smart, D. F., M. A. Shea, and E. O. Flückiger: 2000, 'Magnetospheric Models and Trajectory Computations'. *Space Science Reviews* **93**, 305–333.

Smart, D. F., M. A. Shea, E. O. Flückiger, A. J. Tylka, and P. R. Boberg: 1999b, 'Calculated Vertical Cutoff Rigidities for the Int. Space Station During Magnetically Active Times'. In: *Proc. 26th Int. Cosmic Ray Conf.*, Vol. 7. pp. 398–401.

Smith, E.: 2001, 'The heliospheric current sheet'. *J. Geophys. Res.* **106**.

Snowball, I. and P. Sandgren: 2002, 'Geomagnetic field variations in northern Sweden during the Holocene quantified from varved lake sediments and their implication for cosmogenic nuclide production rates'. *The Holocene* **12**, 517–530.

Solanki, S. K., I. G. Usoskin, B. Kromer, M. Schüssler, and J. Beer: 2004, 'Unusual activity of the Sun during recent decades compared to the previous 11,000 years'. *Nature* **431**, 1084–1087.

Solanki, S. K., I. G. Usoskin, B. Kromer, M. Schüssler, and J. Beer: 2005, 'Climate: How unusual is today's solar activity? (reply)'. *Nature* **436**, E4–E5.

Solomon, S., D. W. Rusch, J. C. Gérard, G. C. Reid, and P. J. Crutzen: 1981, 'The effect of particle precipitation events on the neutral and ion chemistry of the middle atmosphere: II. Odd hydrogen'. *Planet. Space Sci.* **29**, 885–893.

Soon, W. and S. Baliunas: 2003, 'Proxy climate and environmental changes of the past 1,000 years'. *Climate Research* **23**, 89–110.

Soon, W. W.-H.: 2005, 'Variable solar irradiance as a plausible agent for multidecadal variations in the Arctic-wide surface air temperature record of the past 130 years'. *Geophys. Res. Lett.* **32**, 16712–+.

Spahni, R., J. Chappellaz, T. F. Stocker, L. Loulergue, G. Hausammann, K. Kawamura, J. Flückiger, J. Schwander, D. Raynaud, V. Masson-Delmotte, and J. Jouzel: 2005, 'Atmospheric Methane and Nitrous Oxide of the Late Pleistocene from Antarctic Ice Cores'. *Science* **310**, 1317–1321.

Sreenivasan, S. R. and H. Fichtner: 2001, 'ACR modulation inside a non-spherical modulation boundary'. In: *The Outer Heliosphere: The Next Frontiers*. pp. 207–+.

St-Onge, G., J. S. Stoner, and C. Hillaire-Marcel: 2003, 'Holocene paleomagnetic records from the St. Lawrence Estuary, eastern Canada: centennial- to millennial-scale geomagnetic modulation of cosmogenic isotopes'. *Earth Planet. Sci. Lett.* **209**, 113–130.

Stanev, T.: 2004, *High energy cosmic rays*, Springer-Praxis books in astrophysics and astronomy. Springer.

Stocker, T., G. K. C. Clarke, H. Le Treut, R. S. Lindzen, V. P. Meleshko, R. K. Mugara, T. N. Palmer, R. T. Pierrehumbert, P. J. Sellers, K. E. Trenberth, and J. Willebrand: 2001, 'Physical climate processes and feedbacks'. In: J. T. H. et al. (ed.): *Climate Change 2001: The Scientific Basis. Contribution of Working Group I to the Third Assessment Report of the Intergovernmental Panel on Climate Change*. pp. 419–470, Cambridge University Press, Cambridge.

Stone, E. C., A. C. Cummings, F. B. McDonald, B. C. Heikkila, N. Lal, and W. R. Webber: 2005, 'Voyager 1 Explores the Termination Shock Region and the Heliosheath Beyond'. *Science* **309**, 2017–2020.

Störmer, C.: 1950, *The Polar Aurora*. Oxford University Press, London.

Strong, A. W., I. V. Moskalenko, and O. Reimer: 2000, 'Diffuse Continuum Gamma Rays from the Galaxy'. *Astrophys. J.* **537**, 763–784.

Stuiver, M., T. Braziunas, P. Grootes, and G. Zielinski: 1997, 'Is There Evidence for Solar Forcing of Climate in the GISP2 Oxygen Isotope Record?'. *Quatern. Res.* **48**, 259–266.

Sun, B. and R. S. Bradley: 2002, 'Solar influences on cosmic rays and cloud formation: A reassessment'. *Journal of Geophysical Research (Atmospheres)* **107**, 5–1.

Sun, B. and R. S. Bradley: 2004, 'Reply to comment by N. D. Marsh and H. Svensmark on "Solar influences on cosmic rays and cloud formation: A reassessment"'. *Journal of Geophysical Research (Atmospheres)* **109**, 14206–+.

Svensmark, H.: 1998, 'Influence of Cosmic Rays on Earth's Climate'. *Phys. Rev. Lett.* **81**, 5027–5030.

Svensmark, H. and E. Friis-Christensen: 1997, 'Variation of cosmic ray flux and global cloud coverage-a missing link in solar-climate relationships'. *Journal of Atmospheric and Terrestrial Physics* **59**, 1225–1232.

Tauxe, L.: 1993, 'Sedimentary records of relative paleointensity of the geomagnetic field: Theory and practice'. *Rev. Geophys.* **31**, 319–354.

Taylor, J. H. and J. M. Cordes: 1993, 'Pulsar distances and the galactic distribution of free electrons'. *Astrophys. J.* **411**, 674–684.

Thorsett, S. E.: 1995, 'Terrestrial implications of cosmological gamma-ray burst models'. *Astrophys. J. Lett.* **444**, L53–L55.

Tinsley, B. and F. Yu: 2004, 'Atmospheric ionization and clouds as links between solar activity and climate'. *Geophys. Monogr.* **141**, 321–340.

Tinsley, B. A. and G. W. Deen: 1991, 'Apparent tropospheric response to MeV-GeV particle flux variations: A connection via electrofreezing of supercooled water in high-level clouds?'. *J. Geophys. Res.* **96**, 22283–22296.

Tinsley, B. A. and R. A. Heelis: 1993, 'Correlations of atmospheric dynamics with solar activity evidence for a connection via the solar wind, atmospheric electricity, and cloud microphysics.'. *J. Geophys. Res.* **98**, 10375–10384.

Troshichev, O. A., L. V. Egorova, and V. Y. Vovk: 2003, 'Evidence for influence of the solar wind variations on atmospheric temperature in the southern polar region'. *Journal of Atmospheric and Terrestrial Physics* **65**, 947–956.

Tsyganenko, N. A.: 1989, 'A magnetospheric magnetic field model with a warped tail current sheet'. *Planet. Space Sci.* **37**, 5–20.

Tsyganenko, N. A.: 1995, 'Modeling the Earth's magnetospheric magnetic field confined within a realistic magnetopause'. *J. Geophys. Res.* **100**, 5599–5612.

Tsyganenko, N. A.: 1996, 'Effects of the solar wind conditions in the global magnetospheric configurations as deduced from data-based field models (Invited)'. In: *ESA SP-389: International Conference on Substorms*. pp. 181–+.

Tsyganenko, N. A.: 2002, 'A model of the near magnetosphere with a dawn-dusk asymmetry 2. Parameterization and fitting to observations'. *Journal of Geophysical Research (Space Physics)* **107**(A8), 10–1.

Tsyganenko, N. A., H. J. Singer, and J. C. Kasper: 2003, 'Storm-time distortion of the inner magnetosphere: How severe can it get?'. *Journal of Geophysical Research (Space Physics)* **108**(A5), 18–1.

Tsyganenko, N. A. and M. I. Sitnov: 2005, 'Modeling the dynamics of the inner magnetosphere during strong geomagnetic storms'. *Journal of Geophysical Research (Space Physics)* **110**(A9), 3208–+.

Usoskin, I. G., O. G. Gladysheva, and G. A. Kovaltsov: 2004a, 'Cosmic ray-induced ionization in the atmosphere: spatial and temporal changes'. *J. Atmos. Terr. Phys.* **66**, 1791–1796.

Usoskin, I. G., N. Marsh, G. A. Kovaltsov, K. Mursula, and O. G. Gladysheva: 2004b, 'Latitudinal dependence of low cloud amount on cosmic ray induced ionization'. *Geophys. Res. Lett.* **31**, 6109.

Usoskin, I. G., N. Marsh, G. A. Kovaltsov, K. Mursula, and O. G. Gladysheva: 2004c, 'Latitudinal dependence of low cloud amount on cosmic ray induced ionization'. *Geophys. Res. Lett.* **31**, 16109–+.

Usoskin, I. G. and K. Mursula: 2003, 'Long-Term Solar Cycle Evolution: Review of Recent Developments'. *Solar Phys.* **218**, 319–343.

Vakulenko, N., V. Kotlyakov, A. Monnin, and D. Sonechkin: 2004, 'Evidence for the leading role of temperature variations relative to greenhouse gas concentration variations in the Vostok ice core record'. *Dokl. Russian Acad. Sci., Earth Sciences* **397**, 663–667.

Valet, J.-P., L. Meynadier, and Y. Guyodo: 2005, 'Geomagnetic dipole strength and reversal rate over the past two million years'. *Nature* **435**, 802–805.

van Geel, B., O. Raspopov, H. Renssen, J. van der Plicht, V. Dergachev, and H. Meijer: 1999a, 'The role of solar forcing upon climate change'. *Quaterly Sci. Rev.1* **18**, 331–338.

van Geel, B., O. Raspopov, H. Renssen, J. van der Plicht, V. Dergachev, and H. Meijer: 1999b, 'The role of solar forcing upon climate change'. *Quat. Sci. Rev.* **18**, 331–338.

van Geel, B., J. van der Plicht, M. Kilian, E. Klaver, J. Kouwenberg, H. Renssen, J. Reynaud–Farrera, and H. Waterbolk: 1998, 'The sharp rise of Δ^{14}C ca. 800 cal BC: Possible causes, related climatic teleconnections and the impact on human environment,'. In: J. v. d. P. W.G. Mook (ed.): *Proc. 16th Intern. ^{14}C Conference*, Vol. 40. pp. 535–550, Radiocarbon.

van Loon, H., G. A. Meehl, and J. M. Arblaster: 2004, 'A decadal solar effect in the tropics in July-August'. *Journal of Atmospheric and Terrestrial Physics* **66**, 1767–1778.

Veizer, J.: 2005, 'Celestial climate driver: a perspective from four billion years of the carbon cycle'. *Geoscience Canada* **32**, 13–28.

Veizer, J. and et al.: 1999, '^{87}Sr/^{86}Sr, δ^{13}C and $\delta^{18}O$ evolution of Phanerozoic seawater'. *Chem. Geol.* **161**, 59–88.

Veizer, J., Y. Godderis, and L. M. François: 2000, 'Evidence for decoupling of atmospheric CO_2 and global climate during the Phanerozoic eon'. *Nature* **408**, 698–701.

Veizer, J. and F. Mackenzie: 2004, 'Evolution of Sedimentary Rocks'. In: H. Holland and K. Turekian (eds.): *Treatise on Geochemistry*, Vol. 7. pp. 369–407, Elsevier.

Velinov, P. I. Y., M. B. Buchvarova, L. Mateev, and H. Ruder: 2001, 'Determination of electron production rates caused by cosmic ray particles in ionospheres of terrestrial planets'. *Advances in Space Research* **27**, 1901–1908.

Veretenenko, S. V., V. A. Dergachev, and P. B. Dmitriyev: 2005, 'Long-term variations of the surface pressure in the North Atlantic and possible association with solar activity and galactic cosmic rays'. *Adv. Space Res.* **35**, 484–90.

Verschuren, D., K. Laird, and B. Cumming: 2000, 'Rainfall and drought in equatorial east Africa during the past 1,100 years'. *Nature* **403**, 410–414.

Viau, A., K. Gajewski, P. Fines, D. Atkinson, and M. Sawada: 2002, 'Widespread evidence of 1500 yr climate variability in North America during the past 14000 yr'. *Geology* **30**, 455–458.

Vogt, S., G. F. Herzog, and R. C. Reedy: 1990, 'Cosmogenic nuclides in extraterrestrial materials'. *Reviews of Geophysics* **28**, 253–275.

von Storch, H., E. Zorita, J. Jones, Y. Dimitriev, F. González-Rouco, and S. Tett: 2004, 'Reconstructing Past Climate from Noisy Data'. *Science* **306**, 679–682.

Wagner, G., J. Masarik, J. Beer, S. Baumgartner, D. Imboden, P. W. Kubik, H.-A. Synal, and M. Suter: 2000, 'econstruction of the Geomagnetic Field Between 20 and 60 kyr BP from Cosmogeni c Radionuclides in the GRIP Ice Core,'. *Nuclear Instruments and Methods in Physics Research* **B 172**, 597.

Wang, Y., H. Cheng, R. L. Edwards, Z. S. An, J. Y. Wu, C.-C. Shen, and J. A. Dorale: 2001, 'A High-Resolution Absolute-Dated Late Pleistocene Monsoon Record from Hulu Cave, China'. *Science* **294**, 2345–2348.

Wang, Y., H. Cheng, R. L. Edwards, Y. He, X. Kong, Z. An, J. Wu, M. Kelly, C. Dykoski, and X. Li: 2005, 'The Holocene Asian Monsoon: Links to Solar Changes and North Atlantic Climate'. *Science* **308**, 854–857.

Warren, S. E.: 1999, *Antarctic Encylopedia of Climate and Weather*, pp. 32–39. OUP, New York.

Washimi, H., T. Tanaka, and G. P. Zank: 2005, 'A Global V-Shaped Channel Structure of the Termination Shock Due to a Magnetic Pressure Effect, and Its Physical Connection to Bipolar Flow Type Planetary Nebulae'. In: *AIP Conf. Proc. 781: The Physics of Collisionless Shocks: 4th Annual IGPP International Astrophysics Conference*. pp. 289–293.

Waters, L. S. E.: 1999, 'MCNPX User's Manual–Version 2.1.5'. Technical report, Los Alamos Natl. Lab.

Webber, W. R. and P. R. Higbie: 2003, 'Production of cosmogenic Be nuclei in the Earth's atmosphere by cosmic rays: Its dependence on solar modulation and the interstellar cosmic ray spectrum'. *Journal of Geophysical Research (Space Physics)* **108**, 2–1.

Webber, W. R. and J. A. Lockwood: 2001, 'Voyager and Pioneer spacecraft measurements of cosmic ray intensities in the outer heliosphere: Toward a new paradigm for understanding the global modulation process: 2. Maximum solar modulation (1990-1991)'. *J. Geophys. Res.* **106**, 29333–29340.

Webber, W. R. and J. A. Lockwood: 2004, 'Onset and amplitude of the 11-year solar modulation of cosmic ray intensities at the Earth and at Voyagers 1 and 2 during the period from 1997 to 2003'. *Journal of Geophysical Research (Space Physics)* **109**, 9103–+.

Webber, W. R. and A. Soutoul: 1998, 'A Study of the Surviving Fraction of the Cosmic-Ray Radioactive Decay Isotopes ^{10}Be, ^{26}Al, ^{36}Cl and ^{54}Mn as a Function of Energy Using the Charge Ratios Be/B, Al/Mg, Cl/Ar, and Mn/Fe Measured on HEAO3'. *Astrophys. J.* **506**, 335–340.

Weng, H.: 2005, 'The influence of the 11 yr solar cycle on the interannual–centennial climate variability'. *J. Atm. Solar-Terrestr. Phys.* **67**, 793–805.

Whang, Y. C., L. F. Burlaga, Y.-M. Wang, and N. R. Sheeley: 2004, 'The termination shock near 35° latitude'. *Geophys. Res. Lett.* **31**, 3805–+.

Wibberenz, G., I. G. Richardson, and H. V. Cane: 2002, 'A simple concept for modeling cosmic ray modulation in the inner heliosphere during solar cycles 20-23'. *Journal of Geophysical Research (Space Physics)* pp. 5–1.

Wielen, R.: 1977, 'The diffusion of stellar orbits derived from the observed age-depen dence of the velocity dispersion'. *Astron. & Astrophys.* **60**, 263–275.

Wild, M., H. Gilgen, A. Roesch, A. Ohmura, C. N. Long, E. G. Dutton, B. Forgan, A. Kallis, V. Russak, and A. Tsvetkov: 2005, 'From Dimming to Brightening: Decadal Changes in Solar Radiation at Earth's Surface'. *Science* **308**, 847–850.

Wiles, G. C., R. D. D'Arrigo, R. Villalba, P. E. Calkin, and D. J. Barclay: 2004, 'Century-scale solar variability and Alaskan temperature change over the past millennium'. *Geophys. Res. Lett.* **31**, 15203–+.

Willard, D., C. Berhardt, D. Korejwo, and S. Meyers: 2005, 'Impact of millennial-scale Holocene climate variability on eastern North American terrestrial ecosystems: pollen-based climatic reconstruction'. *Global Planet. Change* **47**, 17–35.

Windley, B.: 1984, *The Evolving Continents*. Wiley Press, New York.

Wolfendale, A. W.: 1973, *Cosmic rays at ground level*. London: Institute of Physics.

Worm, H.-U.: 1997, 'A link between geomagnetic reversals and events and glaciations'. *Earth Planet. Sci. Lett.* **147**, 55–67.

Xu, H., Y. Hong, Q. Lin, Y. Zhu, B. Hong, and H. Jiang: 2006, 'Temperature responses to quasi-100-yr solar variability during the past 6000 years based on δ^{18}O of peat cellulose in Hongyuan, eastern Qinghai–Tibet plateau, China'. *Palaeogeogr. Palaeoclim. Palaeoecol.* **230**, 155–164.

Yabushita, S. and J. Allen: 1998, 'On the impact vs GMC model of the K/T boundary event'. *Astronomy and Geophysics* **39**, 28–+.

Yang, S., H. Odah, and J. Shaw: 2000, 'Variations in the geomagnetic dipole moment over the last 12000 years'. *Geophysical Journal International* **140**, 158–162.

Yeghikyan, A. and H. Fahr: 2004a, 'Effects induced by the passage of the Sun through dense molecular clouds. I. Flow outside of the compressed heliosphere'. *Astron. & Astrophys.* **415**, 763–770.

Yeghikyan, A. and H. Fahr: 2004b, 'Terrestrial atmospheric effects induced by counterstreaming dense interstellar cloud material'. *Astron. & Astrophys.* **425**, 1113–1118.
Yeghikyan, A. G. and H. J. Fahr: 2003, 'Consequences of the Solar System passage through dense interstellar clouds'. *Annales Geophysicae* **21**, 1263–1273.
Young, G., V. von Brunn, D. Gold, and W. Minter: 1998, 'Earth's Oldest Reported Glaciation: Physical and Chemical Evidence from the Archean Mozaan Group (≈2.9 Ga) of South Africa'. *J. Geol.* **106**, 523–538.
Yu, F.: 2002, 'Altitude variations of cosmic ray induced production of aerosols: Implications for global cloudiness and climate'. *J. Geophys. Res.* **248**, 248.
Zank, G. P.: 1999, 'Interaction of the solar wind with the local interstellar medium: a theoretical perspective'. *Space Science Reviews* **89**, 413–688.
Zank, G. P. and P. C. Frisch: 1999, 'Consequences of a Change in the Galactic Environment of the Sun'. *Astrophys. J.* **518**, 965–973.
Zank, G. P. and H.-R. Müller: 2003, 'The dynamical heliosphere'. *Journal of Geophysical Research (Space Physics)* pp. 7–1.
Zuccon, P.: 2002, 'A Monte Carlo Simulation of the Cosmic Rays Interactions with the Earth's Atmosphere'. *Internat. J. Mod. Phys. A,* **17**, 1625–1634.